Effect of second phase distribution and morphology on the bake hardening behavior of dual phase steels

A Dissertation submitted

in partial fulfillment of the requirements

for the degree of

Master of Engineering

in

Production Engineering

by

Arnab Chakraborty

Regd. No. 801482003

Under the supervision of:

Dr. Tarun Nanda
Assistant Professor, MED,
Thapar University, Patiala

Dr. B. Ravi Kumar
Principal Scientist, MST,
CSIR-NML, Jamshedpur

MECHANICAL ENGINEERING DEPARTMENT

THAPAR UNIVERSITY, PATIALA-147004, PUNJAB, INDIA

JULY, 2016

Certificate

I hereby declare that the thesis entitled "**Effect of second phase distribution and morphology on the bake hardening behavior of dual phase steels**" is an authentic record of my study carried out as requirements for the award of the degree of **Master of Engineering** in **Production Engineering** at **Thapar University, Patiala** under the supervision of **Dr. Tarun Nanda**, Assistant Professor, Mechanical Engineering Department, Thapar University, Patiala and **Dr. B. Ravi Kumar**, Principal Scientist, MST Division, CSIR-NML Jamshedpur during July, 2014–2016. The matter embodied in this report has not been submitted in partial or full to any other university or institute for the award of any degree.

Date: 11/7/2016

Arnab Chakraborty

It is certified that the above statement made by the student is correct to the best of my/our knowledge and belief.

Dr. Tarun Nanda
Assistant Professor
Mechanical Engineering Department
Thapar University, Patiala - 147004

Dr. B. Ravi Kumar
Principal Scientist
MST Division
CSIR-NML Jamshedpur

Countersigned by

Dr. S.K. Mohapatra
Sr. Professor & Head
Mechanical Engineering Department
Thapar University, Patiala – 147004

Dr. S.S Bhatia
Dean of Academic Affairs
Thapar University, Patiala - 147004

Acknowledgement

Though only my name appears on the cover of this dissertation, a great many people have contributed to its production. I owe my gratitude to all those people who have made this dissertation possible and because of whom my graduate experience has been one that I will cherish forever.

My deepest gratitude is to my advisor, Dr. Tarun Nanda. I have been amazingly fortunate to have an advisor who gave me the freedom to explore on my own, and at the same time the guidance to recover when my steps faltered. His patience and support helped me overcome many crisis situations and finish this dissertation. My co-advisor, Dr. B. Ravi Kumar, has been always there to listen and give advice. I am deeply grateful to him for the long discussions that helped me sort out the technical details of my work. I am also thankful to him for his un-ending encouragement and motivation during the entire duration of my stay in Jamshedpur.I would like to acknowledge Mrs. Manashi Adhikary for numerous discussions and lectures on related topics that helped me improve my knowledge in the area.

I am also indebted to the members of the *National Metallurgical Laboratory* with whom I have interacted during the course of my graduate studies. Particularly, I would like to acknowledge Mr. Anindya Das for the many valuable discussions that helped me understand my research area better. My special thanks to the following technical staff of NML-Jamshedpur for their ready assistance during my experimentation phase – Mr. Lalit Gupta, Mr. Lalan Patro and Mr. Rajiv Jonko

Many friends have helped me stay sane through these difficult years. Their support and care helped me overcome setbacks and stay focused on my graduate study. I greatly value their friendship and I deeply appreciate their belief in me. Most importantly, none of this would have been possible without the love and patience of my family. My family has been a constant source of love, concern, support and strength all these years. I would like to express my heart-felt gratitude to my family.

ARNAB CHAKRABORTY

Abstract

The present scenario of rapid boom in automotive industry has ushered tremendous improvement and growth in the steel processing technology. Advanced High Strength Steels (AHSS) have fulfilled most of the aspects concerning better utilization and fabrication of light weight steels for automobile applications. Various grades of AHSS have been processed over the past few decades, however, the search for even better mechanical properties and subsequently fuel efficient-light weight structures has deemed a deep research prospect in dual phase steels (DP steels), a category of AHSS. DP steels is the most commonly used AHSS grade for automotive industry. Dual Phase steels also known as DP steels consist of a hard martensite/ or bainite phase embedded within a softer ferrite phase. This peculiar combination of a hard phase (martensite) and a soft phase (ferrite) provides a perfect balance of strength and ductility in these steels. The typical production process of DP steels involves inter-critical annealing of low carbon steels which is followed by a rapid quenching or cooling techniques to obtain DP microstructure wherein, martensite is distributed along the grain boundaries of the ferrite grains. DP steels are mostly used for fabricating the exterior members of automobile bodies like the roof or floor panels and the cross member regions. The finished or heavily formed (simulated by pre-straining in this research work) auto-body is given a finishing paint curing treatment which helps in proper curing or adhesion of the paint coat over the entire exterior panels in the vehicles. This finishing operation is industrially referred to as the Bake Hardening treatment. The term hardening is associated with the improvement in final yield strength of the automobile body after this treatment. The increase in final yield strength is due to the presence of free or available interstitial solute carbon atoms in DP steels during its processing. These interstitial solute atoms upon receiving sufficient diffusion energy (during baking treatment) pin or lock the dislocations created during various forming operations (stamping, bending, extrusion etc.) thus, a rise in final yield strength is always obtained. Hence, in addition to curing of the paint coat, the dent resistance of the final component also improves at no extra production cost. In the present research work, bake hardening characteristics of a conventionally processed DP steel viz. Continuous Annealing Line (CAL) process was evaluated against a modified Continuous Annealing Line (mod-CAL) process. A typical industrial continuous annealing line (CAL) process was employed to anneal a 67% cold rolled steel to obtain the dual phase microstructure. Subsequent to this conventional annealing, the steel was now subjected to an

improved process (mod-CAL) with modified initial heating rate and peak annealing temperature. The processed specimens (through CAL and mod-CAL respectively) were further pre-strained in the range 1–5 % followed by the bake hardening treatment at 170 ℃ for 20 minutes. It was observed that the CAL processed specimen showed a peak of about 70 MPa in bake-hardening index at 2 % pre-strain level. At higher pre-strain values (in excess of 2 %), a gradual drop in bake-hardening index was observed. On the contrary, the mod-CAL processed specimens showed near uniform bake-hardening response at all pre-strain levels and a decrease could be noted above 4% pre-strain. The evolving microstructure at each stage of annealing process and after bake-hardening treatment was studied using field emission scanning electron microscopy. The microstructure analysis distinctly revealed the differences in the martensite spatial distribution and interface morphologies developed by the two annealing processes. The modified process showed predominant formation of martensite within the ferrite grains with serrated lath martensite interfaces. This nature of the martensite was considered responsible for the observed improvement in the bake-hardening response. Furthermore, along with improved bake-hardening response, negligible loss in tensile ductility was also noted. This behavior was correlated with delayed micro-crack initiation at martensite interface due to the serrated nature of the lath martensite.

Table of Contents

List of Figures

List of Tables

List of Acronyms & Symbols

List of Acronyms

AHSS	Advanced High Strength Steels
AR	As Received
BH	Bake Hardening
CAL	Continuous Annealing Line
CP	Complex Phase
DP	Dual Phase
DSC	Diffraction Scanning Calorimetry
EBSD	Electron Beam Scattered Diffraction
HSLA	High Strength Low Alloy
IF	Interstitial Free
ICA	Inter Critical Annealing
LIP	Light Weight Induced Plasticity
LNQ	Liquid Nitrogen Quenched
MART	Martensitic
mod-CAL	Modified Continuous Annealing Line
OM	Optical Microscope
PS	Pre Strained
PPM	Parts per million
Q&P	Quench and Partitioning
QT	Quench Temperature
RVE	Representative Volume Element
SEM	Scanning Electron Microscope
SIP	Shear Band Induced Plasticity
TE	Total Elongation
TEM	Transmission Electron Microscope
TRIP	Transformation Induced Plasticity
TS	Tensile Strength
TWIP	Twinning Induced Plasticity
UTS	Ultimate Tensile Strength

XRD	X-Ray Diffraction
YS	Yield Strength

List of Symbols

V_m	Martensite Volume Fraction
ΔY	Rise in Yield Strength
HV	Vickers Micro Hardness
$Rp_{0.2}$	Yield Strength
R_m	Ultimate Tensile Strength
α	Ferrite
γ	Austenite

Chapter 1

Introduction

1.1 General

Advanced high strength steel (AHSS) grades have multiphase microstructure resulting from precise control on heating and cooling processes [1, 2]. Materials used in automotive applications are selected so as to minimize weight, while maintaining critical features which include crash performance, stiffness, and forming requirements [3]. Different types of AHSS ensure that the parts meet varied performance demands in different areas of the vehicle, including both the crumple zone and passenger compartment. Forged and sheet materials for automobile applications demand both high strength and formability. High strength allows for the use of thinner gauge material for structural components, which reduces weight and increases fuel efficiency. Another major advantage of higher strength material is the improved passenger safety owing to the higher crash resistance of the material [4, 5]. Thus, the high strength material must also be formable to allow efficient and cost effective mass-produced automotive parts. AHSS grade steels have been generally classified under metallurgical characteristics which inherently affect the mechanical properties of these grades [4]. AHSS grades have been divided into three generations; the first generation AHSS are primarily ferrite based steels. This generation includes dual-phase (DP) steels, transformation-induced plasticity (TRIP) steels, martensitic (MART) steels, and complex-phase (CP) steels [5, 6]. The first generation AHSS steels exhibit far superior mechanical strength when compared to conventional low carbon or High Strength Low Alloy (HSLA) steels. However, formability is an issue in this generation. Limited elongation or ductility forced the hunt for even better materials. The second generation of advanced high strength steels solved this problem. It includes twin induced plasticity (TWIP), light-weight with induced plasticity (L-IP) steels, and shear band formation-induced plasticity (SIP) steels. The second generation AHSS steels show improved mechanical formability properties (ductility, elongation), but these are austenitic grades which need considerable amount of alloying elements resulting in a significant cost increase [6, 7]. Thus a clear tradeoff between mechanical properties and cost effectiveness was the need of the hour. This was meted out by the third generation of AHSS steels. The concept of lean composition and enhanced processing routes for the AHSS grades developed the third generation which sorted out the concerns of both the first and second

generation AHSS steels like enhanced DP steels, Quench and Partitioning (Q & P route) steels [8, 9].

1.2. Advanced High Strength Steels (AHSS)

AHSS are complex in nature, particularly with their mcrostructure which is usually multiphase for a mended combination of strength and ductility. This balance is vigilantly constructed to meet performance requirements while maintaining excellent formability. AHSS often has other advantageous mechanical properties, such as high strain-hardening capacity and high energy absorption capacity.

1.2.1. Need for AHSS

Several aspects are needed to be looked into for material selection in automotive applications which include safety, fuel efficiency, good environment, manufacturability, durability, and quality. In the rapidly evolving competitive automotive industry, cost is an extremely important parameter for material selection. As the motivation for vehicle mass reduction continues to grow, automakers tend to maximize the efficiency of their materials selection. Analyzing the parts to identify opportunities to redesign geometries within constraints; and to achieve these desired shapes for weight reduction, newer materials are sought. Considering AHSS during this optimization process is very advantageous, partly because the wide range of grades allow for design flexibility [9, 10]. Using stronger steel enables engineers to use thinner steel, or a reduced gauge, to produce a lighter-weight part while maintaining or improving the strength and other performance properties.

1.2.2. Defining AHSS

The terms “high-strength” and “advanced high-strength” refer mostly to steels which share a common family of behaviors. Generally, AHSS differ from the early HSS (IF, BH, HSLA) since they were developed later for improved strength and ductility to enhance formability. In reality, the steels fall into a continuum of strengths. The distinction between HSS and AHSS is somewhat arbitrarily done. While a typical definition for steels with 210 to 550 MPa yield strength is “high-strength” and anything stronger is “advanced high-strength.” AHSS steels are also sometimes called “ultra high-strength steels” for tensile strengths exceeding 780 MPa [8]. Equally important with increasing YS and UTS was the achievement of appropriate combination of formability, weld-ability, and other characteristics necessary for the automotive application of

steel in a competitive market. This necessity generates the large variety of grades in different stages of development.

1.3. Generations of AHSS

The AHSS can be classified into three generations based on their microstructural properties [5, 6]. AHSS steels are classified as first generation which are "primarily ferrite-based steels", second generation "austenitic grades with high manganese and sometimes aluminium contents". Because of the tradeoff between poor elongation and formability seen in first generation, while high alloying cost of second generation, a new third generation was developed keeping in mind the above mentioned constraints. The properties of this third generation AHSS were superior to the first generation and were much cost effective than the second generation AHSS due to leaner compositions [5]. The classification of AHSS is represented in Figure1.1 below.

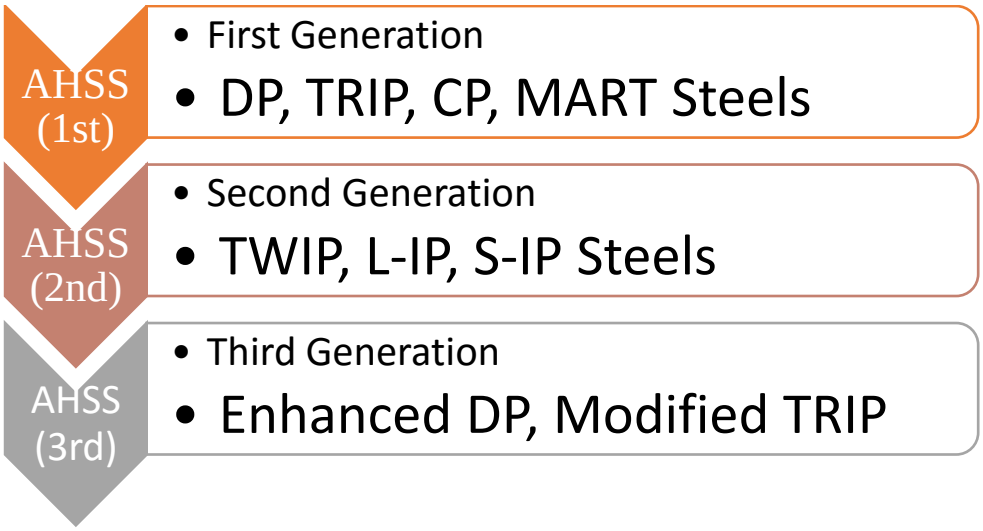

Figure 1.1 Classification of AHSS.

1.3.1. First generation AHSS

The First Generation of AHSS includes Dual-Phase (DP) steels, Transformation Induced Plasticity (TRIP) steels, Complex Phase (CP) steels and Martensitic (MART) steels. The first generation AHSS concepts were developed in fairly lean compositions and are primarily ferrite-based multiphase microstructures. The strength achieved in the first generation of AHSS far exceeded that of the conventional HSLA steels but it limited the ductility. Thus formability remains a problem [6].

1.3.2. Second generation AHSS

Second generation AHSS are basically austenitic steels with high alloying contents e.g. TWIP, L-IP, S-IP etc. Due to presence of retained austenite in the microstructure, these steel offer excellent combination of strength and formability which helped in overcoming the problem in first generation AHSS of low ductility. While, a shortcoming associated in this generation was addition of heavy alloying elements which meant, the industrial processing, specifically of the TWIP steels with high manganese content was very challenging. The TWIP steels are also prone to delayed cracking [3, 6].

1.3.3. Third generation AHSS

The third generation of AHSS was developed to impart better combination of strength and ductility (than the first generation of AHSS) while at a lower cost than (the second generation AHSS). The mechanical properties of the third generation of AHSS filled the opportunity band which existed between the first and second generation of AHSS e.g. 1000 MPa tensile strength and 30 % elongation [9], as can be seen from Figure 1.2.

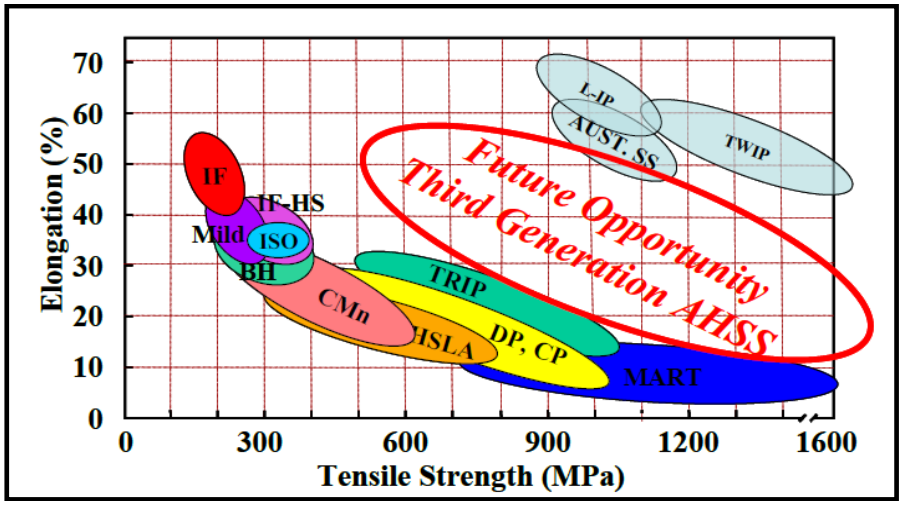

Figure 1.2: Overview of tensile strength and total elongation combinations for various classes of conventional and advanced high strength sheet steel (AHSS) grades [6].

For optimizing the results of this generation, techniques for lean alloy steel compositions are used for developing such grades of AHSS. Since, microstructure determines the behavior and performance of AHSS steels, the proper design and control of the microstructure becomes essential in the third generation of AHSS. Third generation AHSS are the extension of first generation steels by improvements seen in mechanical properties through grain refinement. The

strategies pursued for the third-generation AHSS steels include processing to enhance properties of DP steels, modifications made to traditional processing of TRIP steel, development of ultra high-strength steels with ultrafine bainite microstructures, implementation of new processing routes like quenching and partitioning (Q&P) and ultra-rapid heating and cooling, and development of high-Mn content TRIP steels [6, 9, 10, 11, 12].

1.4. Dual Phase Steels (DP Steels)

The dual phase steel consists of a ferrite matrix, additionally containing islands of high hardness martensite. The presence of martensite, a hard second phase within a soft and ductile ferrite matrix in a dual phase steel promotes better distribution of strain. In other words, this results in efficient load transfer between deformable ferrite and relatively non-deformable martensite [13, 14, 15]. The dual phase (DP) steel offers a characteristic continuous yielding phenomena, high work hardening rate, low yield to tensile strength ratio and high uniform and total elongation [15]. The second phase development primarily relies on the processing route adopted. It is quite well established that the final microstructure of DP steels depends on a lot of factors like heating rate, soaking temperature (austenitizig temperature), soaking time, cooling medium and cooling rate. The relationship between processing factors and final microstructure and hence mechanical properties in DP steel is completely determined by austenite stability during the annealing process which in turn depends on chemistry of the steel and time given for pearlite dissolution and austenite homogenization with respect to carbon [14, 15].

1.4.1. Processing of Dual Phase Steels

The development of DP steels has attracted great interest in the automobile industry because of a potential weight reduction by using inexpensive alloying without sacrificing mechanical properties [13]. DP steels mainly consist of two phases' viz. ferrite and martensite. But, in addition to martensite, the microstructure may also contain small amounts of other phases such as retained austenite, new ferrite, pearlite and bainite, depending on the cooling rate and thermo-mechanical processing route. Some of the authors have produced DP steels by direct quenching from temperature above A_{C1} temperature (i.e. inter-critical temperature). Microstructure produced comprised of ferrite and martensite [13, 14]. Some authors have produced DP steels by initially performing slow (air) cooling up to desired ferrite transformation stage from fully austenitic state and then quenching for transforming the remaining austenite to martensite (done according to CCT diagram) [15]. Very limited work has been reported to produce the

bainite/ferrite or martensite/ ferrite microstructure of dual phase steels by laminar cooling than ultra-fast cooling up to coiling temperature and finally by coil cooling up to room temperature of hot rolled strip [14]. Mechanical properties obtained viz the last method are better than all other methods due to grain refinement of microstructure and proper volume fraction of the constituent phases. The DP steels thus produced properly fit in the region of third generation AHSS. However, in this method, there is a difficulty in controlling the different rates of cooling required from the austenization temperature to the room temperature.

1.4.2. Properties and Applications of Dual Phase Steels

The combination of high strength and ductility in modern AHSS can allow thinner components to be used in car construction and also to improve the safety due to their high energy-absorption capabilities. The greatest prospect of application of DP-type steels is in automotive industry. It is predicted, that their total share in a car structure can reach over 50 % [2]. These steels usually contain 0.05–0.2 % C, 1.2–1.6 %Mn, 0.03–0.6 %Si and micro additions of V, Nb and Ti up to concentration of 0.1 % [2, 3].

1.5 Bake Hardening behavior in DP steels

Bake-hardening (BH) phenomena is one such process which results in enhanced yield strength of finished component, but often at the cost of its final ductility or total elongation [16]. BH operations in industrial (automobile) processing, is a finishing treatment, where the paint coating of the automotive body is baked at temperatures of 150-200^{o}C for 20-30 minutes [16, 17, 18]. This leads to the solute diffusion toward dislocations and the formation of Cottrell atmosphere and hence the strengthening effect [19, 20, 21]. This process of baking is beneficial in ways that it improves the final overall dent resistance without any additional production cost. DP steels also show excellent bake hardening (BH) properties for which it assumes the role of prime material in automotive industry for the exterior members of a vehicle like door panels and B-Pillars etc [1, 2, 3].These press formed finished components are passed through a paint curing operation that helps bind the paint coat as well as enhance the final yield strength post forming and painting, thereby improving the dent resistance at no extra production cost. Typical BH effect comes into play during paint curing operation which is performed within a chamber held at a temperature of about 170 ℃ for about 20 minutes [22, 23]. A pictorial representation of bake hardening in DP steels is shown below in Figure 1.3.

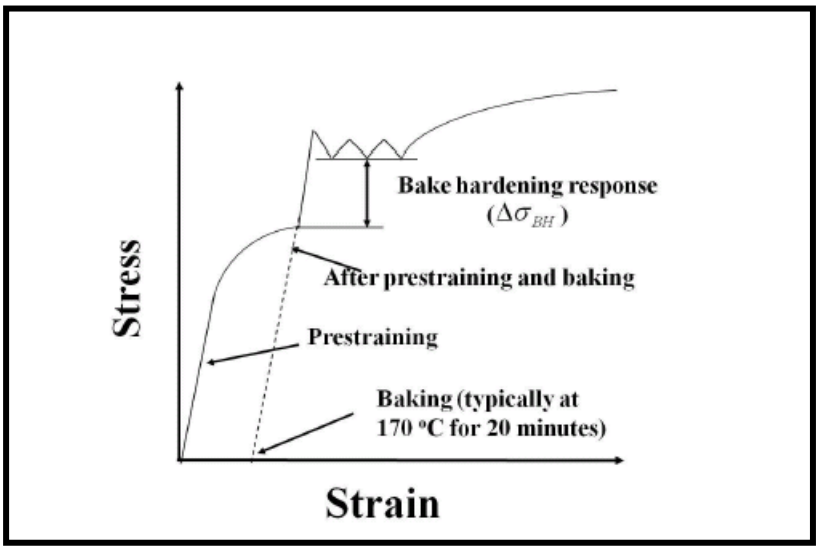

Figure 1.3: Reprsentation of BH behavior [17].

It is well studied and reported now that this low temperature baking aids the diffusion of solute carbon atoms present in the microstructure of DP steels to the dislocations generated at a) ferrite grain boundaries during the phase transformation from austenite to martensite during the cooling stage, and b) from the external deformation (pre-straining) while forming of auto-body components [24, 25, 26]. The accumulation of these solute interstitial atoms near the generated dislocation sites initiates “Cottrell Atmosphere” formation and simultaneous pinning of the mobile dislocations by these solute atoms begin. The driving force for the solute redistribution emanates from the reduction in lattice energy.

1.6 Stages in Bake Hardening

Bake hardening has been defined to occur in three successive stages of occurrence. These stages are both time and temperature dependent [17, 18, 19, 20]. Figure 1.4 below shows the pictorial representation of stages involved in bake hardening. It clearly shows the effect of baking time and temperature on the variable hardening stages evolving out of baking of press formed components. Three stages are generally defined for bake hardening: a) First Stage; b) Second Stage; c) Third Stage. The stages are briefly discussed in the next section.

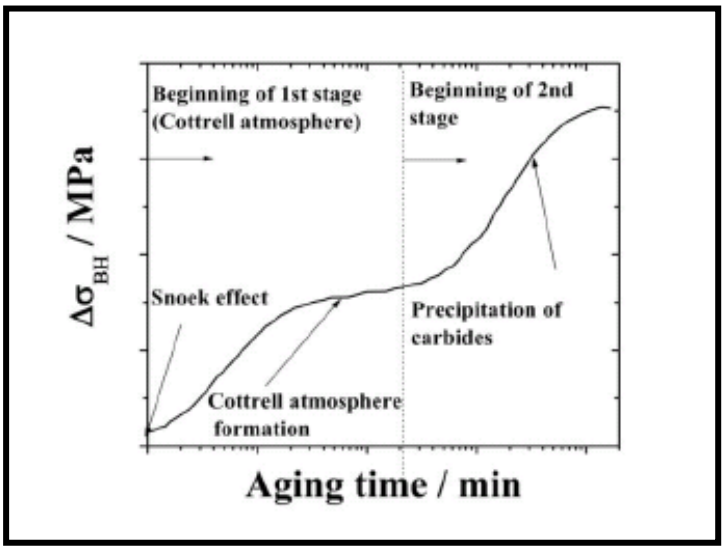

Figure 1.4: Various stages in bake hardening [17]

1.6.1. Snoek rearrangement

It refers to a low temperature short range diffusion of solute atoms nearby the deformation zone which happens so quickly that it is hardly measurable. The diffusion is simply rearrangement of randomly distributed solute atoms upon any external deformation (pre-straining). The rearranged solute atoms occupy kinetically and energetically most favourable interstitial sites in the solvent matrix [17, 18, 27]. The rearrangement very seldom leads to fixing of very few dislocation sites by these interstitial atoms thus providing mild to negligible strengthening action. Hence, its effect will not be studied in the present work henceforth.

1.6.2. First stage

Accelerated strengthening can occur at slightly higher temperatures around 150-200 ℃ wherein the interstitial solute atoms gain sufficient diffusion energy to lock the dislocations (created by prior pre-straining) viz long range diffusion. Solute atoms get attracted to the strain field generated by the dislocations; as a result an atmosphere of solute atoms is formed nearby these sites. This effect was first observed by Cottrell and the atmosphere created was named after him as “Cottrell Atmosphere”. The *first stage* is often referred to as the “Cottrell Atmosphere” formation [17].

1.6.3. Second stage

The *second stage* of BH is believed to occur due to segregation of solute atoms in the form of ϵ carbides from the “Cottrell Atmosphere”. This stage is reached only after all the dislocation sites

have been “locked” or “pinned” by the interstitial solutes. The core of the “Cottrell Atmosphere” becomes the most preferable site for the precipitation of these carbides to take place. This precipitation leads to additional hardening which is termed as the *second* stage of bake hardening [24, 25].

1.6.4. Third stage

Prolonged segregation of interstitial solute carbon atoms on the dislocation sites can lead to an eventual saturation stage when the precipitate concentration induces cluster formation with increasing aging time leading to coarsening of ϵ carbides. This stage is reported to be the *third stage* of BH [26, 28, 29].

1.7. Factors influencing BH behaviour in DP steels

Industrially DP steels are produced through continuous annealing route. In DP steels, the BH depends on available solute carbon and its interaction with the dislocations post straining and paint baking operations [17, 19, 20, 23, 25, 26]. The solute carbon available depends on factors like annealing temperature, austenite stability, and amount of carbon in solution in ferrite during rapid cooling [22]. Figure 1.5 shows the relationship between solute carbon concentration and the bake hardening response. It was observed to increase with increasing carbon content.

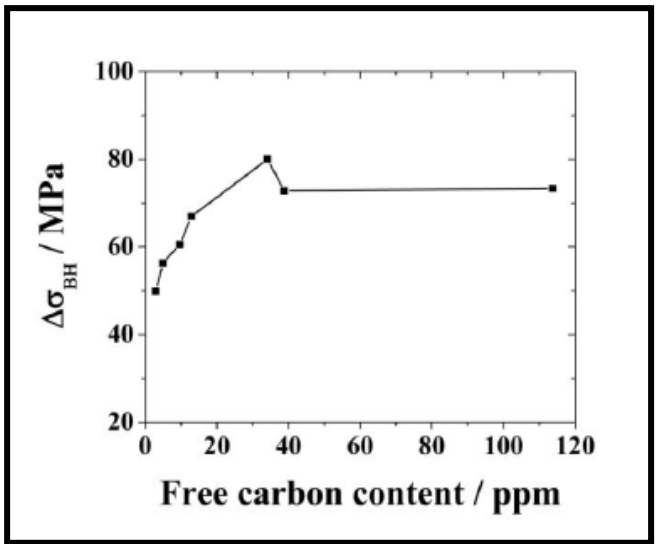

Figure 1.5: Effect of solute carbon content on BH behavior of low carbon steels [17].

Higher solute content only ensured more pinning of dislocations, however only upto a certain value. Beyond a particular content, any increase in solute had no significant effect on the bake

hardening behavior since at higher solute levels most of the dislocations have already been locked and it leaves no more dislocation to be pinned thereby no further improvement in yield strength is possible. Effect of BH can be modulated by altering the interaction of solute carbon atoms with the dislocations. It has been reported that the different morphology and distribution of lath martensite (second phase) is expected to behave differently under stress/ tensile loading with respect to deformation it is also expected to alter the effect of interaction of mobile dislocations near the interface and therefore the BH [16,19]. BH response also depends on the amount of pre-strain, bake-hardening temperature-time and on the formation of mobile dislocations in ferrite as a result of martensitic transformation, and therefore contribution of dislocation pinning leading to an increase in bake-hardening response is significant [20]. In this work, an attempt has been made to study the ferrite/ martensite interface size and shape effect along with the martensite spatial distribution on BH and total elongation of two different inter-critically annealed DP590 steel grade specimens. Second phase morphology and distribution was engineered by simulating industrial and lab designed annealing processing conditions. The change in interface area of second phase was found to impact the BH and tensile behaviour in this steel under the simulated annealing conditions. The usual BH behavior in DP steels is observed to rise and peak to a certain pre-strain amount and then fall beyond that maximum pre-strain value. A well studied and detailed analysis of BH behavior is seen in Figure 1.6 with regards to baking temperature and pre-strain values.

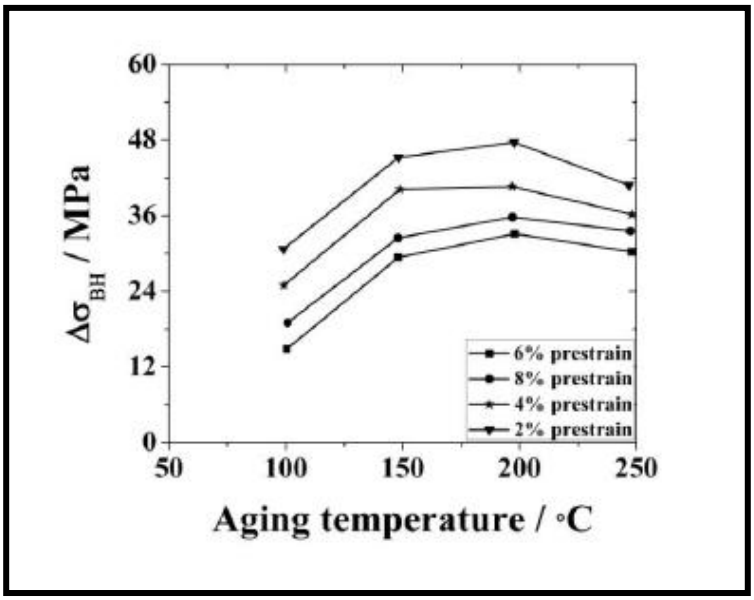

Figure 1.6: Effect of temperature and pre-straining on BH for low carbon steels [17].

1.8. Summary of the Chapter

This chapter elucidates the role of advanced high strength steels in present day automotive industry and its microstructure benefits which ably suit them for modern day use in vehicles. DP steels is one of the grades of AHSS and is being currently focused on improving the fuel efficiency and crash absorption resistance of automobiles due to its unique microstructure of a soft and hard phase. This DP steel also shows very decent bake hardening behavior which ultimately results in improved yield strength at no extra production cost. Typical BH behavior seen in DP steels has been discussed in the concluding sections of this chapter as-well.

Chapter 2

Literature Review

2.1 General

The following chapter is devoted to the review of the various literatures which were studied to understand the annealing processes established to obtain DP steels and study the effect of various operating parameters on the bake-hardening properties of these steels.

2.2 Review of the Literature

Adamczyk and Grajcar (2006) [13] investigated the effect of heat treatment conditions on the structure and mechanical properties of Dual Phase (DP) type steel. For the experimentation, steel of composition (C:0.09; Mn:1.5; Si:0.26; Ni:0.07; P:0.014; S:0.009; B:0.003; Al:0.029; N:0.012:Fe: balance; all in wt %) was melted and continuous casting of 100x100mm slabs was done. After solidification the slabs were hot-rolled and forged in order to obtain the rods with a section of 24x24 mm. The heat treatment of the specimens was realized according to three routes. In the routes I and II, the steel was heated to a temperature of 910 ℃ ($\alpha + \gamma$ region), held at this temperature for 30 min. In route I, specimen was air cooled to room temperature then again heated to750 ℃ and water quenched. In route II specimen was water quenched from both temperatures viz: 910 ℃ and 750 ℃. The route III consists in austenitizing of steel at a temperature of 910 ℃ and air cooling for 45 s to a temperature of 750 ℃ in order to realize the partial γ to α transformation, followed by water quenching. Route I led to formation of the ferrite structure with an irregular envelope of martensite on grain boundaries. In route II, during heating the steel to an under hardening temperature, the nucleation of austenite mainly occurred on the boundaries of martensite laths formed after primary quenching from a temperature of 910 ℃. The predominated martensite fraction occurred mainly as thin fibers located in surroundings of grain boundaries. Moreover, in surroundings of martensite, especially at a boundary zone of large grains of the alpha phase, small grains of the recrystallized ferrite could be identified. In routeIII, martensite was located on grain boundaries of the alpha phase. The optimum fraction of martensite averaging 20% occurred after air cooling of the specimens for 45 s. The used conditions of heat treatment led in obtaining the DP-type steels of comparable fractions of ferrite and martensite. The optimum fraction of martensite was from 21% to 24%, and the grain size of α phase was in the range 7–10 μm. The diversified morphology of martensite had a influence on various mechanical properties of the steel. The optimum strength and ductile properties were

achieved by route II. The yield point of this steel was about 520 MPa, tensile strength about 800 MPa, total elongation 20%, and uniform elongation about 16%.

Gunduz*et* et al. (2008) [20] investigated the strain aging behaviour of DP steel pre-strained to 4% (tensile) and aged at temperatures between 25–250 ℃. For the study steel of plate thickness 5 mm and a chemical composition of; 0.17C- 1.4Mn-0.4Si-0.020S-0.025P (wt%) was used. The DP microstructure was obtained by heating the bars in the inter-critical temperature range of 735 ℃ to 780 ℃ for 15 min, followed by quenching into cold water. Samples for microscopic evaluation were etched with 2 % Nital followed by immersion in 10 % sodium-metabisulfite solution. This technique revealed martensite as a brown colored phase. The authors calculated the martensite volume fraction obtained by heating at ICT of 735 ℃ and 780 ℃ which were 14% and 22% respectively. Figure 2.1 shows the microstructure after annealing at above mentioned temperatures. Tensile specimens of 25 X 5 X 3 mm were prepared and pre-strained for aging treatment. The processed and pre-strained specimens were aged for 30 minutes at temperatures between 25 and 250 ℃ in a furnace and subsequently air cooled.

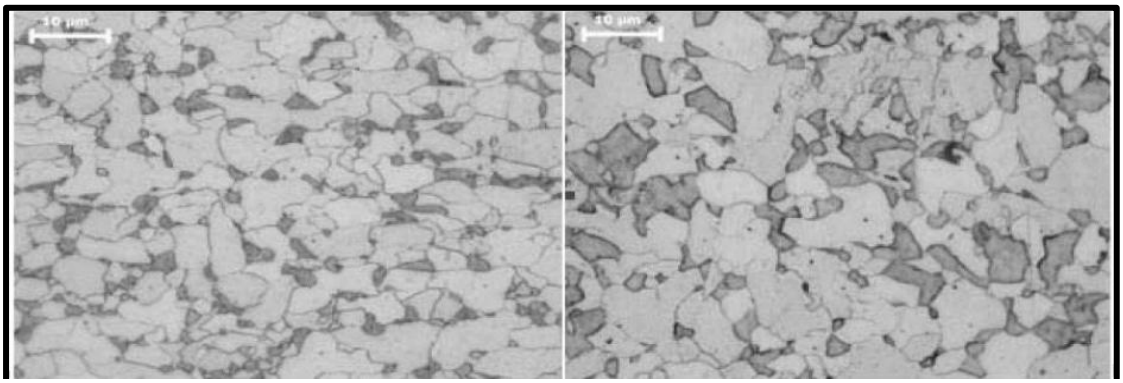

Figure 2.1: (a) Microstructure after annealing at 735 ℃, (b) at 780 ℃ [20].

The authors observed that dual phase steels had rounded (continuous) stress strain curves prior to aging, however, under pre-strained conditions discontinuous yielding behaviour returned. This return in discontinuity is attributed to the pinning of the dislocations within the ferrite by interstitial carbon atoms. The studies on strain aging also showed that with reappearance of the lower yield point upon pre-straining there was also significant increase in YS and thereby ΔY as can be seen in Figure. 2.2. The authors also observed that at higher aging temperatures of 250 ℃, besides the static strain aging effect there is also a softening effect, a result of tempering of martensite which decreases the strength of DP steels as evident from Figure 2.3.

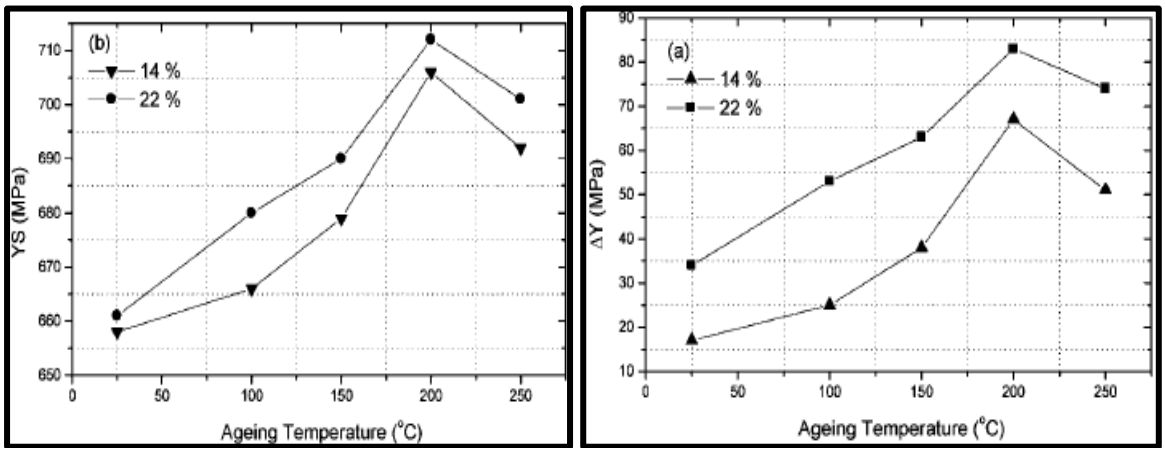

Figure 2.2: Effect of martensite by volume and aging temperature changes on (a) ΔY& (b) YS [20].

At a given aging temperatureΔY, YS and UTS increased with increasing martensite. Thus the authors concluded that DP steels with 14% and 22% martensite were strongly susceptible to strain aging which caused an increase in strength at the cost of ductility.

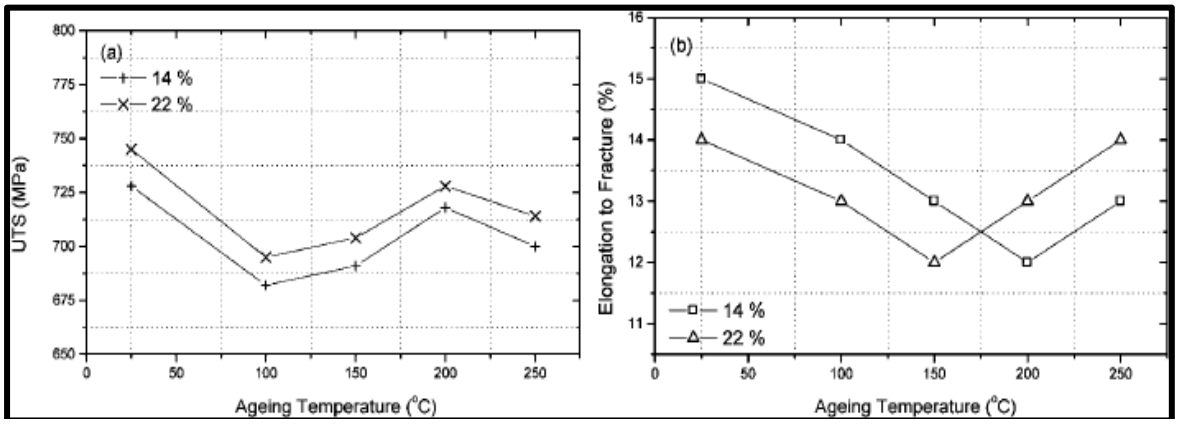

Figure 2.3: Effect of martensite by volumes and aging temperatures on changes in (a) UTS and (b) elongation [20].

Maggi and Murgia (2008) [4] have provided an overview of the different Advanced High Strength Steel (AHSS) grades and their fundamental characteristics which are now regularly used in industries worldwide. According to the authors, the most common classification of these grades were primarily based on metallurgical characteristics from low carbon steels (Carbon steels, IF Steels), High Strength Steels or HSS (C-Mn, BH, HSIF) to AHSS (DP, TRIP, MP/CP, MART). A similar classification of all these grades was possible based on their strength characteristics with HSS showing yield strength (YS) in the range of 210–550 MPa and tensile strength (TS) within 270–700 MPa, while AHSS showed YS greater than 550 MPa and TS more than 700 MPa. A third classification was based on mechanical characteristics or formability

parameters, as can be seen in Figure 2.4.

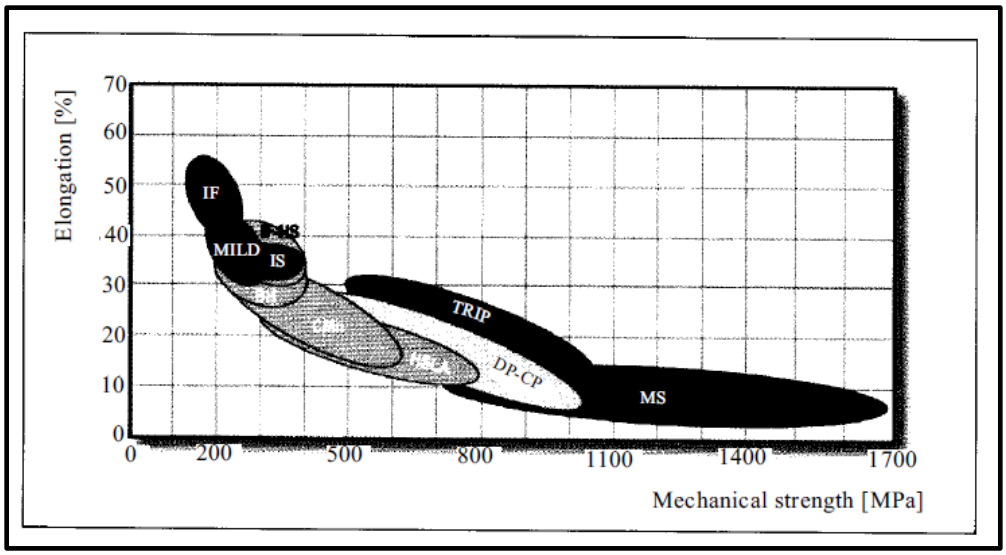

Figure 2.4: Classification of certain conventional (HSS, in grey) and AHSS (black-white) for automobile use, based on mechanical characteristics [4].

The authors noted that the basic difference between HSS and AHSS lied in the microstructure of the two. HSS happened to be pre-dominantly ferrite based, while AHSS were multi-phase steels containing residual ferrite, martensite, bainite, and austenite in desirable quantities for the required mechanical characteristics. It was also seen that the AHSS grades shared a common aspect regarding the precise control of cooling rates from the austenitic or austenitic-ferritic field. In order to unambiguously identify individual grades, a designation system, based on a code representing the metallurgical and strength characteristics was also prepared as listed below in Table 2.1. The authors then highlighted the AHSS grades and their respective metallurgical characteristics one by one.

Table 2.1: Tensile characteristics of several of the main steels for automobile use [4].

Designation (grade)	**Yield Strength (MPa)**	**Rupture Strength (MPa)**	**Elongation at rupture (%)**
HSLA 350/450	350	450	23-27
DP 300/500	300	500	30-34
DP 350/600	350	600	24-30
TRIP 450/800	450	800	26-32
DP 500/800	500	800	14-20
CP 700/1000	700	1000	12-17
MS 1250/1520	1250	1520	4-6

Firstly dual phase (DP) steels were discussed which are composed of a ferritic matrix, containing islands of high hardness martensite. Depending upon the chemical composition and the manufacturing method adopted these steels also showed significant quantities of bainite at times. Ferrite being the softer phase offered optimal ductility, while martensite/ bainite conferred hardness and strength to it. Matrix hardening was also possible by addition of some alloying elements like Mn, Cr, Mo and Ni. DP steels also showed decent bake hardening ageing along with excellent weldability and spring back resistance. Next the authors discussed the Transformation Induced Plasticity Steels better known as TRIP steels. The microstructure consisted of retained austenite (R.A) surrounded by matrix of ferrite with islands of martensite and bainite. Higher carbon content compared to DP was observed during the stabilization of the austenitic phase. During the controlled deformation state, R.A transformed into martensite which showed work hardening effects along with improved ductility. Complex Phase steels (CP) also known as multi-phase steels (MP) were considered next. A controlled cooling rate was followed, so as to delay the formation of ferrite and pearlite, instead here the austenite was transformed into fine grained bainitic matrix, with islands of residual martensite. Delay in recrystallization promoted further grain refinement with the addition of micro-alloying elements like Ti, Nb and V. These steels showed better tensile strength than DP or TRIP steels. Martensitic steels (MART) were also discussed which had pre-dominantly martensitic microstructure with modest quantities of ferrite and bainite. Hardening was for the martensitic matrix due to higher carbon content. These were often subjected to tempering to improve its ductility, so as to bestow suitable formability. Another major grade of AHSS namely Twinning Induced Plasticity Steels or TWIP steels was also investigated which were characterized by very high quantities of Mn (17–24 %) and C (0.5–0.70 %). Besides the well known dislocation movement mechanism, these steels also had characteristics twinning phenomena. Without doubt the TWIP grades had the best performance in terms of both mechanical strength and ductility but were not cost effective for the mass scale industrial or automotive application. Finally hot-formed steels (HF) were talked about which showed excellent hardenability and were specifically used to make parts with complex geometries by hot forming after suitable austenization. An extension of this type of steel namely Post forming heat treated steel (PFHT) was also included in the final discussion. The common treatments offered post forming to these types were water and air tempering. The objectives of such type of steels were to maintain the desired geometry of the part during and following the heat treatment. Despite the results obtained, driven by the automobile industry, the steel industry has continued the ongoing development of AHSS steels. The driving forces behind such developments were certainly reduced specific weight, increased strength to weight ratio and/or

elongation at rupture.

Momeni et al. (2008) [18] investigated the effects of various annealing temperature along with role of pre-straining and baking temperature on bake hardenability of low carbon steels. The material used for this investigation was of the following composition as is listed in Table 2.2.

Table 2.2: Chemical composition of investigated steel [18].

Element	**C**	**Si**	**Mn**	**P**	**S**	**Cr**	**Mo**	**Ni**	**Cu**	**Al**
Weight,%	0.034	0.004	0.022	0.004	0.013	0.009	0.002	0.031	0.031	0.041

Annealing treatment were performed at 680 ^{o}C, 730 ^{o}C and 780 ^{o}C for soaking periods of 10, 20 and 30 mins under different cooling media; Furnace, Air and Water. The optimum annealing cycle was observed for samples treated at 780 ^{o}C when soaked for 30 mins and water quenched which enhanced the cementite breaking down rate at higher temperature and time thus providing more free solute carbon atoms. The authors also observed that higher the cooling rate lesser was the time available for long range carbon diffusion for formation of cementite, thus leaving most of the carbon in the entire solvent matrix as free solute atoms. More the available carbon solute atoms better would be the interaction with dislocations generated during pre-straining thereby improved strengthening effect would be seen post baking treatment. For checking this hypothesis, the authors then conducted tensile straining of samples from the optimized annealing process (780 ℃; 30 mins) which were pre-strained to 4%, 6% and 8% followed by performing baking operation at 150 ℃, 180 ℃ and 210 ℃ for 20 mins. The effect of pre-straining values and different baking temperatures on the investigated steel is seen in Figure 2.5.

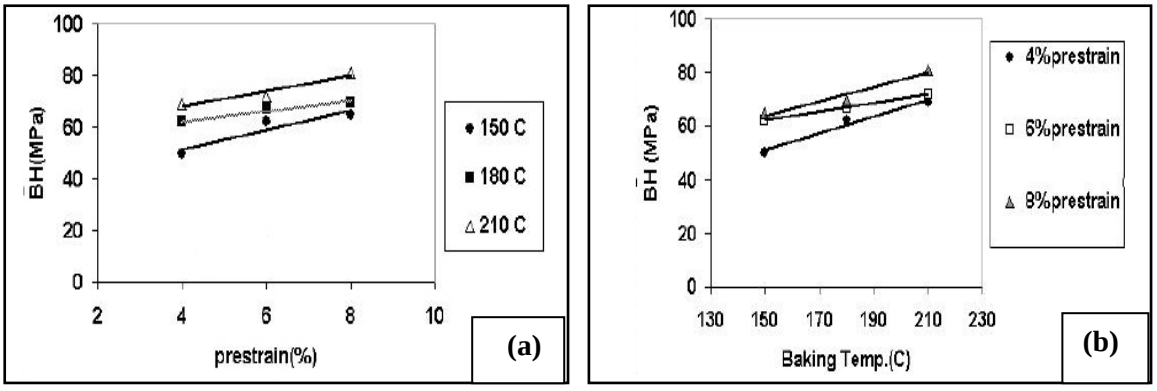

Figure 2.5: (a) Effect of pre-straing on BH; (b) Effect of Baking temperature on BH [18].

The authors observed that with increasing pre-strain values the BH effect improved while similar results were also noticable with baking temperature. They analyzed that dislocation are generated during pre-straining stage. Increasing pre-strain values thereby resulted in increased number of dislocations in the low carbon steel. Hence, more number of available carbon solute atoms interacted with the dislocations thus improving the bake hardenability. It was also observed that rate of diffssion of these solute atoms depended on the temperature of baking operation. Thus increasing baking temperature led to more diffusion of carbon solute atoms to these dislocation sites resulting in improved pinning action hence an increase in BH was again seen. Thus the authors concluded that increase in annealing temperature and time along with increasing pre-strain and baking temperature improved the bake hardenability of low carbon steels used for automotive applications.

Zhang et al. (2008) [21] studied the bake hardening behaviour in TRIP and DP steels under varying pre-straining values. The chemical composition of the experimental steel was C 0.11; Mn 1.67; Si 1.19 (% by wt). Samples processed by TRIP process underwent annealing at 780 ℃ for 300 seconds, which was further austempered at 400 ℃ for 300 seconds and finally air cooled to obtain a primary ferrite matrix surrounded by islands of bainite and some retained austenite. The DP microstructure of ferrite and martensite was obtained by isothermal annealing at 780 ^{o}C for 300 seconds and then water quenched to room temperature. The annealing temperature ensured 60% volume fraction of ferrite in each process. Tensile and pre-straining of specimens processed above were done on CMT 5305 type tensile tester. As-processed initial microstructure was observed using SEM (Hitachi S570) and OM (Nikon EPIPHOT300). Six samples each of TRIP and DP processed steel were pres-strained at 0%, 2%, 4%, 8% and 10% to observe the bake hardening response when baked at 170 ℃ for 20 minutes. The authors observed a BH peak of around 70 MPa at 2% pre-strain for TRIP steel which gradually dropped to sub zero values at 10%, while DP observed highest BH value at 0% state while it showed a continual decrease in BH at higher pre-strain values. The higher martensite volume fraction (40%) in DP steels was deemed responsible for severe plastic flow inhibition of ferrite at higher pre-straining values. This resulted in high amount of internal stress generation within the ferrite matrix which eventually got relaxed due to baking at low temperature of 170 ℃ for 20 mins, hence the fall in BH effect was realized. Due to lesser work hardenability and lesser martensite volume fraction of TRIP steels over DP steels the amount of stress relaxation was also lesser thereby better BH was noticed. The authors also investigated the loss in ductility with increasing pre-strain, while

TRIP steels showed (Uniform Elongation) UEl of 16% at maximum pre-strain of 10% the same for DP steel was noted to be below 5%. The better ductility response in TRIP processed specimens was explained due to the transformation of austenite to martensite on applying deformation (pre-straining) which increased the local hardness of the transformed zone. The deformation would then be lowly transferred to other nearby zones thus delaying the necking phenomena. The authors finally concluded that pre-straining had a major role in the bake hardening behaviour of DP and TRIP steels. However, due to difference in second phase microstructure TRIP steels showed better BH behaviour than DP steels.

Timokhina et al. (2010) [30] have studied the effect of carbon on the aging behaviour of different phases in multiphase DP and TRIP steels using a unique combination of TEM and APT (Atomic Probe Tomography). Table 2.3 shows the composition of the investigated steel while standard cold rolling and inter-critical annealing (ICA) at 780 ℃ for 180 s was performed. DP steel was followed by quenching while the TRIP steel was cooled to 400 ℃ and held for 300 s and finally quenched.

Table 2.3: Composition of studied steels [30].

Steel		C	Si	Mn	Al	Cu	Cr	Ti
TRIP	wt%	0.12	1.77	1.39	0.031	0.005	0.02	0.003
	at%	0.55	3.44	1.38	0.062	0.004	0.02	0.004
DP	wt%	0.036	1.065	1.08	0.018	0.004	0.083	-
	at%	0.17	2.09	1.08	0.037	0.0035	0.088	-

Tensile samples were prepared for each steel and pre-strained in tension to 5% and then baked at 175 ℃ for 30 min. Mechanical properties at room temperature were established by INSTRON tensile testing machine with specimens of dimension 25mm X 6mm X 2mm over a crosshead speed of 0.5 mm/min. The results are tabulated below in Table 2.4.

Table 2.4: Mechanical properties of steels [30].

Steel		UTS, (MPa)	YS, (MPa)	Total El, (%)	Uniform El, (%)	Average BH Response, (MPa)
TRIP	IA	795±10	520±10	31±2	27±3	60±3
	PS/BH	810±8	735±5	27±2	21±3	
DP	IA	633±10	425±10	24±3	23±2	80±2
	PS/BH	678±7	676±7	17±3	14±2	

Optical microscopy and image analysis was done to estimate volume fraction of ferrite, while XRD was performed to evaluate volume fraction of retained austenite (R.A). Microstructure characterization was done using TEM. An average dislocation density was calculated using TEM study and results of which are compiled in Table 2.5. Further selected samples were nital etched (2%) and particle analysis was done using EDXS (Energy Dispersive X-ray Spectroscopy). Finally APT analysis was conducted to study rearrangement of carbon (in martensite) after PS-BH treatment. The authors observed presence of 75 ± 5 % polygonal ferrite (PF) , 15 ± 4 % martensite (M) for DP against 70 ± 3 % for PF and 20 ± 3 % R.A that of TRIP steel.

Table 2.5: Dislocation density of PF & M [30].

	DP			TRIP	
	As-rec		PS/BH	As-rec	PS/BH
	average	PF/M interface	average	average	average
Dislocation Density, $x10^{14}m^{-2}$	0.96±0.04	5±0.8	2.4±0.09	1.75±0.09	2.7±0.05

Figures from the above optical microscopy and TEM analysis are shown in Figure 2.6.

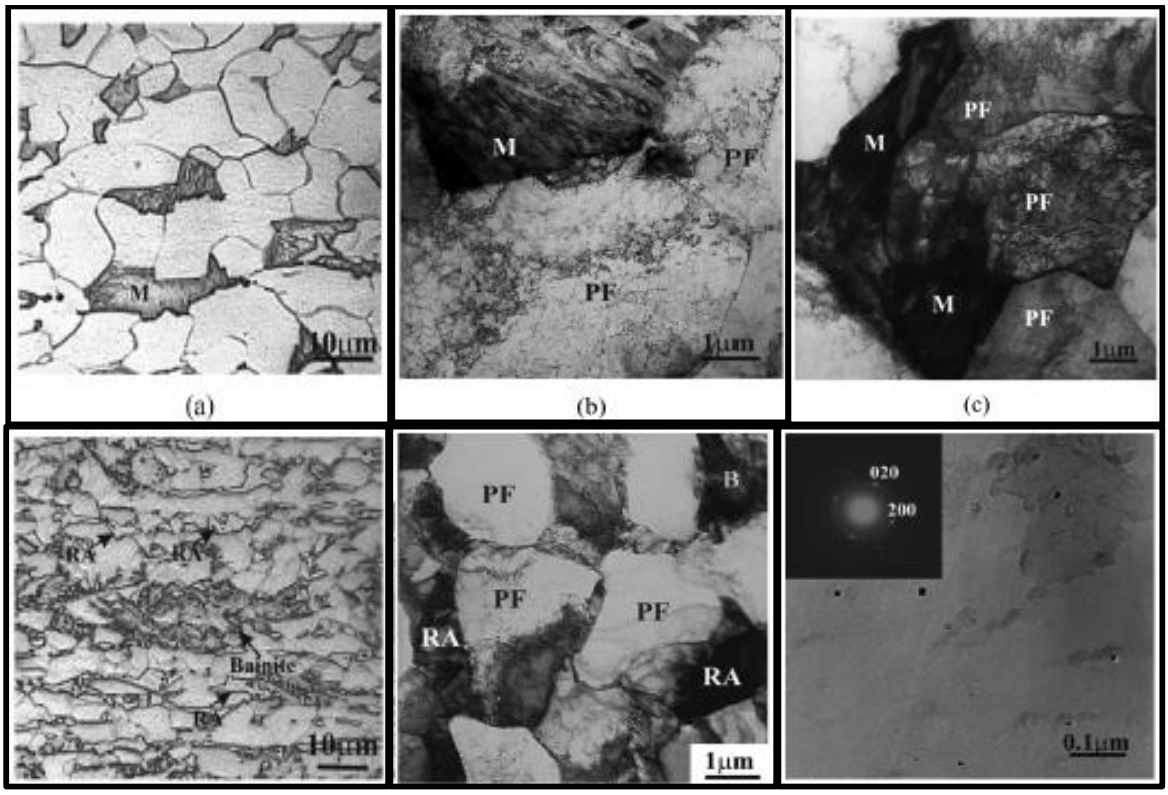

Figure 2.6: Microstructure of DP steel: (a) optical micrograph, general view after ICA, (b) TEM micrograph, post ICA, (c) local increase in dislocation density of ferrite near martensite, (d), (e), (f) corresponding figures for TRIP steel [30].

Since BH behaviour of the DP steel is controlled by the concentration of interstitial carbon in ferrite to pin the dislocations, it was necessary to measure the solute redistribution in the various phases using APT. While all the atom maps of martensite crystals in the DP steel after ICA had uniform redistribution of carbon, after PS/BH, the authors found segregation of carbon to linear features, which were believed to be dislocations in ferrite of DP steel. APT also confirmed formation of rod like carbides in martensite after PS/BH. Similarly carbon atom maps for TRIP steel after PS/BH showed segregation of carbon to particular atomic planes within the sample volume. With these observations the authors were able to conclude that BH in case of DP steels was a consequence of the mobile dislocations pilling up near the ferrite/martensite interface within the ferrite phase due to the volume expansion accompanying the austenite to martensite transformation during quenching. In case of TRIP steels, BH was defined as formation of dislocation cell structure in ferrite and high carbon content of ferrite. This definition was associated with the additional effects of austenite twinning during pre-straining which increased the number of dislocations in ferrite. Thus it was also established that BH phenomena was much more pronounced in DP than in TRIP steels because of carbon segregation to dislocations within ferrite.

Chiang et al. (2011) [23] investigated the effects of soaking temperature, slow cooling rates and rapid cooling starting temperature conditions during continuous annealing process on the bake hardening behaviour of Ultra Low Carbon bake hardening steels (ULC-BH). The chemical composition of the starting material consisted of 0.0021% C, 0.008% Nb and some Ti and Mn additions to the solid solution. Samples collected from hot rolled conditions of continuous production lines were cold rolled to 77 % and given a final thickness of 0.7mm Annealing process were performed on tensile samples of 75 X 22 mm dimensions in an environment of 7 % H_2 & 93 % N_2 (by vol.).

Table 2.6: Annealing conditions [23].

	Annealing temperature	Slow cooling	Rapid cooling	Quenching
No.1	TA1, TA2, TA3, TA4		GJ to R.T.	
No.2	TA2	Rsc1, Rsc2, Rsc3	GJ to R.T.	
No.3	TA2	Rsc3	Trc1~Trc5	GJ to R.T.

Four samples were annealed within a temperature range of 700-900 ^{o}C (T_{A1}; T_{A2}; T_{A3}; T_{A4}) and were gas-jet quenched to room temperature. The entire summary of the annealing processes followed to observe the annealing process parameters on BH is presented in Table 2.6. Rapid quenching performed had cooling rates exceeding 100 ℃/s thus preventing formation of any

carbides and resulted in super saturated solute carbon concentration in every annealing condition. Bake hardening test were performed at 170 ℃ for 20 mins. OM and Internal Friction Measurement (IFM) was used to study the influence of grain size and solute carbon on BH while tensile testing was done to evaluate yield stress variation with annealing temperature.

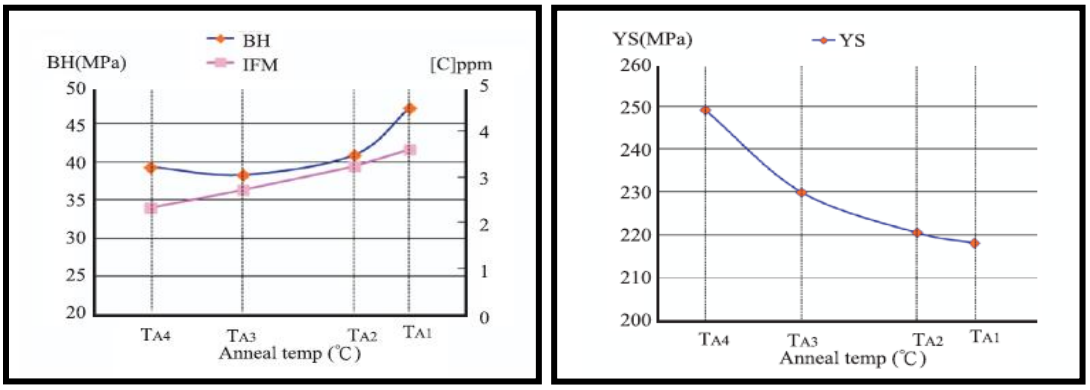

Figure 2.7: (a) BH and solute carbon variation with annealing temperature, b) Yield Stress variation with annealing temperature [23].

The authors observed the effect of soaking temperatures (T_{A1}; T_{A2}; T_{A3}; TA4) and rapid quenching on the BH response for 77 % cold rolled processed ULC-BH steel. The results are shown above in Figure 2.7. Higher soaking temperature ensured higher amount of solute carbon thus resulting in improved BH behaviour. Next the authors observed the effect of slow and rapid cooling rates on the BH behaviour. Samples annealed within temperature range of T_{A2}-T_{A4} were slow cooled at different cooling rates (all < 20 ℃/s) while a sample annealed at T_{A2} was quenched by gas-jet technique to evaluate rapid cooling response.

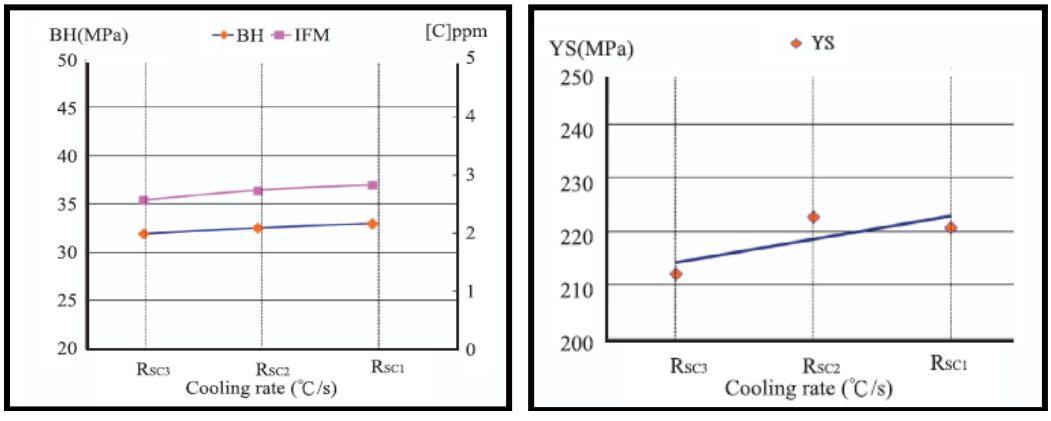

Figure 2.8: (a) BH and solute carbon variation with different slow cooling rates; b) Yield Stress variation with different slow cooling rates [23].

Figure 2.8 also shows increasing trend for both BH and carbon solute with increasing (slow) cooling rates. The variation for rapid cooling rates is shown in Figure 2.9. From Figure 2.9 it became evident that rapid cooling starting temperature did not much influence either the BH or the carbon solute concentration (ppm).

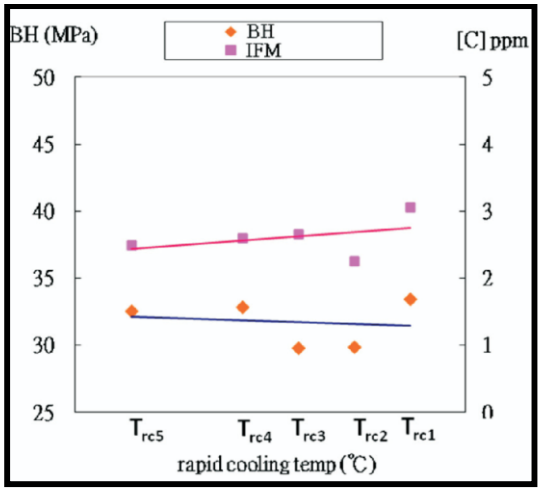

Figure 2.9: BH and solute carbon variation with different rapid cooling rates [23].

The authors thus vehemently concluded that increasing soaking temperature led to increased dissolution of carbides which eventually resulted in higher solute carbon concentration in the solid solution. Another critical observation was that higher (slow) cooling rates inhibited re-precipitation of carbides since it leaves lesser time for the solute carbon to diffuse and form a super saturated carbon concentration in the matrix. Hence rise in BH was noticed with increasing cooling rates due to higher availability of solute carbon.

Kadkodharpur et al. (2011) [31] provided a detailed analysis of the microstructure and failure mechanism of dual phase steel with respect to different strain levels. A commercial grade DP800 steel was used for the investigation which was galvannealed. Tensile samples were cut along rolling direction of the received sheet. Analysis of the process of void nucleation, growth and coalescence were done by performing interrupted tensile test to different engineering strains of ε = 0.12 and ε = 0.17. SEM analysis of deformed specimens was carried out to study the damage accumulated along the gauge length after uni-axial tensile testing. The authors observed that the failure mechanism was influenced broadly by three parameters which were; (i) large (>4μm) martensite phase, (ii) medium sized ceramic inclusion (1-2 μm), (iii) small carbide particles. However, the chief factor controlling damage mechanism remained martensite size. They found that lesser amount of smaller sized martensite showed diffused necking while higher amount of it

involved failure at observed strain values. Further, SEM analysis revealed that void nucleation in dual phase steel occurred primarily at ferrite grain boundaries where it shared long boundaries with harder martensite. Typical strain distribution mismatch was seen as the sole reason for this phenomena, while void initiation was observed between closely spaced martensite grains. It was concluded that martensite morphology and distribution had a crucial role to play in deciding the failure mechanism in DP steels as it affected the damage accumulation capability significantly. The authors also proposed a model based on experimental observations and simulations to predict the failure mechanism in DP steels. They concluded that microstructural in-homogeneity at the interface of ferrite and martensite grains favoured localized deformation patterns thus influencing the failure mechanism profoundly.

Ghadbeigi et al. (2013) [32] studied local deformation and damage mechanism for a commercial DP600 steel using in-situ tensile testing conditions inside a SEM in combination with DIC. Two different gauge geometries were prepared to evaluate the damage evolution processes during tensile testing upto failure. Strain distribution measurements were done for both ferrite and martensite to identify particular damage mechanism. According to the strain maps given through FEM simulation it was seen that, large plastic deformation of the value of 4.5 were recorded in ferrite phase along with severe localized deformation and slip band formation. DIC results also showed martensite plastic strain of 0.9 along the phase boundaries. The authors observed that the martensite failure predominantly occurred viz. micro-crack initiation at the boundaries with ferrite followed by crack propagation towards the centre of the islands. Although the ferrite-martensite interface remained strong and cohesive it was concluded that localized damage within the ferrite matrix adjacent to the interface occurred primarily by sub-micron void formation only. This was contrary to earlier results of interface separation along the phase boundary or within the ferrite grains itself due to localized damages.

Cora and Koc (2014) [7] provided an overview for the world auto industry by reviewing the benefits and problems encountered in the development and implementation of high strength steels. With current scale of improvement programs carried worldwide the authors argued that most of the mild steel applications in current vehicle designs would be replaced by ultra/advanced high strength steels (U/AHSS). AHSS grades were designed to achieve unique material and mechanical properties.

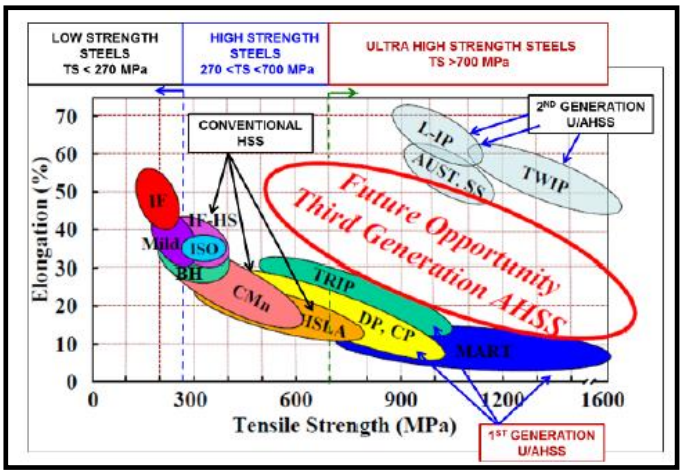

Figure 2.10: Conventional, current and prospective automotive steels and their corresponding elongations and strengths [7].

Their chemical compositions were carefully selected and multiphase microstructures were controlled through precise heating and cooling processes so that desired strength, ductility, toughness, and fatigue properties were obtained. The first, second and third generation U/AHSS materials as well as conventional high strength steels are shown in Figure 2.10 which was also referred as "*banana curve"*. As it can be inferred from the Figure 2.10 that in first generation AHSS, the higher yield strength the lower elongation was experienced. To overcome this problem second generation AHSS materials with high strength and superior elongation was developed. Nonetheless, the application of second generation AHSS may not be widespread due to high cost of alloying elements (e.g. Ni, Mn). A cost-effective alternative to weight reduction was possible through the development and use of third generation AHSS materials which had ultra-high strength (above 1200 MPa in UTS) along with elevated ductility (at least 30 %). Increasing safety, fuel efficiency, and reducing tailpipe emission regulations were always needed to be addressed by auto industry in a cost-effective manner. Although materials such aluminum, magnesium, carbon-reinforced composites had higher potential from mass reduction point of view, AHSS had superior features over its rivals. Some of the reaping benefits that were synonymous with AHSS grades were its availability and cost, environmental effects (lesser greenhouse gas emissions during its production, use and disposal), crash energy absorption and the much obvious higher formability. However, along with the noteworthy benefits certain challenges propped up with the utilization of U/AHSS materials. The first was increased die wear, as the strength of AHSS sheets were higher than conventional types, higher forming forces were required that lead to increased wear at contact surfaces and deteriorated the surface quality

of the products. Next big issue was that of spring-back phenomena which occurred during elastic recovery after forming (bending etc). Welding of AHSS parts differed from mild steel parts as higher carbon and alloying elements (such as C, Al, Si, Mn) made AHSS more sensitive to the welding. In addition, with rapid heating and cooling during the welding process, steel chemistry was highly affected so were the microstructure, mechanical properties, and fatigue life of the AHSS material. Therefore tight control of welding parameters was required. Edge cracking was also one of the roadblocks of U/AHSS implementation, with smaller gages that may be used with AHSS blanks for light-weighting purposes, stresses increased in edges as well as over the weld region and potentially shorten the fatigue life and durability of auto-body structures. Some of the challenges discussed were addressed in modern times like for die wear a suitable powder metallurgical vapour deposition technique over the blank specimens was implemented. Similarly improved welding techniques like MAG welding enhanced the weld-ability to certain extents, while local softening technology based on induction and laser heating principles were employed to improve the fracture (edge cracking) problems. Thus the authors were able to conclude that with increased knowledge on weld-ability and joining, prediction and controlling springback and fracture, increased fatigue performance would eventually lead to exploitation of AHSS by other industries.

Ramazani et al. (2014) [22] conducted experiments to quantify the effect of pre-straining, holding time and aging temperature on the bake hardening (BH) behaviour of multiphase microstructures. Two industrially processed hot rolled DP600 and cold rolled TP700 steel were investigated by the authors. The chemical composition of both the steels is given in Table 2.7.

Table: 2.7 Chemical compositions of the investigated DP600 and TRIP700 steels in (wt.%). tshows the thickness of the steel sheets (in mm) [22].

Steel	C	Si	Mn	P	Cr	Al	N	t (mm)
DP600	0.076	0.06	1.02	0.030	0.44	0.03	0.006	2.0
TRIP700	0.221	0.09	1.68	0.012	0.02	1.49	0.002	0.9

The light optical micrographs revealed DP600 steel consisted of 20 % martensite particles embedded in a ferrite matrix whereas the microstructure of TRIP700 steel consisted of 70 % ferrite, 15 % bainite and 15 % retained austenite. Firstly, tensile samples were cut from DP600 and TRIP700 sheet, in a direction parallel to the rolling direction and fracture tests were conducted at a cross head velocity of 4 mm/ min. For every condition, three parallel tests were

carried out. Pre-strain values from 0−10 % with a subsequent BH annealing cycle within temperature range of 60–220 ℃ for 1 to 10,000 minutes were conducted to quantify the parameters affecting BH properties in the two steels. It was observed from the experiments that under condition of 170 ℃ / 20 min baking, with increase in the level of pre-straining both the steels started showing discontinuous yielding (see Fig. 2.10a), while, the effect was more pronounced at higher degrees of pre-straining. Also a rise in yield and ultimate strength was observed with higher degree of pre-straining. The strengthening effect improved with increasing BH temperature (because of increase in solute atom diffusion). BH values were then compared with BH^* (BH value calculated from true stress-strain diagram) at different bake hardening temperatures (60 ℃, 170 ℃ and 220 ℃) and the authors noticed that DP steel reached highest BH^* value at 2 % pre-straining level while for TRIP steel highest BH^* value was observed at 5 % pre-straining level.

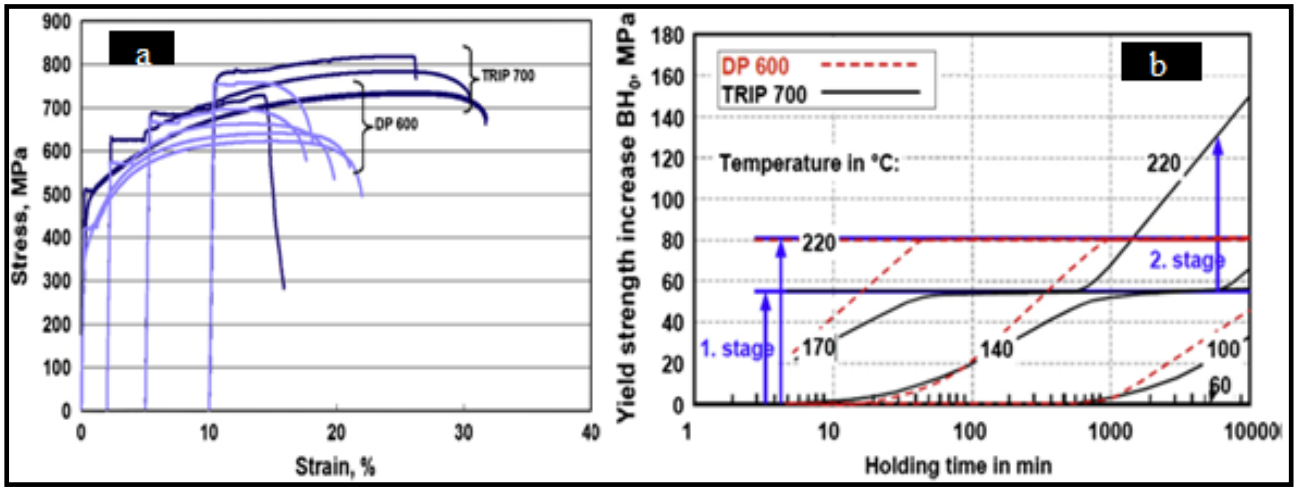

Figure 2.11: (a) Stress-strain curves of DP600 and TRIP700 in the BH condition 170 ℃/20 min for various degrees of pre-straining (b) Comparison of BH0 values in dependency of the BH time and temperature for DP600 and TRIP700 steels [22].

Thereafter, the effect of aging time (holding time) and temperature was studied on BH behaviour of both the steels (in the absence of pre-straining). It was observed from Figure 2.11 (b) that, with higher BH temperatures the holding time required decreased. The 60 ℃ treatment hardly showed BH effects so it was inferred by the authors that these steels were highly stable against room temperature ageing. With higher BH temperatures of 140 ℃ a first stage strengthening plateau was reached at around 80 MPa for DP600 and about50 MPa for TRIP700 grade. With the 220 ℃ annealing BH values already started out from the plateau above 80 MPa, but a second strength increase up to 150 MPa was noted for TRIP700 steel for holding times longer than 500

min. Further, this second strength level was reached for all BH treatments when pre-strains were of 2% or 5%.

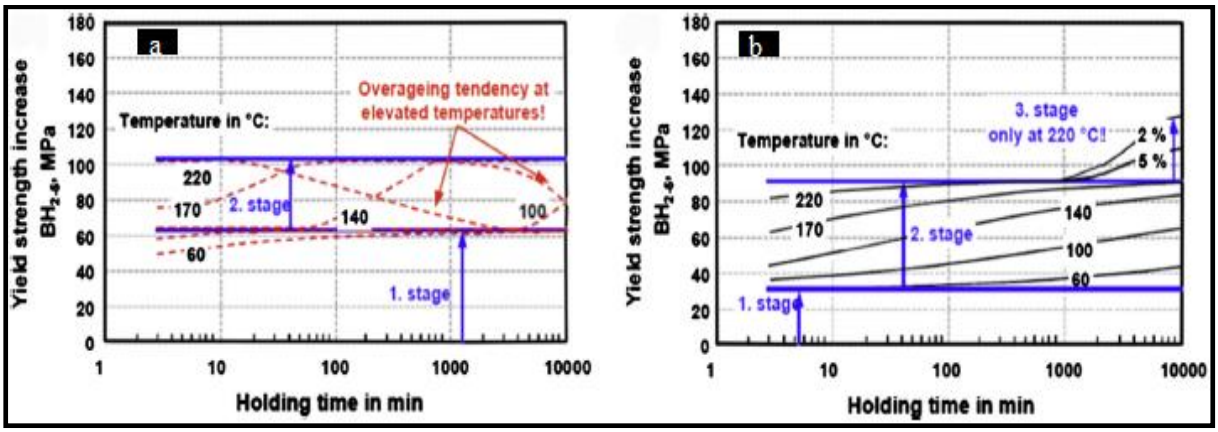

Figure 2.12: Comparison of BH values in dependency of the BH time and temperature for the (a) DP600 and (b) TRIP700 steel [22].

Figure 2.12 (a) and (b) show the effect of holding temperature and time on the BH values. The authors observed that, with increasing pre-strain values and higher BH temperatures above 170 ℃ DP600 steel showed a decrease in BH values again which occured due to overaging effect. In contrast, TRIP700 steel kept a constant BH value and even displayed a tendency towards a third step of ageing under BH conditions of 220 ℃ and long holding time. Furthermore, a significant decrease of retained austenite from 17% to 4% was observed at 220 ℃ (BH Temperature) with holding times longer than 100 min. However, for 170 ℃, the reduction in retained austenite due to BH effect was rather small (reduced from 17% to 15%) and that too at long holding times. With lower BH temperatures, no decay of the residual austenite could be found. The 3rd stage of strength increase in TRIP for 220 ℃ correlated with the austenite destabilization. From the above results it was concluded by the authors that the retained austenite seemed to be quite insensitive to industrial paint baking processes (generally occurs at 170 ℃ and for 20min). BH treatments at higher temperatures supported diffusion so higher strengthening was achievable. Same was true for holding time, with increasing holding times up to10,000 min the observed steels displayed two steps of yield strength increase for BH_0. For the BH_{2-5}values, DP600 steel showed over-aging effect. In contrast, TRIP700 steel revealed some tendency towards a third step of ageing with higher BH values at 220 ℃ without any overaging.

Cao et al. (2015) [19] have studied the effect of temperature and strain rate on the mechanical behaviour of dual phase (DP) steels. Mechanical properties were investigated by uniaxial tensile

tests covering applicable temperatures (−60 ℃ to 100 ℃) and strain rates (1×10^{-4} to $1 \times 10^{2} s^{-1}$) experienced during automotive crash situations. Commercial dual phase steel (DP 800) supplied by Swedish Steel AB (SSAB) in the form of rolled sheet with a thickness of 2 mm was investigated. Table 2.8 represents the compositional details of the investigated steel specimen.

Table 2.8: Chemical composition of the steel studied (wt.%) [19].

Elem.	C	Si	Mn	P	S	Cr	Ni	Mo	Cu
Comp.	0.111	0.2	1.4	0.0091	0.0038	0.03	0.05	0.010	0.01
Elem.	V	Al	Sn	Ti	As	B	Nb	Co	N
Comp.	0.0063	0.0424	0.0029	0.0024	0.0016	0.0003	0.0136	0.015	0.0086

The microstructure consisted of ferrite (F) grains and martensite (M) islands together with some percentage of retained austenite (A). Deformation to 3.5% at room temperature at a strain rate of $10^{-4} s^{-1}$ and subsequent heat treatment at 180 ℃ for 30 min in air was used to simulate pressing of plates followed by the paint-bake cycle involved in the manufacturing process of automobile body structures. Tensile specimens were machined with the tensile direction parallel to the original rolling direction. The strain rate was varied by more than 6 orders of magnitude, from 1×10^{-4} to $1 \times 10^{2} s^{-1}$. The testing temperature ranged from −60 ℃ to +100 ℃. High strain rate testing (upto $10^{2}\ s^{-1}$) were performed at room temperature by using Instron VHS 8800. Results from the above tests are shown below in Figure 2.13.

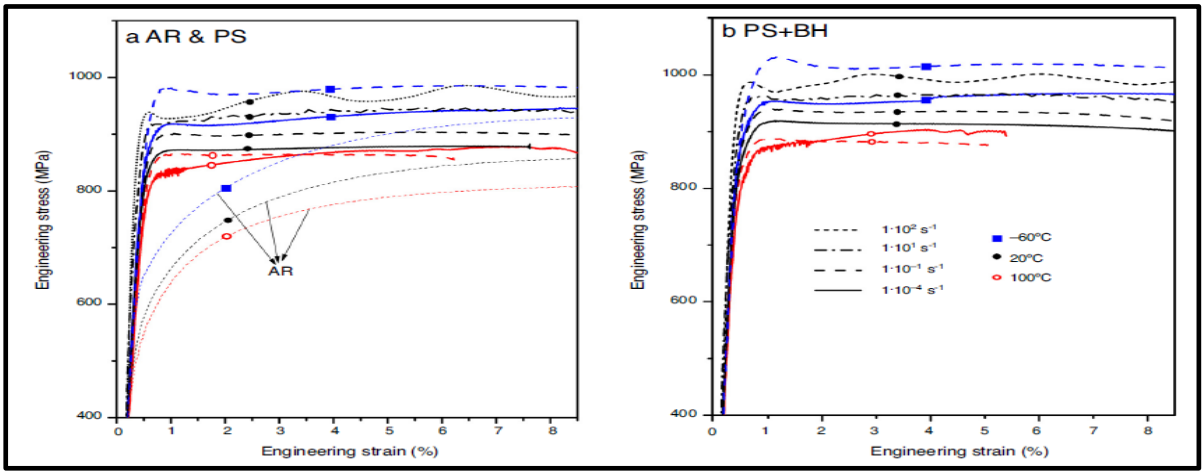

Figure 2.13: Engineering stress–strain relationships for different pre-treatments: (a) as-received (AR) and pre-strained (PS) respectively; (b) pre-strained (PS) + bake hardened (BH) [19].

Based on the results from uni-axial tensile tests the authors observed that pre-straining and superimposed bake-hardening led to increased strength, decreased strain hardening, and smaller ductility at all temperatures and strain rates. In addition, pre-straining lead to yield phenomena through strain aging which was further enhanced by subsequent bake-hardening. An increase in yield and ultimate tensile strengths was generally observed when the strain rate was increased or when the temperature decreased as seen in Figure 2.14 (a) & (b) below.

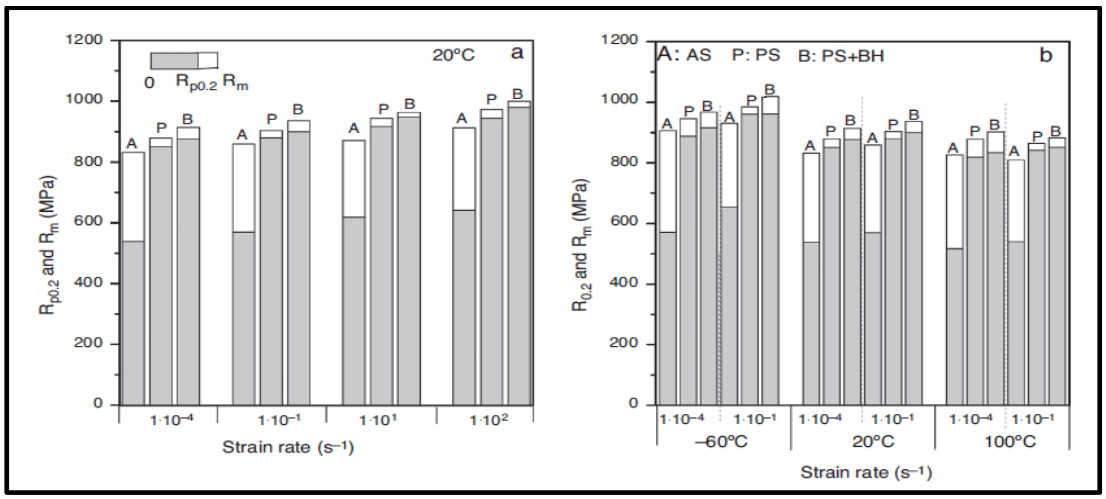

Figure 2.14: Ultimate tensile strength and yield strength of the steel studied [19].

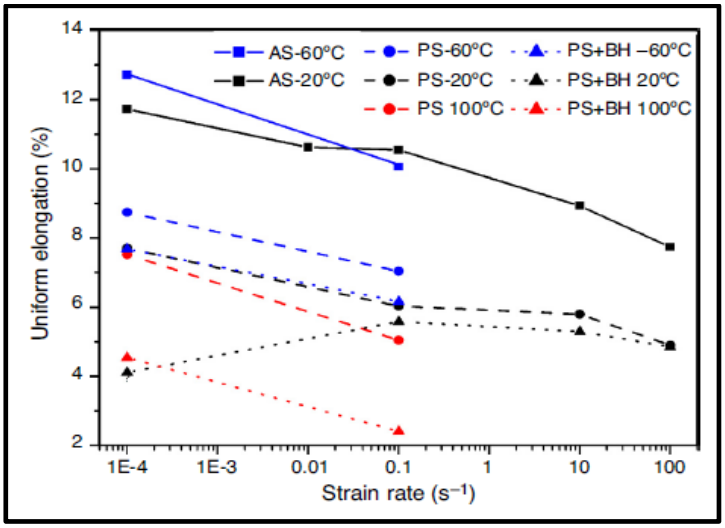

Figure 2.15: Uniform elongation as a function of strain rate and temperature [19].

From Figure 2.15 the authors observed that for almost all conditions of pre-treatments, an increase in strain rate lowered the uniform elongation. The authors finally concluded that, macroscopically the hardening could be interpreted as a two phase behaviour with elastically stressed inclusions of martensite in a plastic ferritic matrix.

Concepcion et al (2015) [33] studied the effect of carbon content on microstructure and mechanical properties of DP steels. To achieve the objective, bars of four different conventional carbon steels with nominal carbon content between 0.05 and 0.38wt% were used. Table 2.9 depicts the chemical composition of analyzed material along with their respective critical temperatures measured by Optical Emission Spectrometry (OES) and Linear Thermal Dilatometry (LTD) using heating rate of 15 ℃/min, respectively.

Table 2.9: Chemical composition of analyzed material (wt%) and critical temperatures (℃) [33].

Material	C	Mn	Si	P	S	Ac_1	Ac_3
S1	0.08	0.77	0.21	0.017	0.012	732	873
S2	0.11	0.69	0.21	0.025	0.021	733	865
S3	0.20	1.45	0.40	0.015	0.028	720	776
S4	0.38	1.43	0.37	0.024	0.033	736	805

Samples were heat treated at different inter-critical temperatures to obtain DP steel grades with varying martensite (M) content. Figure 1 below depicts the heat treatment schematically, with a holding time of 30 minutes, followed by water quenching. Table 2.10 also shows the different temperatures chosen to cover a wide range of M content.

Table 2.10: Intercritical temperatures applied on HT for DP [33].

Identification	%C (wt%)	Intercritical temperatures (°C)
S1	0.05	795; 810; 820; 840
S2	0.10	740; 750; 760; 770; 780; 790; 800; 820; 840; 860; 880
S3	0.20	740; 760; 780; 800; 820
S4	0.35	740; 750

Microstructural analysis was done using Light Microscope that yielded ferritic-martensitic microstructure. Martensite was quantified by quantitative metallography test (ASTM E562) with volume fraction varying between 23 – 96 % whose fraction increased with increasing inter-critical temperature as shown in Figure 2.16. Mechanical properties determining Vickers microhardness (HV_1) and tensile test were conducted to obtain yield strength ($Rp_{0.2}$), Ultimate tensile strength (R_m) and elongation (A %). Fracture surfaces were observed by optical stereomicroscopy (SLM). In all cases, the authors observed an increase in HV_1, $Rp_{0.2}$and R_m with increasing martensite, consistent with an increase in inert-critical temperature. Figure 2.17

(a–e) shows the relationship between the various mechanical properties as a function of martensite percentage.

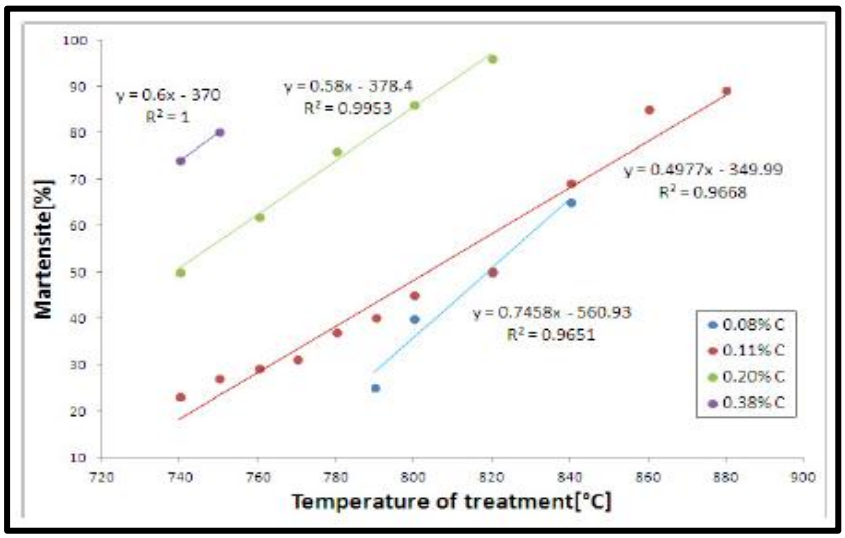

Figure 2.16: Martensite percentage as function of heat treatment temperature for each material [33].

Thus the authors observed that hardness too increased with M, associated to an increase of the carbon content in martensitic phase while A% decreased with increasing C. They finally postulated that, the best combination of properties for DP steels was possible at about 50 % of martensite fraction and in this case it was to be achieved for S2 steel (0.10 % C) with values represented in Table 2.11.

Table 2.11: Mechanical properties of S2-50 sample [33].

Sample	**HV1**	**Rp0.2 [MPa]**	**Rm [MPa]**	**Rm/Rp0.2**	**A [%]**
S 2-50	250 ± 6	435	839	1.93	16.1

Thus the influence of C content on the microstructure and its associated mechanical properties was investigated successfully.

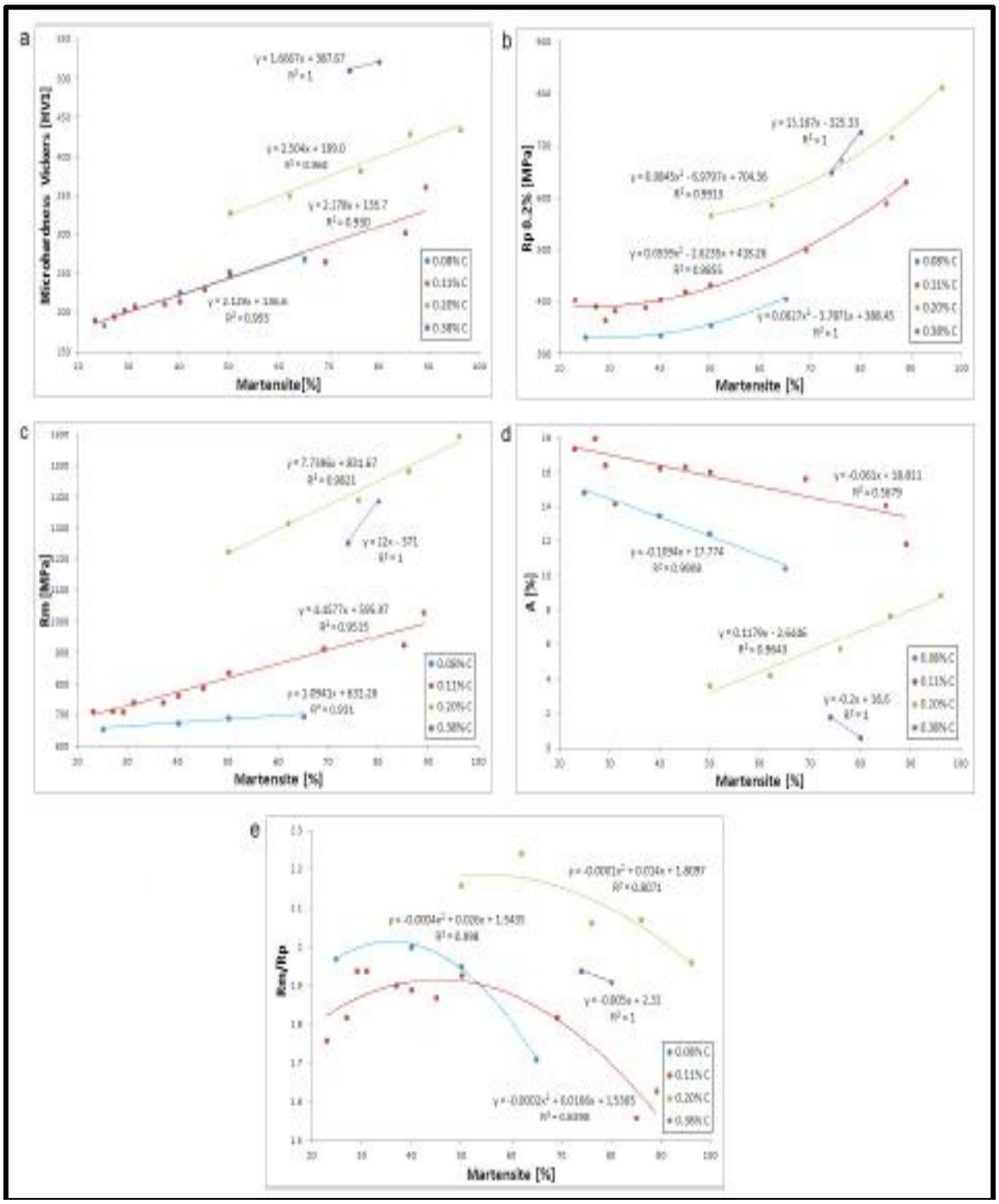

Figure 2.17: Mechanical properties of DP vs M for different C: (a) HV; (b) $Rp_{0.2}$; (c) R_m; (d) A%; (e) SR [33] .

Lai et al. (2015) [34] studied the effects of martensite volume fraction (V_m) on the damage and fracture behaviour of DP steels. The steel grade used in this work consisted of 0.1 % C and 3.4 % Mn by weight. The DP microstrucuture was obtained by quenching of hot rolled ingot from 900 ^{o}C which was followed by cold rolling to 1 mm thickness with 70% reduction. Further tempering

of this as-received material was done which was finally followed by inter-critical annealing at 700 ^{o}C for duration ranging from 20 mins to 6 hours. Standard metallographic techniques were used to prepare samples for SEM analysis while quantitative image analysis for calculating phase fraction was done viz Image J. Nano Indentation test were performed to locally probe martensite hardness. Mechanical properties were evaluated with the help of tensile testing machine with standard dog bone tensile samples of 25 mm gauge length and keeping a standard strain rate of 0.001/s. DP microstructure with 15 %, 19 %, 28 % and 37 % V_m were obtained by annealing at 700 ℃ for different soaking period. The tensile properties of the different annealing conditions are listed in Table 2.12 Thus it was observed that tensile strength increased with increasing V_m but at the cost of uniform elongation and true strain. This was mostly attributed to the progressive elasto-plastic transititon with higher $V_{m.}$ The authors also observed that V_m had a significant effect on the fracture behaviour of the observed specimens.

Table 2.12: Mechanical properties of DP steel involving different V_m [34].

Samples	Tensile strength (MPa)	Uniform elongation	Fracture strain
QT-700-15%	691 ± 4	0.164 ± 0.002	1.06 ± 0.06
QT-700-19%	765.5 ± 13	0.143 ± 0.009	0.75 ± 0.11
QT-700-28%	928 ± 25	0.124 ± 0.011	0.4 ± 0.01
QT-700-37%	1058 ± 18	0.116 ± 0.002	0.33 ± 0.02

It was proposed that fracture in DP steels was either due to interface decohesion at ferrite-marteniste boundary or due to micro crack initiation and growth along the martensite islands. It was reported by the authors that micro void initiation was followed by interface decohesion in case of DP microstructure with lesser $V_{m.}$ However, martensite fracture leading to micro void initiation happened with increasing V_m in DP steels. Figure 2.18 also support the observed phenomena under SEM. The authors thus concluded that DP steels mainly showed ductile fracture behaviour at lower V_m, however, cleavage or brittle failure was observed at higher V_m. The interconnectivity of martensite islands with higher V_m resulted in constrained plastic flow of the ferrite matrix by confining the active slip systems.

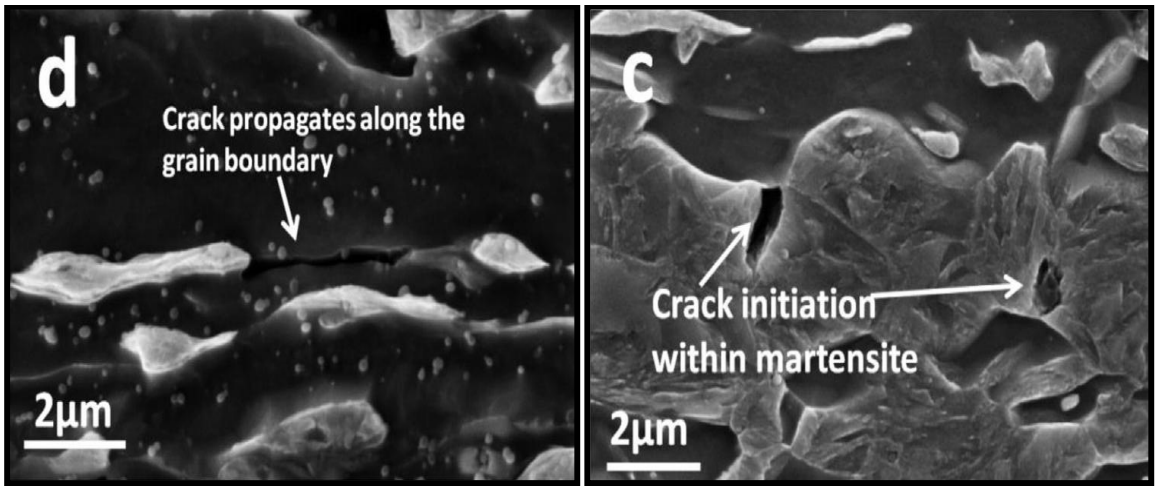

Figure 2.18: SEM image of a) Interface decohesion observed for DP steel with V_m (15%); b) Martensite crack observed for DP steel with V_m (28%) [34].

Thereby, once a martensite islands breaks, a cleavage crack is initiated in the ferrite grains due to severe local stress build up at the crack tip.

2.3. Summary of Literature

- Several authors have focused on AHSS generations and their proper classification techniques while elaborating the benefits of them over conventional steels. Some have even reported the challenges of implementing such grades in modern day industries worldwide and have provided solutions to tackle such issues at large. Special attention has been given to studies concerning processing of DP steels due to their immense applicability in automotive industries. **[4, 7, 13]**.
- Several authors have reported on the role of annealing process parameters on the final free carbon solute content during processing of low carbon steels. Discussions related to the effect of soaking temperature and cooling rates on the final carbon solute content which ultimately influence the final mechanical properties of these steels has been reviewed by many authors **[21, 23, 33]**.
- Some authors have highlighted the effect of pre-straining and bake hardening (BH) treatment on DP and TRIP steels which is also a very common finishing operation in the manufacturing of automobile bodies and components. Reports on strain and age hardening, along with BH values for such steels have been talked at length and the correlation of BH parameters with the overall mechanical properties has been discussed **[19, 20, 22, 30]**.
- Some authors have analyzed the role of second phase volume fraction, size, and distribution on various forms of deformation under uni-axial tensile testing of DP steels. Failure

mechanism have been studied as a function of true strain by some authors while, effect of martensite morphology on the nucleation, initiation and growth of micro-cracks has been studied under in-situ tensile testing conditions by few authors **[31, 32, 34]**.

2.4. Gaps in Literature

- Very limited literature is available to highlight the influence of annealing process parameter (heating rate, and annealing temperature etc.) variations on the bake hardenability of DP steels
- Although several authors have discussed the role of second phase volume fraction, (martensite) morphology, size, and distribution on the mechanical properties of dual phase steels, not much work has been reported of its influence on the BH properties of DP steels.
- The consequences of hardening achieved by baking operation on the final ductility with respect to the martensite spatial distribution in DP steels is an area which has not been examined very distinctly
- The extent of grain boundary damage upon tensile straining of bake hardened samples with respect to different lath martensite and ferrite-martensite interface morphology is another area which has not been thoroughly studied.

Chapter 3

Design of the Study

3.1. General

The purpose of this chapter is to present the detailed design structure of the proposed research work. It exhibits the overall objective of the proposed research methodology, and the experimental procedure to be adopted. It also specifies the machines, equipment, and the software that were needed to meet the designed objective.

3.2. Establishment of the Objective Function

Dual phase (DP) steels consist of a hard second phase (martensite) embedded within a soft-ductile ferrite matrix. This particular combination provides a perfect blend of strength and ductility in these steels. The dual phase microstructure shows continuous yielding behaviour, high work harden-ability, and a low yield to tensile strength ratio. The presence of mobile dislocations as is evident by the continuous yielding phenomena in these steels also offers very decent opportunity for bake hardening (BH) behavior in DP steels. The second phase (martensite) volume fraction, morphology, and spatial distribution are the critical factors which influence the overall mechanical properties viz. yield strength, tensile strength, uniform and total elongation along with bake-hardenability of DP steels. Thus, altering the critical factors can result in significant changes in the final mechanical properties of DP steels. The critical factors are in turn dependent on the various annealing process parameters such as heating rate, soaking temperature, soaking time, cooling regime, and cooling rate. Therefore, tailoring of the second phase's size, distribution, and morphology is possible by controlling the annealing parameters. In the present research work, two different inter-critical annealing processes were employed to obtain dual phase microstructure with distinctively varying martensite spatial distribution and ferrite-martensite ("*lath*") interface morphology. The overall objective of achieving different martensite distribution and morphology was undertaken to evaluate the bake hardening properties achieved in the two annealing processes. To achieve the said objective, annealing simulations were performed in a custom designed and developed annealing simulator. Annealing experiments were conducted on standard tensile specimens (25 mm gauge length as per ASTM standard E-8M) were cut along the rolling direction of the as-received sheet. The annealing atmosphere and cooling medium was a gas mixture of 10 % H_2 and balance N_2. The simulator

consisted of a heating chamber wherein the appropriate soaking temperature was reached. The simulator also consisted of a cold chamber wherein nitrogen quenching (H_2 + N_2 mixture) was performed at the requisite cooling rates to obtain the final dual phase microstructure. The temperature was monitored using K-type thermocouple soldered to the mid-section of a dummy tensile specimen fitted within the movable chamber which nested the specimens.

Several authors have studied the effect of second phase size, distribution, and morphology on the mechanical properties of DP steels [31–35]. However, the impact of second phase size, spatial distribution, and ferrite-martensite interface morphology (under similar volume fraction but different annealing processes) on the bake hardening properties and the resulting final ductility (post baking) in DP steels have not yet been thoroughly investigated. The present work was an attempt to fill this gap. It was observed through the present research that bake hardening properties had an intrinsic relationship with the distribution and morphology of the second phase martensite in DP steels. The present study established and explained the observed differences in BH response of specimens processed under different annealing conditions with their respective second phase (martensite) microstructure variations. This second phase microstructure variation also gave providence in explaining the differences observed in the final ductility of pre-strained and bake hardened specimens.

The objective of the present research work was to study the effect of martensite spatial distribution and ferrite-marteniste interface (lath) morphology on the bake-hardening properties of a dual phase steel grade DP590.

The key issues to be taken up during the research work are as follows:

- To characterize the microstructure of the as-received cold rolled ferrite-pearlite steel sheet using optical microscopy and SEM analysis.
- To anneal the as-received steel under two different processing conditions for obtaining varying martensite spatial distribution and ferrite-martensite interface (lath) morphology. The two different processing conditions were (i) the industrially used conventional CAL process, and (ii) the newly developed mod-CAL process.

  The purpose of performing the two annealing processes was to obtain DP microstructure with similar tensile properties (YS, UTS, TE) but different second phase spatial distribution and lath morphology.
- Evaluation of tensile properties (YS, UTS, TE) of the annealed specimens processed by the two different processing routes viz. CAL and mod-CAL processes.

- Quantitative phase fraction analysis of each phase present in the microstructure with the help of image analyzing software 'ImageJ'. Determining the average grain size distribution of each phase using "analySIS FIVE".
- Further, to observe and study the differences in second phase (marteniste) spatial distribution and ferrite-martensite interface morphology in the post annealed specimens (CAL & mod-CAL processes) using SEM.
- To pre-strain each specimen processed by the two different annealing conditions at values in the range, 1–5 % (in increment of 1 %) before baking them in an oven (*Carbolite Furnace*) at 170 ℃ for 20 minutes.
- To evaluate the tensile properties of the pre-strained and baked specimens obtained from both the annealing processes (viz. CAL and mod-CAL). Thereafter, the specimens which showed the maximum and minimum BH properties (Bake Hardening Index, BHI and Total Elongation, TE) were further investigated. This was done to evaluate the effect of second phase spatial distribution and lath martensite morphology on the resulting BH characteristics. For this, the following steps were adopted:

  (i) SEM micrographs were analyzed to study the role of martensite distribution and lath martensite morphology on the bake hardening properties.

  (ii) Nano-indentation test was conducted to characterize the lath martensite obtained from the two annealing processes (CAL and mod-CAL).

  (iii) Experimental validation of the observed bake hardening characteristics (BHI) in the specimens processed under the two different annealing cycles (CAL and mod-CAL) was done by X-ray diffraction test. It also helped in qualitative estimation of available solute carbon presence in the two heat treated specimens.

  (iv) The deformation mechanism of the pre-strained and bake hardened specimens (CAL and mod-CAL processed) were studied by performing interrupted tensile test. This test also helped in understanding the role of lath morphology on the deformation behaviour for the DP microstructure obtained from the two annealing processes.

3.3. Experimental Procedure

The experimental procedure followed in the present work is described in this section.

3.3.1 Starting Material

The starting material was a low carbon 67 % cold rolled sheet of 0.82 mm thickness. The chemical composition is tabulated in Table 3.1.

Table 3.1 Chemical composition of the as-received steel.

Element	C	Mn	Si	S	P	Al	N	Fe
% wt.	0.074	1.83	0.43	0.002	0.012	0.026	0.0032	Balance

The microstructure of the as-received steel consisted of ferrite and pearlite. Characterization of the as-received steel specimen was done by performing standard metallographic analysis which included grinding, mounting, paper polishing, cloth polishing and etching etc. Nital etchant (solution of 2 % nitric acid in 10 ml ethanol) was prepared to reveal the phases present in the steel by using optical microscopy. Nital helped in etching ferrite phase as white while pearlite was observed as dark brownish/ black when seen under optical microscope.

3.3.2. Determination of Annealing Parameters

After analysing the microstructure of the as-received material, the next step was to determine the annealing process parameters to obtain the two varying DP microstructure using CAL and mod-CAL processes. Annealing parameters like inter-critical temperature range (lower and upper critical temperature of the steel under investigation), heating rates, soaking time periods, and cooling rates to be followed were determined with the help of existing literature [36, 37] and also through further investigations,. The following two subsections cover the details of annealing processes which were employed to obtain different DP microstructure for evaluating bake hardening and tensile properties.

3.3.2.1. Continuous Annealing Line Process (CAL)

The first annealing process was the industrially utilized process, called, Continuous Annealing Line (CAL). This conventional process exhibited second phase (martensite) distribution at the ferrite-ferrite grain boundaries along with very fine and sharp ferrite-martensite interface morphology. Figure 3.1 illustrates the industrially used continuous annealing line process (CAL) simulated in the present research work by using annealing simulator. The parameters (annealing temperature, holding time, cooling stages) used for CAL in the present research are shown in

Figure 3.1. The processing conditions employed in the present research work are similar to those being currently followed for conventional DP steel processing [38, 39].

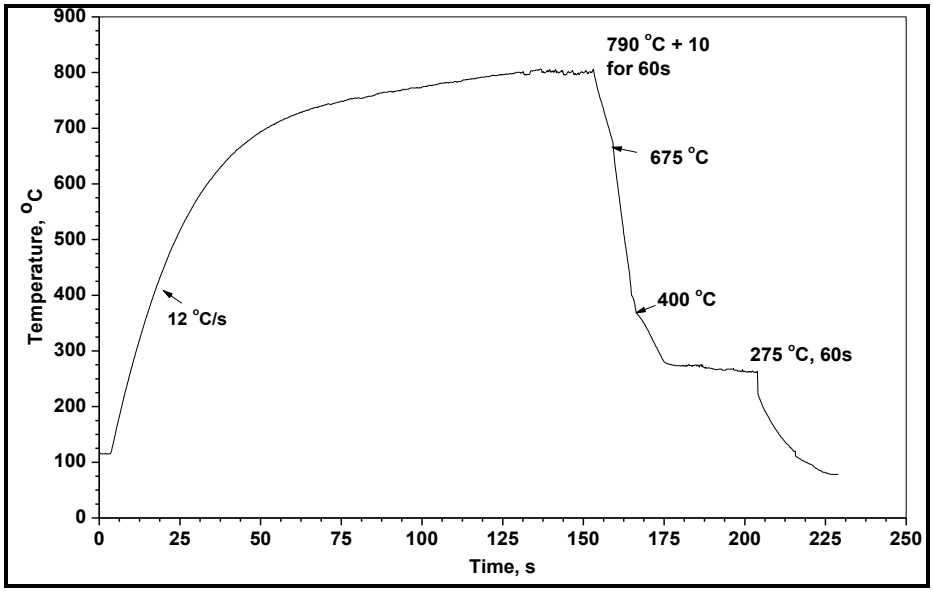

Figure 3.1: Typical temperature-time profile of industrial continuous annealing line (CAL) process.

The CAL process comprises of initial heating of the specimen to the inter-critical temperature of 790 ℃, followed by isothermal holding for 60 s, and finally following a cooling regime as is shown in Figure 3.1. The "heating and soaking" steps during CAL can be viewed as comprising of:

(i) Fast heating in the recrystallization zone (region where ferrite recrystallization is predominant). For example, in the present work (see Figure 3.1), the specimen was initially heated till 710 ℃ at a rate of 10–15 $℃/s$ (here, heating rate was approximately 12 $℃/s$).

(ii) Moderate heating zone (upto the annealing temperature) followed by an isothermal holding stage or soaking zone which helped in pearlite dissolution and austenite nucleation. Thus, an overlapping effect of pearlite dissolution and austenite nucleation was achieved in the second stage of heating. Here, it is also noted that beyond 710 ℃ and upto the peak temperature of 790 ℃, the heating rate was about 1.06 $℃/s$ followed by isothermal holding of 60 s. The isothermal holding ensured sufficient time for austenite nucleation and grain growth along with sufficient carbon enrichment.

The cooling stages employed in the present CAL process involved three stages:

(i) The first stage was slow cooling from soaking tempearure of 790 ℃ to 675 ℃. This stage of slow cooling resulted in further austenite enrichment and ferritic transformation.

(ii) The second stage of rapid quenching from 675 ℃ to 400 ℃ resulted in martensitic transformation and was also employed (under rapid conditions) to ensure avoiding bainitic region during phase transformation.

(iii) The third stage of slow cooling respectively from 400 ℃ to 275 ℃ was performed for effective holding at 275 ℃ to allow overaging of the hard martensite phase. This overaging ensured tempering of newly formed martensite thereby improving the final ductility of the processed DP steel. The tempering of the hard phase also ensured segregation of carbon from martensite in form of carbides such that phenomena of Luder Band (Strecther Strain marks) formation after forming operations performed on DP steel components may be avoided.

The above CAL process showed preferential formation of grain boundary martensite and presence of martensite at grain boundaries is reported to affect the mechanical properties of steels under strain path changes [40–42]. These results are discusses in Chapter 4 (Section 4.3.1.1)

3.3.2.2. Modified Continuous Annealing Line Process (mod-CAL)

The objective of modifying the existing conventional industrial annealing process (CAL) was to alter the distribution of second phase (martensite) and the ferrite-martensite interface morphology. It is well reported in literature that by allowing more ferrite recrystallization before entering into the inter-critical range leads to formation of fine ferrite with well dispersed martensite (which is also of small size). Therefore, (in order to improve upon the existing conventional CAL cycle), in the proposed modified cycle, an attempt was made to slow down the heating rate during 'Stage-I' of the heating cycle. The motive was to allow for more ferrite recrystallization and better dispersion of cementite present in original pearlite. So, in the modified cycle (referred here as mod-CAL), the temperature of 710 ℃ (Stage-I heating) was reached at a relatively slower rate to allow for more ferrite recrystallization and better cementite dispersion (with an average heating rate of~ 6 $℃/s$; see Figure 3.2). Following this, during the second stage of heating (in the inter-critical range) a moderate heating rate of 1.60 $℃/s$ was applied to reach a temperature of 790 ℃ (Stage-II heating). This heating stage allowed further recrystallization of the remaining unrecrystallized grains, if any, (after the first stage of heating) along with the growth of newly recrystallized ferrite grains (which formed during Stage-I

heating). Also, during this Stage-II heating, it was expected that some austenite grains start to nucleate. The austenite nucleation was expected to occur at the dispersed carbide particles (of pearlite) due to the presence of high carbon concentration at these locations. Here, it should be noted that since cementite/ carbide particles are well dispersed, this effective dispersion may promote formation of austenite with fine grains. Also, in the mod-CAL processing, holding during Stage-II heating was eliminated. It was anticipated that holding during heating in CAL cycle leads to austenite grain growth. Therefore, during mod-CAL, instead of holding at the inter-critical annealing temperature of 790 ℃, heating was continued into the third stage to a higher temperature of 840 ℃ (Stage-III heating).

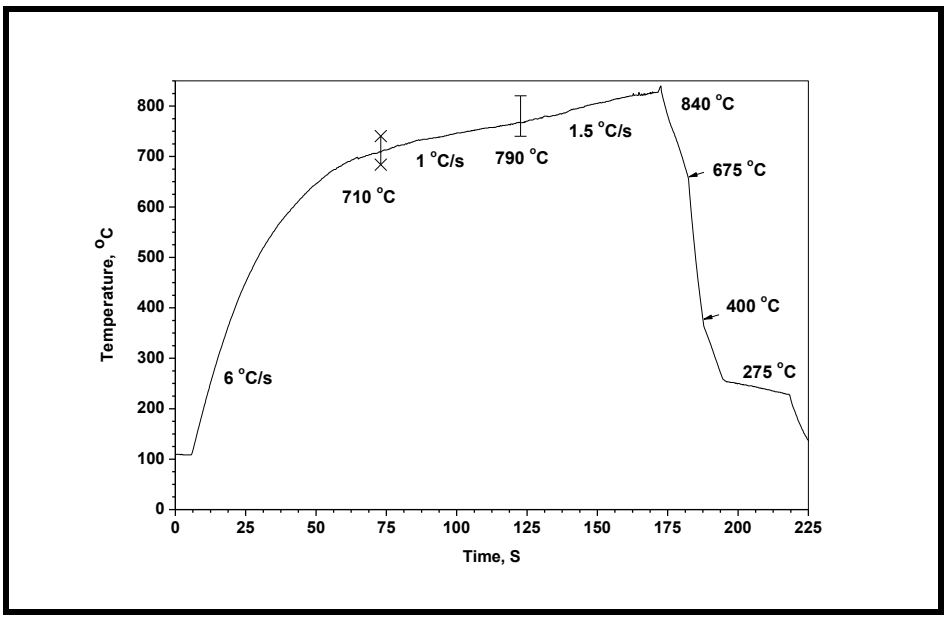

Figure 3.2: Typical temperature-time profile of the modified continuous annealing line (mod-CAL) process.

The Stage-III temperature was chosen in a manner which would achieve similiar austenite fraction (as in CAL) and without any grain coarsening. Peak annealing temperature of 840 ℃ met both these objectives effectively. Finally, cooling regime similar to CAL was used to complete the annealing cycle. Figure 3.2 depicts a typical mod-CAL annealing cycle utilized to produce DP microstructure in the present work.

Therefore, by heat treating the as-received steel by the above discussed two different annealing routes (CAL, and mod-CAL), it was possible to achieve dual phase microstructures in the as-received steel specimens with similar martensite volume fraction. However, the obtained microstructure substantially differed in second phase (martensite) spatial distribution and

morphology. This was the requisite input for comparing the bake hardening response of the two different morphologies, which is the main focus of the present work.

3.3.3. Pre-Straining and Bake Hardening Treatment

The next step in experimental procedure was to pre-strain the heat treated DP specimens from both the CAL and mod-CAL processes. In the actual industrial conditions in the automobile sector, the heat treated steel sheets (i.e. CAL processed) are subjected to various forming operations (viz. press forming, deep drawing etc) to obtain the final dimensions in the car body components. Thereafter, these finished components are subjected to the paint-curing cycle. In the present work, the forming operation and paint-curing cycle were simulated through pre-straining and bake hardening respectively. The range of pre-straining prior to baking was kept in the range 1–5 % which was in accordance with conventional forming limits of automobile industry [15, 16, 18, 19]. The baking was done at a temperature of 170 ℃ for 20 min using a Muffle furnace (*Carbolite*). The baking parameter were decided on the lines of existing literature work [16, 17] which claim that maximum diffusion of solute carbon in the DP microstructure is observed within the temperature range of 150-200 ℃ when baked for 20–30 minutes.

3.3.4 Tensile Testing of PS and BH Specimens

For each heat treated specimen, subsequent to pre-straining and bake hardening treatment, full fracture tensile test were conducted to determine the final yield strength, ultimate tensile strength and elongation (total elongation).

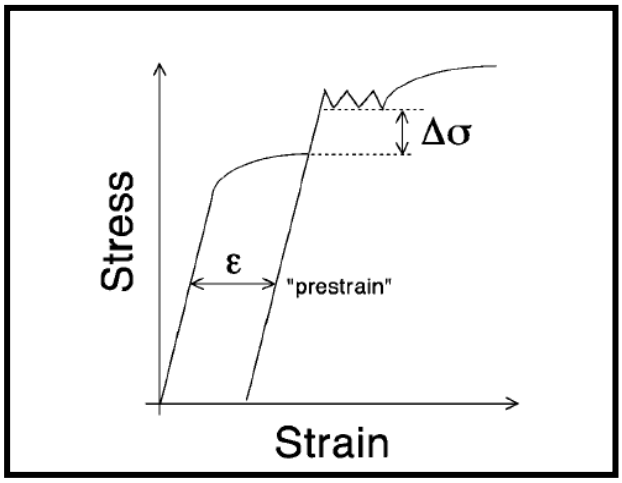

Figure 3.3: Stress-Strain curves of bake hardened and pre-strained specimens indicating bake hardening index [17].

Tensile test were carried out on INSTRON 8862 Servo-hydraulic equipment of 100 kN load capacity with a 25 mm extensometer and crosshead velocity of 0.5mm/min under standard strain rate of 0.001/s. Further, bake hardening index (BHI), which is a measure of the baking response, is the difference in the yield strength after baking and the flow stress obtained after pre-straining (but before baking) as can be seen from Figure 3.3. Mathematically, it can be expressed as seen in equation 1 below.

$$BHI = \text{Final yield strength} - \text{Flow stress just after pre-straining} \quad \ldots\ldots\ldots\ldots\ldots\ldots\ldots\ldots (1)$$

3.3.5. Analysis of Second Phase Post Bake Hardening

The most crucial part of this study was the proper evaluation and analysis of the second phase (martensite) distribution and observing the F/M interface morphologies. Copper mounted specimens were prepared for CAL and mod-CAL processed specimens which were polished, etched, and observed under SEM at a very high magnification range (1000-60000X). The central idea was to capture the variations in "lath" structures obtained by adopting two different inter-critical annealing processes.

The difference in average lath martensite hardness was investigated by Nano-indentation test, while a qualitative analysis of the solute carbon present in the two processed DP microstructures of CAL and mod-CAL was done by X-ray diffraction test. The effect of martensite spatial distribution and F/M interface morphology on the deformation mechanism of the processed specimens (CAL and mod-CAL) was studied by interrupted tensile (necking) test. This test was conducted on specimens pre-strained to 5 % (maximum pre-strain value) followed by baking treatment (170 ℃, 20 mins). The extent of ferrite grain elongation/ deformation was evaluated by simply calculating the "aspect ratio" of the deformed ferrite grains after the interrupted tensile necking test.

3.4. Commercial Software

The software used in the present study are briefly mentioned below.

1) analySIS FIVE

It is a image analysis software (*OLYMPUS* Corporation, Japan) developed specifically for particle detection, grain size measurements, layer thickness and coating measurements, weld measurement etc. In the present work, it was used for quantitative analysis of phase grain size

distribution of individual phases in the DP microstructure. The aspect ratio calculations were also done using this software.

2) ImageJ

It is a public domain Java image processing program inspired by *NIH Image* for *Macintosh Inc.* USA. It can display, edit, analyze, process, save and print 8-bit, 16-bit and 32-bit images. It can read many image formats including TIFF, GIF, JPEG, BMP etc. Quantitative analysis for determining the phase fraction of the individual phases was done using this package.

3) ORIGIN 5.0

Origin (*ORIGINLabs:* Northampton, Massachusetts, USA) is a data analysis and graphing software. It offers advanced analysis tools and applications for peak fitting, surface fitting, statistics, and signal processing. In the present work, this software was used for plotting the tensile test engineering stress-strain curves, nano-indentation hardness versus depth plots, and the peak doublet plot from XRD measurements.

3.5. Annealing Simulator

Lab simulations for the conventional industrial annealing (CAL) process and the modified continuous annealing line (mod-CAL) process to obtain DP microstructures in the present work were carried out in an annealing simulator developed jointly by CSIR-NML and Tata Steels, Jamshedpur (Figure 3.4–3.6). The following is a description of the annealing simulator.

(a) Heating System

The simulator consisted of a hot chamber with maximum achievable temperature around 1050 ℃ (Radiation Heating Furnace) at heating rates greater than 25 ℃/s. Figure 3.4 shows the hot chamber wherein the appropriate annealing temperatures for both the processes (viz. CAL and mod-CAL) were obtained. Guide-ways were constructed along the longitudinal direction of the furnace bed to facilitate movement of the hot chamber to either engage or disengage (post annealing treatment) the cold chamber.

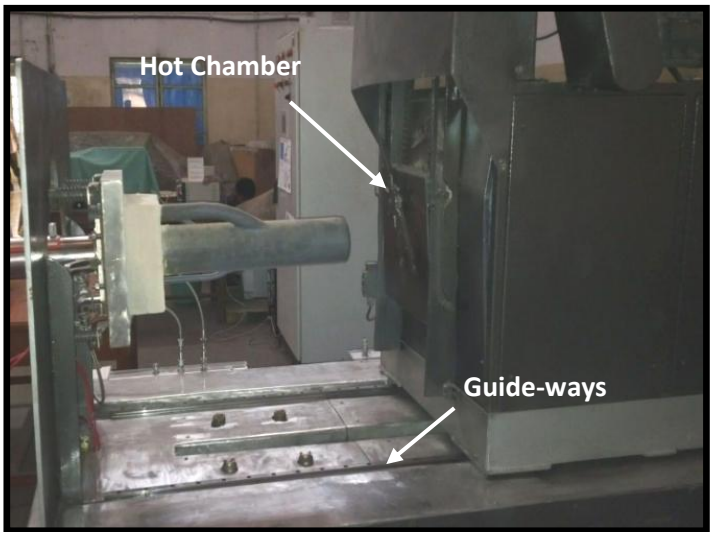

Figure 3.4: Hot chamber of the annealing simulator (Courtsey: NML, Jamshedpur).

(b) Cooling System

Cooling of the specimens is achieved by purging a gas mixture of hydrogen and nitrogen at very high pressures.

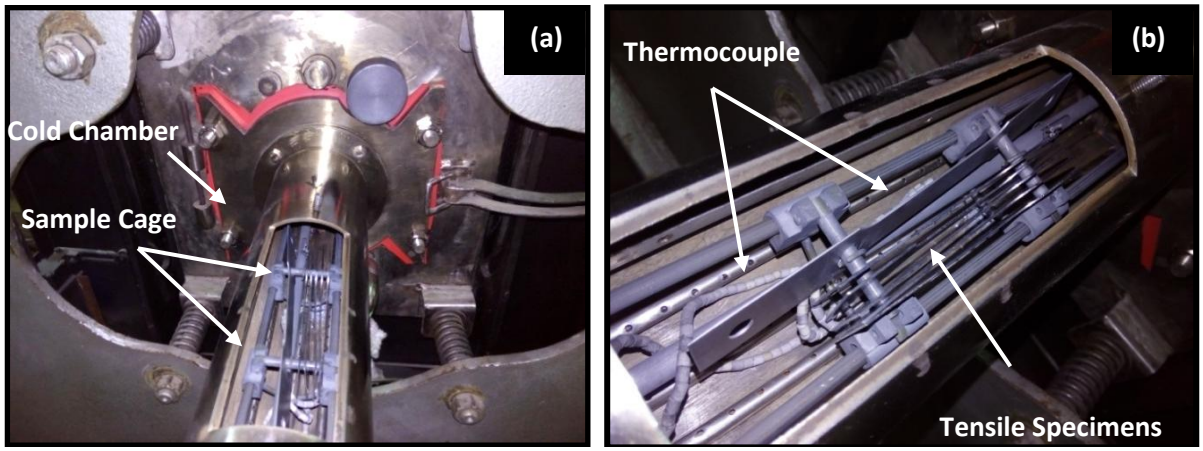

Figure 3.5: (a) Cold Chamber of the annealing simulator, (b) blown up view of the specimen cage (Courtsey: NML, Jamshedpur).

A specimen cage was attached within the cold chamber to hold the tensile specimens while a dummy tensile specimen was permanently attached to it with a K-type thermocouple soldered at its mid-section to record the master temperature.

Figure 3.5a and Figure 3.5b show the specimen cage and thermocouple connections within the cold chamber of the annealing simulator. The specimen cage was adjustable so it could be shut inside the hot chamber once the annealing temperature was reached. Different cooling rates can

be achieved by either changing the percentage of hydrogen gas in the gas mixture or the purging pressure or both.

(c) PLC based Digital Control System

The heart of the system is the PLC based Digital Control System. It provides all the signals necessary to control the annealing simulator variables simultaneously through a digital closed-loop system. The system can be operated in several modes (totally manual control, combination of computer and manual control etc.) to provide maximum versatility in the annealing simulations.

(d) Process Simulation Environment of Annealing Simulator

The annealing environment was gas charged with a mixture of H_2 and N_2 prior to annealing process. While nitrogen helped in maintaining an inert atmosphere, H_2 was used to remove presence of any trace moisture prior to annealing.

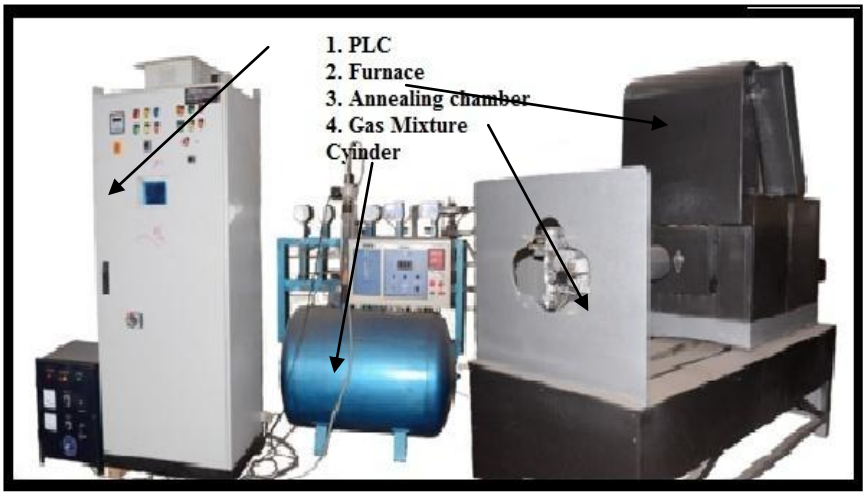

Figure 3.6: Annealing Simulator (Courtesy: NML, Jamshedpur).

The cooling medium employed by gas-jet technique involved a gaseous mixture of 10% H_2 and balance N_2 for all the annealing experiments, similar to industrial practice, to prevent oxidation. Figure 3.6 shows all the parts described above of the annealing simulator.

3.6. Specimen Preparation for Metallography

Typical metallographic specimen preparation involves the following steps: mounting, paper polishing, cloth polishing and etching. These steps help in the proper microstructural evaluation

of the processed specimens. The instruments and equipment needed for proper specimen preparation are discussed in this section.

A) Precision Cutter

The precision cutter (Make: MECATOME T 255/300, *Metal Power Analytical (I) Pvt. Ltd*, Andheri, Mumbai, India) is a multi-purpose cutter used to cut a variety of materials precisely. The steel sheet is mounted between the two clamping vices. The sheet is positioned in a position relative to the cutter wheel, so that the cutter can easily cut the material on lowering it down towards the material. Figure 3.7 illustrates the precision cutter utilized in the present work.

Figure 3.7: Low Speed Precision Cutter (Courtesy: NML, Jamshedpur).

B) Mounting

Mounting is done to facilitate specimen holding (single or even multiple specimens) and preparation. Mounted specimens are prepared from either conducting (Copper) or non-conducting (Bakelite) powder depending on the electrical conductivity of the prepared specimens. Copper is used for mounting when specimen is to be used for SEM analysis. Specimens are hot mounted at a temperature of 160 ℃ which is followed by appropriate cooling cycle to prepare the mount. The edges of the mounted specimens are rounded to minimize the damage to grinding/polishing discs. The mounting press (Make: BAINMOUNT METCO, *Chennai Metco Pvt. Ltd.*, Chennai, India) was used in the present work and is shown in Figure 3.8.

Figure 3.8: Mounting Press (Courtesy: NML, Jamshedpur).

C) Paper Grinding

The surface to be examined by optical microscopy or SEM is first polished with abrasive (SiC) papers of successive finer grades or higher grit number ranging from 320, 400, 600, 800, 1000, 1200, 1500 and 2000 mesh size. The mounted specimen is first rubbed on lower grade SiC paper to prepare desired flatness while switching to successive higher grades by repeatedly rubbing in a direction and then perpendicular to it. The over-heating of specimen is avoided by applying water so that no modification in the microstructure occurs.

Figure 3.9: Abrasive Papers (Courtesy: NML, Jamshedpur).

The pressure needs to be adjusted as high pressure can lead to introduction of deep scratches and low pressure could result in very long duration for polishing. Some SiC papers used in the present work are shown in Figure 3.9.

D) Cloth Polishing

The next step is polishing of specimens on a rotating wheel disc. Polishing wheels are covered with a soft cloth (velvet, canvas, suede etc.) which need to be soaked in a polishing medium (alumina or colloidal) along with appropriate coolant like ethanol/water. The polishing cloth is aqua washed thoroughly in the beginning stage with a brush to remove any (previous alumina or colloidal particles) contaminants which may cause deep scratches on the paper polished mounted surfaces. Figure 3.10 below shows the equipment used for cloth polishing of specimens in the present study.

Figure 3.10: Polishing Machine (Courtesy: NML, Jamshedpur).

The specimen is held on the rotating disc in order to obtain a scratch free surface with mirror like finish. Polishing machine (Make: BANIPOL METCO, Model No: PMV018, *Chennai Metco Pvt. Ltd.,* Chennai, India) of 0.37 kW capacity was used in the present work.

E) Etching

Etching is done in order to reveal the microstructure constituents of any metal/ alloy specimen which has been properly polished and dried through selective chemical attack. The specimen must be thoroughly cleaned before etching. Etchant must be selected and prepared accurately. Etchant may be applied using a cotton bud wiped over the surface for a few times (necessary precautions must be taken while etching, as very small difference occurs between etching and over-etching). Nital (2% HNO_3 in ethanol), a non colour etchant was used in the present work. It revealed the ferrite phase as white and martensite as black.

F) Leveling

The surface to be examined optically should be perfectly flat and leveled. If not, then the viewing area would be out of focus i.e. if the center is focused, the sides would go out of focus or vice versa. By using a specimen leveling press (shown in Fig. 3.11), this problem can be avoided, as it presses the mounted specimen into clay on a microscope slide, making it leveled. A small piece of paper or cloth covers the surface of the specimen to avoid scratching.

Figure 3.11: Leveling Machine (Courtesy: NML, Jamshedpur).

3.7. Equipment for Microstructure Evaluation and Characterization

This section provides brief details of the equipment used for qualitative microstructural analysis including optical Microscopy (OM), scanning electron microscopy (SEM), nano-indentation and X-Ray diffraction test. The equipment used are described as follows.

A) Optical Microscope

Optical microscopy is used for the purpose of magnifying small specimens with the help of visible light and a system of lenses. Metallic materials are usually opaque and therefore investigations of plane cross-sections by incident light prevail in metallographic analysis. Due to the difference in the refractive indices there appear different color shades. Starting from the specimen preparation, to etching of the specimen, and setting up of microscope, all steps should be carefully optimized in order to get maximum information from a microscopic study. The optical microscope (Make: Leica DM2500 M; *Lieca Microsystems,* Wetzlar, Germany) was used in the present study is shown in Figure 3.12.

Figure 3.12: Optical Microscope (Courtesy: NML, Jamshedpur).

B) Scanning Electron Microscope

A scanning electron microscope (SEM) is a type of electron microscope that images a specimen by scanning it with a high-energy beam of electrons. The electrons interact with the atoms that make up the specimen and produce signals that contain information about the specimen's surface topography, composition, and other properties such as electrical conductivity etc. SEM can produce very high-resolution images of the specimen’s surface, revealing details less than 1 nm in size.

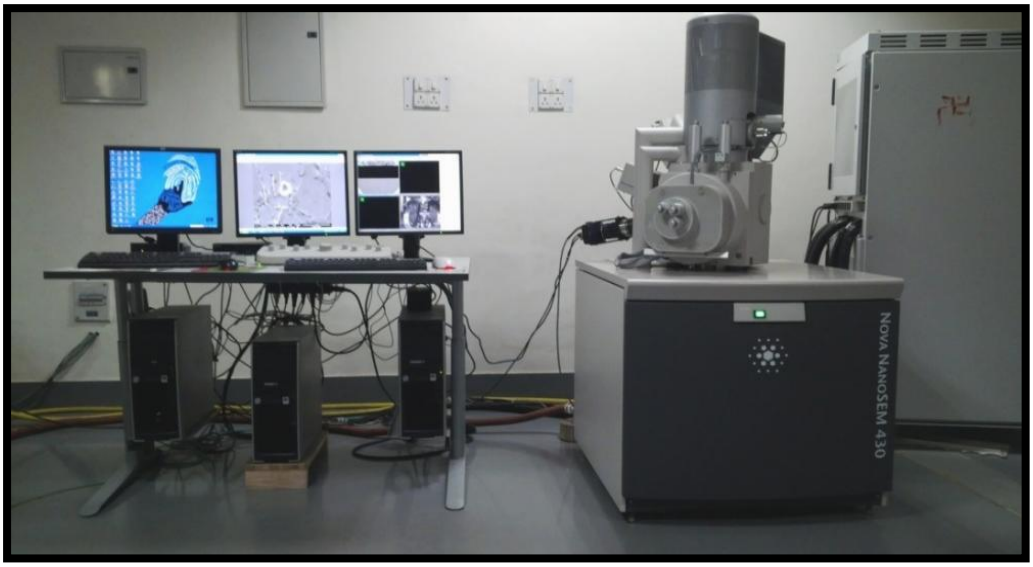

Figure 3.13: Scanning Electron Microscope (Courtesy: NML, Jamshedpur).

Due to the very narrow electron beam, SEM micrographs have a large depth of field, yielding a characteristic three-dimensional appearance useful for understanding the surface structure of a specimen. Figure 3.13 above shows the scanning electron microscope (Make: Nova Nano SEM 430; *Field Emission Inc.*, Hillsboro, USA) was used in the present study.

C) X-Ray Diffraction (XRD)

X-ray diffraction (XRD) is a versatile, non-destructive technique that is widely employed to characterize crystalline solids and extract information about the existing phases and crystallographic structure of materials.

Figure 3.14: X-Ray Diffraction set-up (Courtsey: NML Jamshedpur).

Figure 3.14 shows the XRD testing machine used for present study. In the present work, amount of free or available solute carbon in the two processes was qualitatively determined by performing X-ray diffraction (XRD) technique (Make: Bruker *AXS D8*, Massachusetts, USA) with Cu Kα of 0.154 nm wave length along with fast detector Lynx Eye was used for diffraction experiments.

3.8. Equipment for Bake Hardening and Mechanical Properties Evaluation

This section describes the machines/ equipment used to evaluate the mechanical properties of the material before and after the annealing simulation/ heat treatment performed on the specimens. This equipment is as follows.

A) Carbolite Furnace

Standard tensile specimens after pre-straining were baked in a furnace as shown in Figure 3.15 at a temperature of 170 ℃ for 20 minutes.

Figure 3.15: Carbolite furnace used for baking of pre-strained processed specimens (Courtesy: NML Jamshedpur).

The furnace had a variable heating rate and was set at 5 ℃/ min heating rate to achieve desired baking temperature for the performed test.

B) Tensile Testing Machine

Tensile test were conducted at room temperature under displacement control at a strain rate of 1.3×10^{-4} sec^{-1} using Instron 8862 syatem of 100 kN load capacity. To study the BH effect, the heat treated tensile specimens were first subjected to pre-straining (in the range of 1–5 %) followed by paint curing simulations leading to bake hardening phenomena. Thereafter, tensile properties were determined, for both the pre-strained only as well as of the pre-strained and bake hardened specimens. Figure 3.16 shows the tensile testing machine (Make: Instron 8862 System, *Instron Engineering Corporation*, Norwood, USA) that was used in the present work.

Figure 3.16: Tensile Testing Machine (Courtesy: NML, Jamshedpur).

C) Nano-indentation

Nano-indentation calculates the average hardness of individual phases present in the microstructure using a polished metallic or non-mettalic specimen. Cold mounted specimen specimens are hot glued and placed inside the indent chamber. Specific regions are marked for the indenter to make indents withing those regions for their easy detection post indentation test viz. SEM analysis. In the present work, average hardness of lath martensite obtained from the two different annealing processes (viz. CAL and mod-CAL) was measured by Nano-indentation test. Figure 3.17 shows the Nano-indentation tester used in the present work (Make: MTS *Nano-Indenter XP*, USA) to help characterize the lath marteniste and interface morphology.

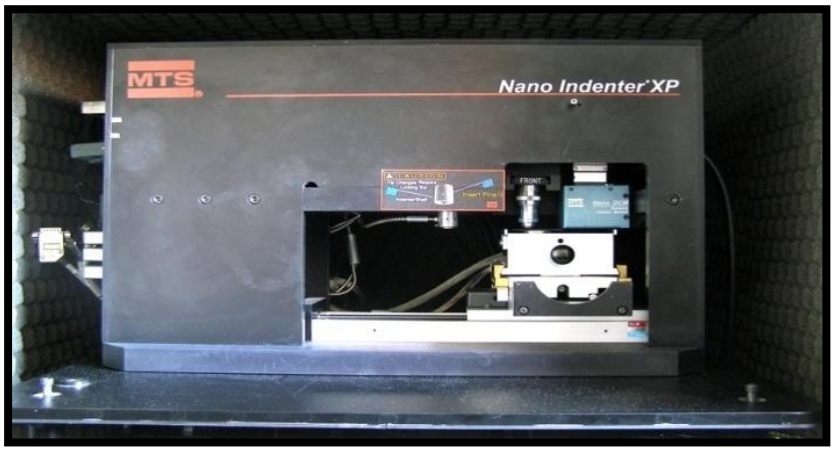

Figure 3.17: Nano-Indenter Tester (Courtesy: NML, Jamshedpur).

In the present study, the Nano-indentation tester was operated at a maximum load of 500 mN (50.8 g) force with an indentation depth of 150 nm. A minimum of seven indents were used for the calculation of average hardness.

3.9. Summary of the Chapter

This chapter brings forward the design of the present study. In this chapter, the objective function and key issues to be considered have been discussed. An overview of the experimental procedure to be followed has been provided. Also, machines and equipment to be used for specimen preparation for metallography, microstructural analysis, and mechanical properties evaluation have been discussed.

Chapter 4

Results and Discussion

4.1. General

This chapter deals with the results and discussion of annealing simulations, pre-straining, and bake hardening treatments provided to the heat treated specimens in the present work.

4.2. Properties of the As-Received Material

The microstructure of the as-received steel consisted of ferrite and pearlite as shown in Figure 4.1a–b.

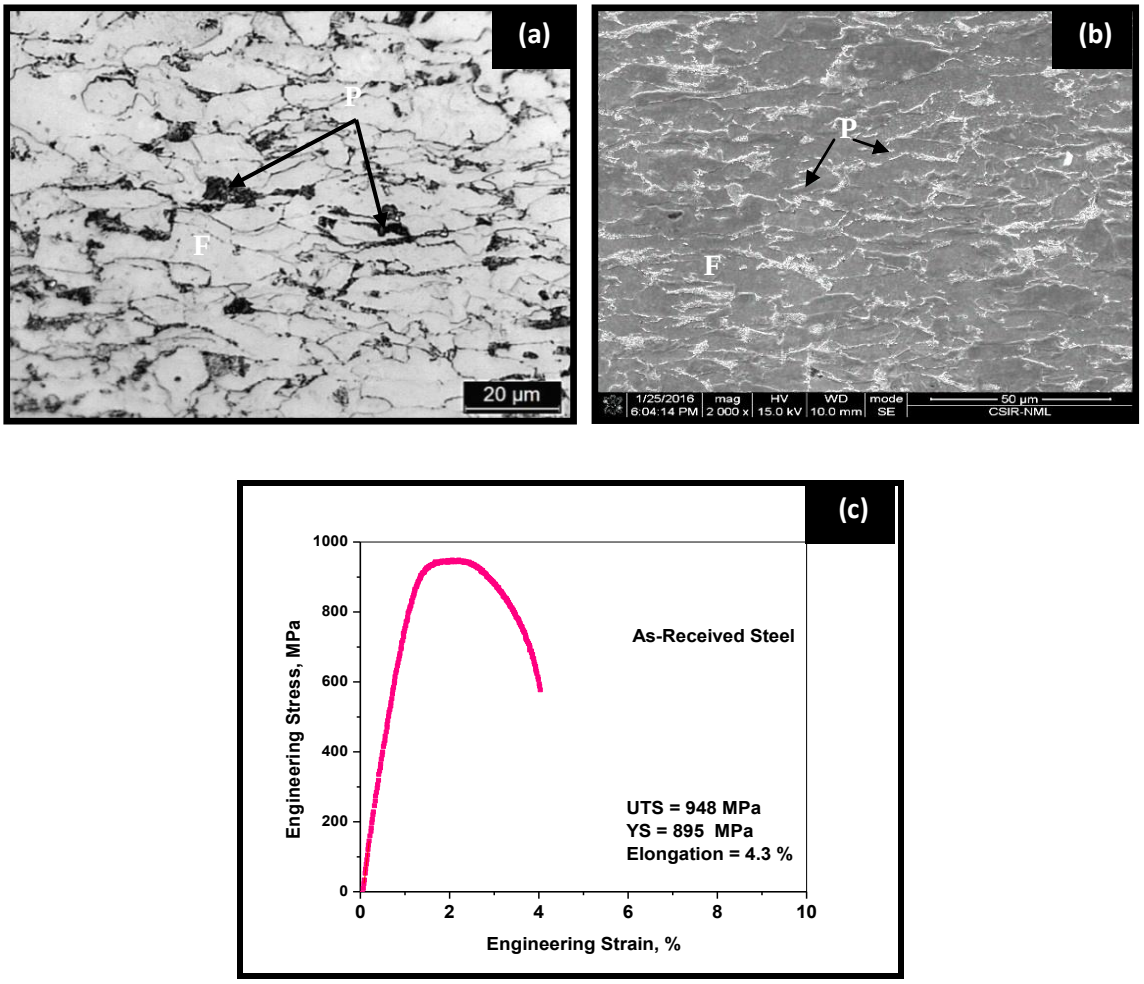

Figure 4.1: Characteristics of the as-received steel sheet (a) Optical micrograph, (b) SEM micrograph, (c) Stress-strain curve, F = Ferrite and P = Pearlite.

Phase fraction analysis was done using “ImageJ” which determined ferrite and pearlite volume fractions at 86 % and 14 % respectively. Figure 4.1c presents the engineering stress-strain plot for the as-received cold rolled steel. A significantly high YS and UTS with very low ductility were characteristic of the heavily deformed initial microstructure. Severe cold rolling increased the presence of dislocations, refined the ferrite and pearlite grain sizes. This all enhanced the strain hardenability of the as-received steel but at the expense of ductility. As discussed in Chapter 3, the as-received steel was subjected to two different set of annealing conditions (viz. CAL and mod-CAL) in order to obtain variations in second phase (martensite) distribution and morphology. This was done in order to investigate the effect of change in martensite distribution and morphology on the bake hardening characteristics of a DP steel grade.

For this purpose tensile specimens of 0.82 mm thickness were cut along the rolling directions from the as-received sheet, with dimensions as shown in Figure 4.2.

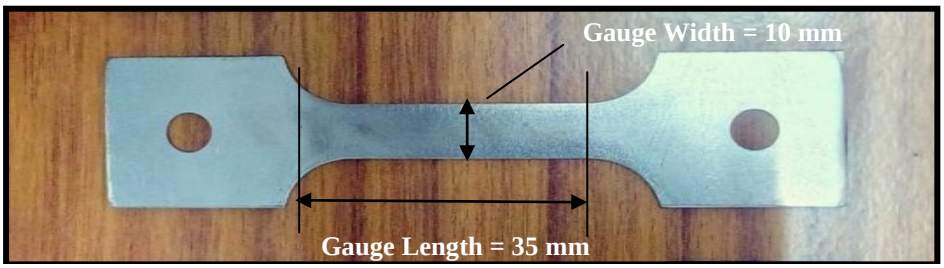

Figure 4.2: Dimensions of the tensile specimens.

4.3. Results of Annealing Simulations

The results of the annealing simulations performed with regards to the microstructural analysis and the mechanical properties are presented as follows.

4.3.1. Microstructural Analysis

This section provides a detailed discussion on the observed variations in the microstructure (viz. martensite-ferrite grain size distribution and morphology) of the as-received steel specimens subjected to CAL and mod-CAL heat treatment processes.

4.3.1.1. Martensite Distribution and Morphology

Figure 4.3a–d show the SEM micrographs of the DP microstructures obtained after subjecting the as-received specimens to CAL (Figure 4.3a and Figure 4.3c) and mod-CAL (Figure 4.3b and Figure 4.3d). Figure 4.3a–b show the distribution of the hard second phase (martensite) for CAL

and mod-CAL processed DP microstructures respectively. CAL processed specimen showed a typical grain boundary distribution of martensite (Figure 4.3a) which was in accordance with the earlier reported literature [13, 31–40, 43]. However, mod-CAL processed specimen showed a mixed distribution of martensite along the grain boundary and also within the ferrite grains (as indicated in black arrows in Figure 4.3b).

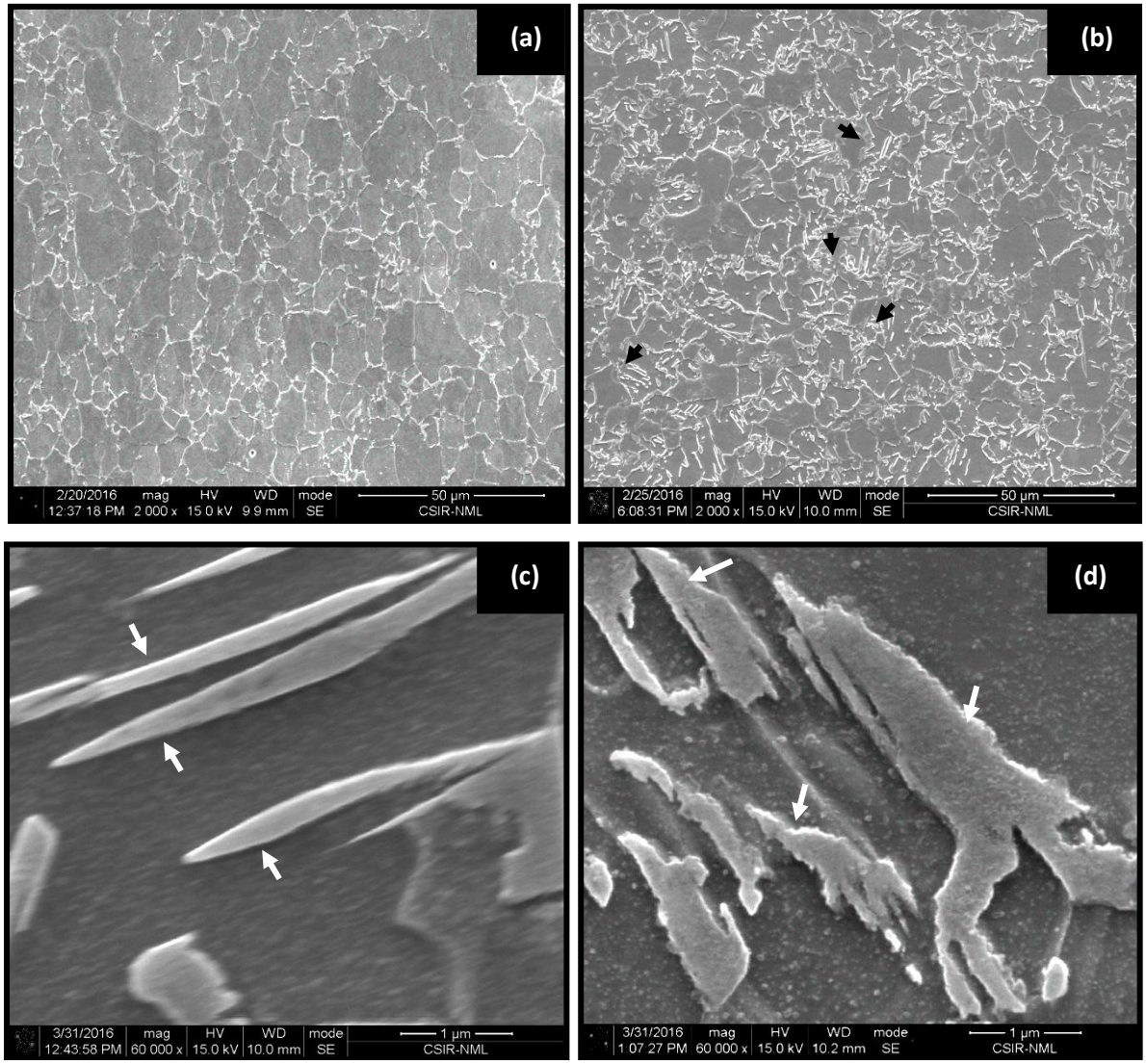

Figure 4.3: DP microstructure obtained after heat treatment (a–b) showing distribution of martensite obtained by CAL and mod-CAL respectively, and (c–d) morphology of lath martensite obtained in CAL and mod-CAL process respectively.

Figure 4.3c–d show the difference in lath morphologies obtained in the steel after the two annealing processes. The CAL processed lath martensite showed fine and sharp edged laths, while mod-CAL processed specimen showed wider and serrated lath edges (as indicated by the white arrows in Figure 4.3c–d respectively). The serrations seen in mod-CAL processed

specimen were observed due to the multi variant growth selection during austenite nucleation at a higher annealing temperature (under continuous heating in the third stage and with no soaking as discussed in section 3.3.2.2 and Figure 3.2). This initiated austenite growth in multiple directions for mod-CAL processed specimen (see Figure 4.3d) instead of a uni-lateral growth of lath martensite as was for CAL processed specimen (see Figure 4.3c).

Along with the qualitative study of martensite distribution and morphology, quantitative analysis was also performed to characterize the differences more efficiently. Phase fraction analysis was carried out using "ImageJ" which found martensite volume fraction as 16.5% and 18% in CAL and mod-CAL processed steels respectively.

Further, grain size distribution analysis of both the phases (ferrite and martensite) was done to determine the frequency or percentage of fine, medium, and large sized ferrite/ martensite grains obtained by respective heat treatment processes of the as-received steel.

4.3.1.2. Average Grain Size Distribution

"analySIS FIVE" software was used to determine the grain size distribution. The manual sketch module was adopted to trace individual grains from three frames, each for the CAL and the mod-CAL processed specimens (to evaluate average grain size distribution of ferrite and martensite phases). Figure 4.4 below shows the results obtained from "analysis FIVE". It was observed from Figure 4.4a that mod-CAL processed specimen contained a very large fraction (>50 %) of extremely fine martensite grains (with size < $0.5\mu m^2$) as compared to CAL processed specimen. Further, Figure 4.4 b depicted that most of ferrite grains (> 60–65 %) in mod-CAL processed specimen were of moderate to large grain size.

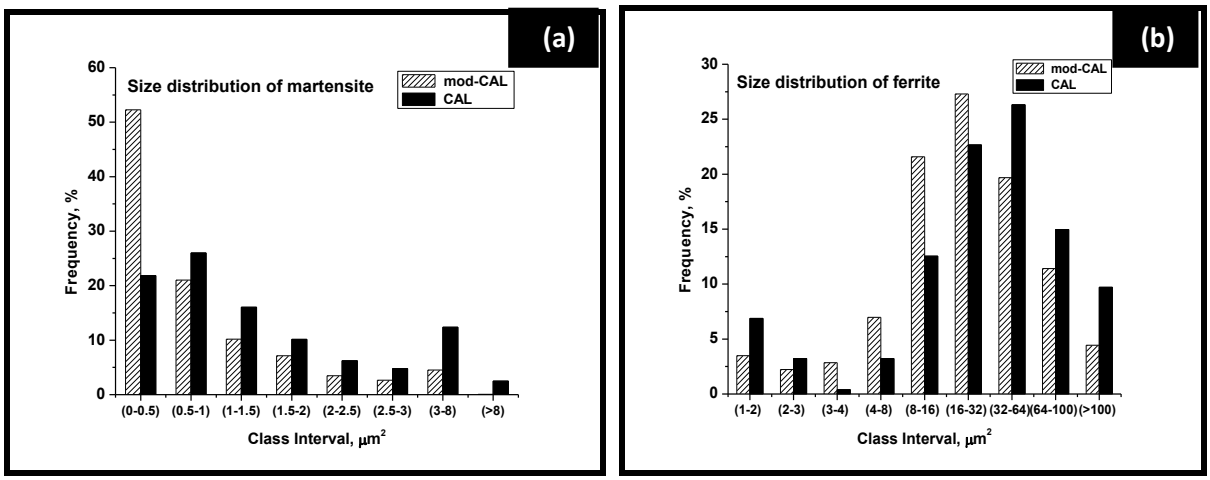

Figure 4.4: Grain size distribution (area) in the heat treated specimens (a) martensite, (b) ferrite.

As a result from these two distinct features observed in the mod-CAL processed specimens, viz. (i) large volume fraction of very fine martensite grains, and (ii) high volume fraction of ferrite grains with moderate to large size the mod-CAL process microstructure showed a mixed distribution of martensite. In this mixed distribution, martensite phase was present both (a) at the grain boundaries, and importantly (as desired), (b) within the ferrite grains (i.e. in-grain martensite).

4.3.1.3. Nano-indentation Test

Nano-indentation tests were performed to characterize the "lath" (martensite) observed in the DP microstructures obtained from the two processes.

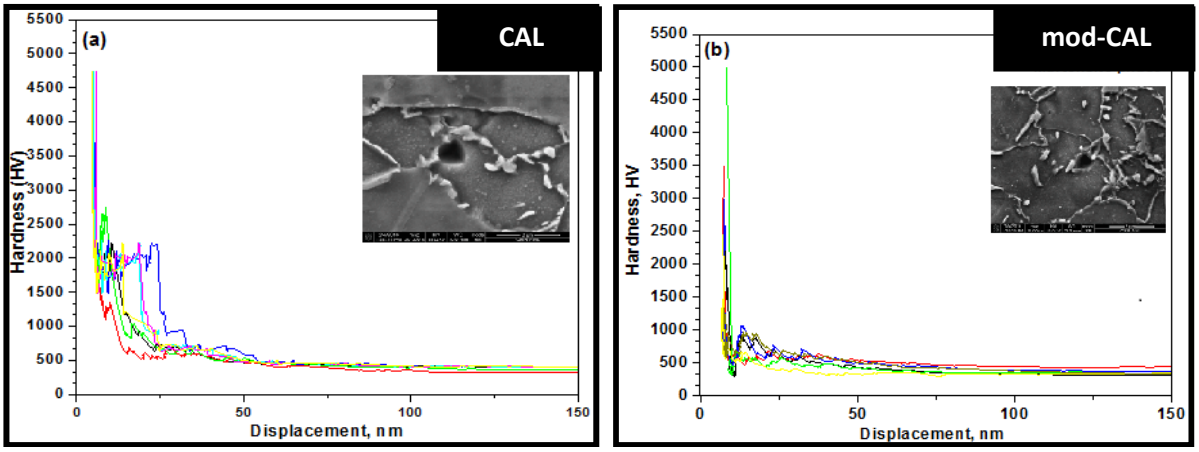

Figure 4.5: Hardness versus depth plot (a) CAL, and (b) mod-CAL specimen. Inset showing one indent each on lath martensite of CAL and mod-CAL respectively.

Specific regions were marked on the specimens to observe the lath martensite morphology and observations (indents) were taken within those specified region only to facilitate subsequent SEM analysis. SEM micrographs (shown in inset of Figure 4.5a–b) reveal that care was taken to make indentation on the second phase of DP microstructure. For each specimen, seven observations (indents) were taken to note the average hardness value of the phase. The typical loading curves of the nano-indentation test for the CAL and mod-CAL processed specimens are shown in Figure 4.5a–b. Average hardness (the stabilized value of hardness observed at depth of 150 nm) was 350 HV and 387 HV for CAL and mod-CAL specimens respectively. This value of hardness confirmed the presence of second phase as martensite in both the specimens [27, 29, 31, 32].

The relatively higher hardness for mod-CAL martensite also suggested higher solute carbon present in them. The higher annealing temperature resulted in enhanced austenite stability which indirectly led to more carbon diffusion during transformation (austenite to martensite) stage [34–37].

4.3.2. Evaluation of Tensile Properties

Tensile properties were next evaluated to ascertain the mechanical behaviour of the CAL and mod-CAL processed DP microstructures respectively.

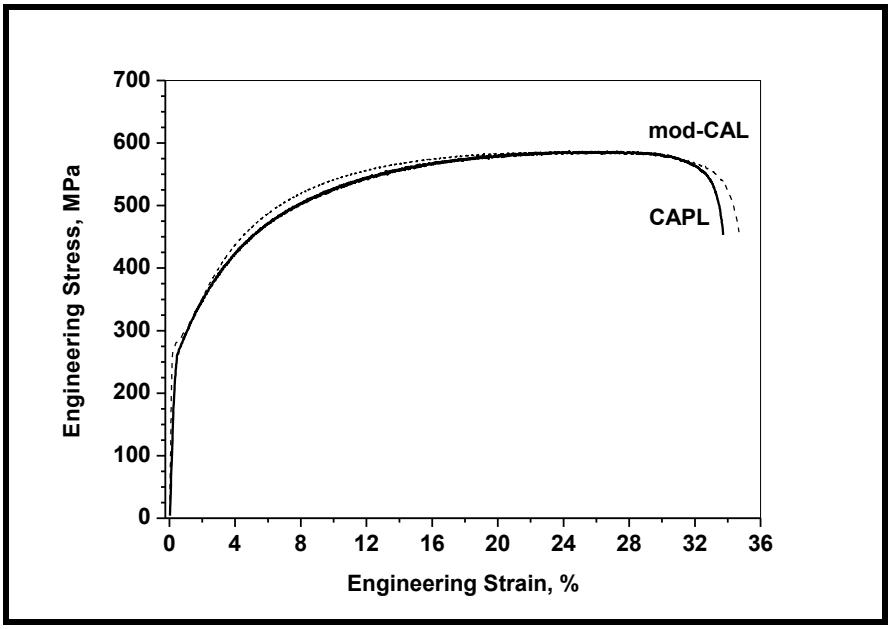

Figure 4.6: Engineering stress-strain curves for heat treated specimens.

The engineering stress-strain plots are shown in Figure 4.6 and properties are summarized in Table 4.1.

Table 4.1: Mechanical properties of the CAL and mod-CAL processed specimens.

Heat Treatment Process	YS, MPa	UTS, MPa	TE, %
CAL	260	586	34
mod-CAL	270	590	35

It can be observed that both processes (CAL and mod-CAL) have resulted in almost similar mechanical properties. Thus, two different starting microstructures (different in terms of martensite morphology and distribution) with almost similar mechanical propertie were obtained.

Further, investigations tried to seek information if these variations in second phase morphology and distribution resulted in different bake hardening characteristics.

4.4. Pre-Straining of As-Processed Specimens

The DP microstructures obtained from CAL and mod-CAL annealing processes were next pre-strained in the range of 1–5% (with intervals of 1 %) to evaluate the flow stress obtained under different pre-straining values. For this purpose, tensile specimens of the annealed specimens were again tensile loaded under standard strain rate of $1x10^{-3}$ s^{-1} at a cross head velocity of 0.5 mm/min.

4.4.1. Pre-Straining of CAL specimens

Table 4.2 presents the details of specimens and the results obtained after tensile testing of pre-strained CAL specimens. It may be noted that in case of tensile testing of pre-strained specimens, loading is only till the particular pre-strain value and the test is interrupted and stopped there e.g. for tensile testing of 2 % pre-strained specimen, loading is done only upto a stress value which generates a strain of 2 % in the specimen, and the test is stopped here (so, stress-strain curve would be generated only upto the pre-defined strain level).

Table 4.2: Details of tensile testing of pre-strained CAL specimens.

S.No.	Pre-strain level, %	Initial dimensions of specimens, mm			Results obtained after tensile testing of pre-strained specimens	
		Width (b)	Thickness (t)	X-section (b × t)	Flow Stress, MPa	Work Hardening, MPa
1.	1	10.06	0.82	8.24	290	290 – 260* = 30
2.	2	10.15	0.82	8.32	373	113
3.	3	10.24	0.82	8.39	412	152
4.	4	10.09	0.82	8.27	425	165
5.	5	10.06	0.82	8.24	499	239
*Yield Strength of the CAL processed specimen without pre-strain.						

It was observed that with increase in pre-straining value, the value of flow stress also increased continuously (see Figure 4.7). These flow stress values corresponding to each pre-strain level are required later for calculating the bake hardening index.

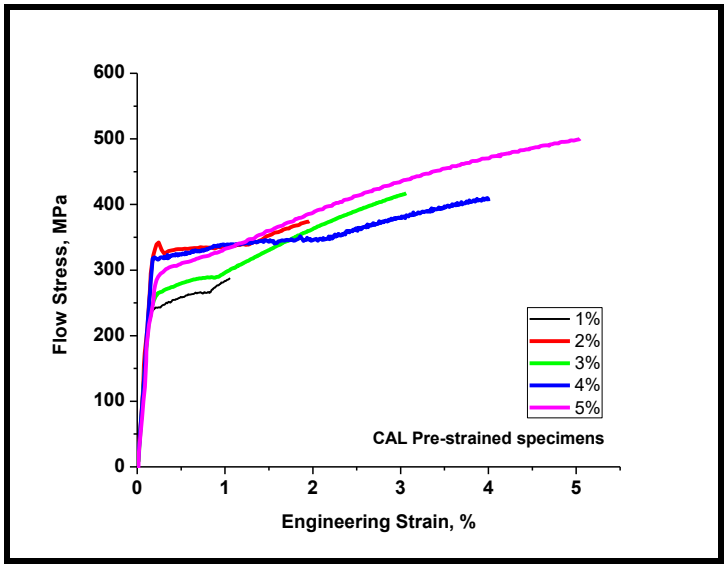

Figure 4.7: Flow stress curves of pre-strained CAL specimens.

4.4.2. Pre-Straining of mod-CAL Specimens

Next, pre-straining of mod-CAL processed specimens was undertaken to obtain flow stress measurements for evaluation of bake hardening indices. The specimen dimensions for pre-straining and the results of tensile testing are provided in Table 4.3.

Table 4.3: Details of tensile testing of pre-strained mod-CAL specimens.

.

S.No.	Pre-strain level, %	Initial dimensions of specimens, mm			Results obtained after tensile testing of pre-strained specimens	
		Width (b)	Thickness (t)	X-section (b × t)	Flow Stress, MPa	Work Hardening, MPa
1.	1	10.12	0.82	8.30	298	298 – 270* = 28
2.	2	10.04	0.82	8.23	360	90
3.	3	10.07	0.82	8.15	420	150
4.	4	10.09	0.82	8.27	451	181
5.	5	10.06	0.82	8.24	488	218
*Yield Strength of the mod-CAL processed specimen without pre-strain.						

From Table 4.3 and Figure 4.8, a similar trend in flow stress values was observed i.e. with rise in pre-strain level, the flow stress value continuously increased.

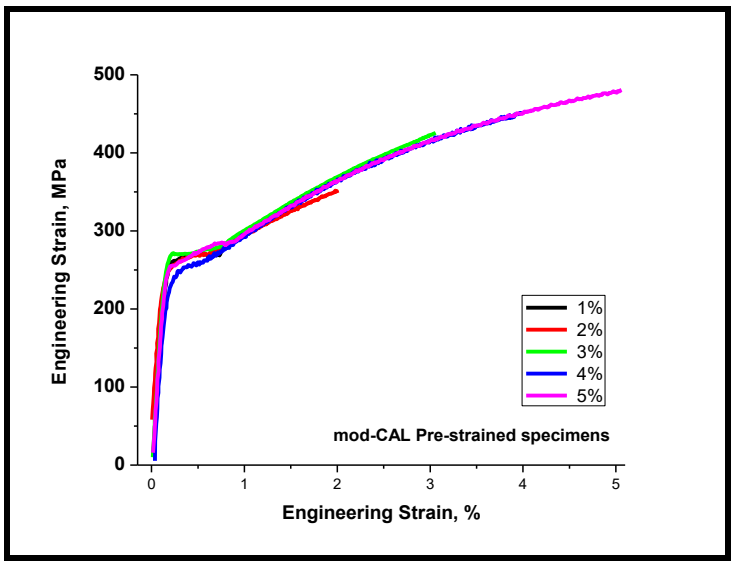

Figure 4.8: Flow stress curves of pre-strained mod-CAL specimens.

4.5. Bake Hardening Treatment

Pre-strained specimens (of both CAL and mod-CAL; and for all pre-straining levels) were now subjected to bake hardening treatment (170 ℃, 20 min). The results of bake hardening treatment are discussed as follows.

4.5.1. Bake Hardening Treatment of CAL processed DP590 specimens

Figure 4.9 depicts the engineering stress-strain plots for the "pre-strained" (PS; showed in solid lines) and also the "pre-strained with bake hardening" (PS+BH; showed in dotted lines) CAL processed specimens.

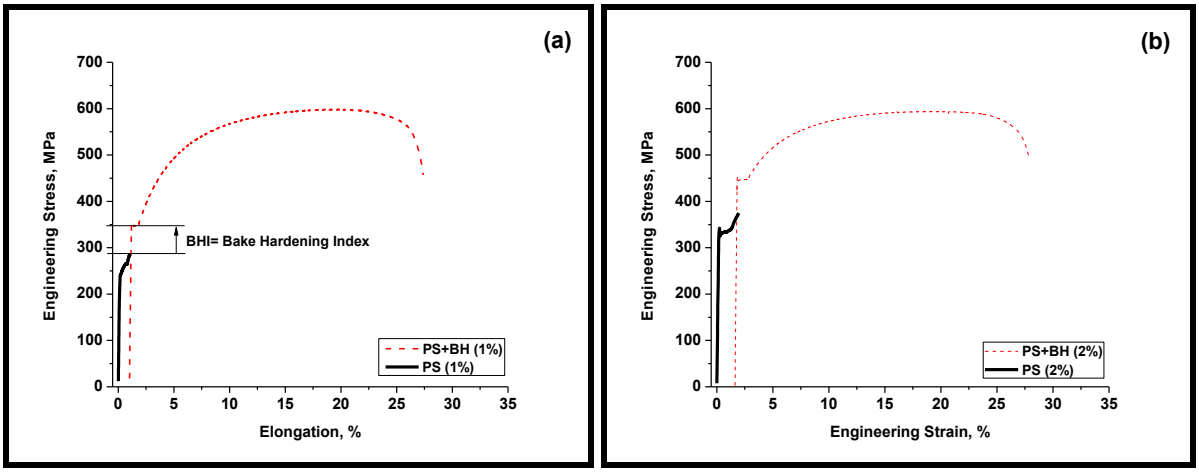

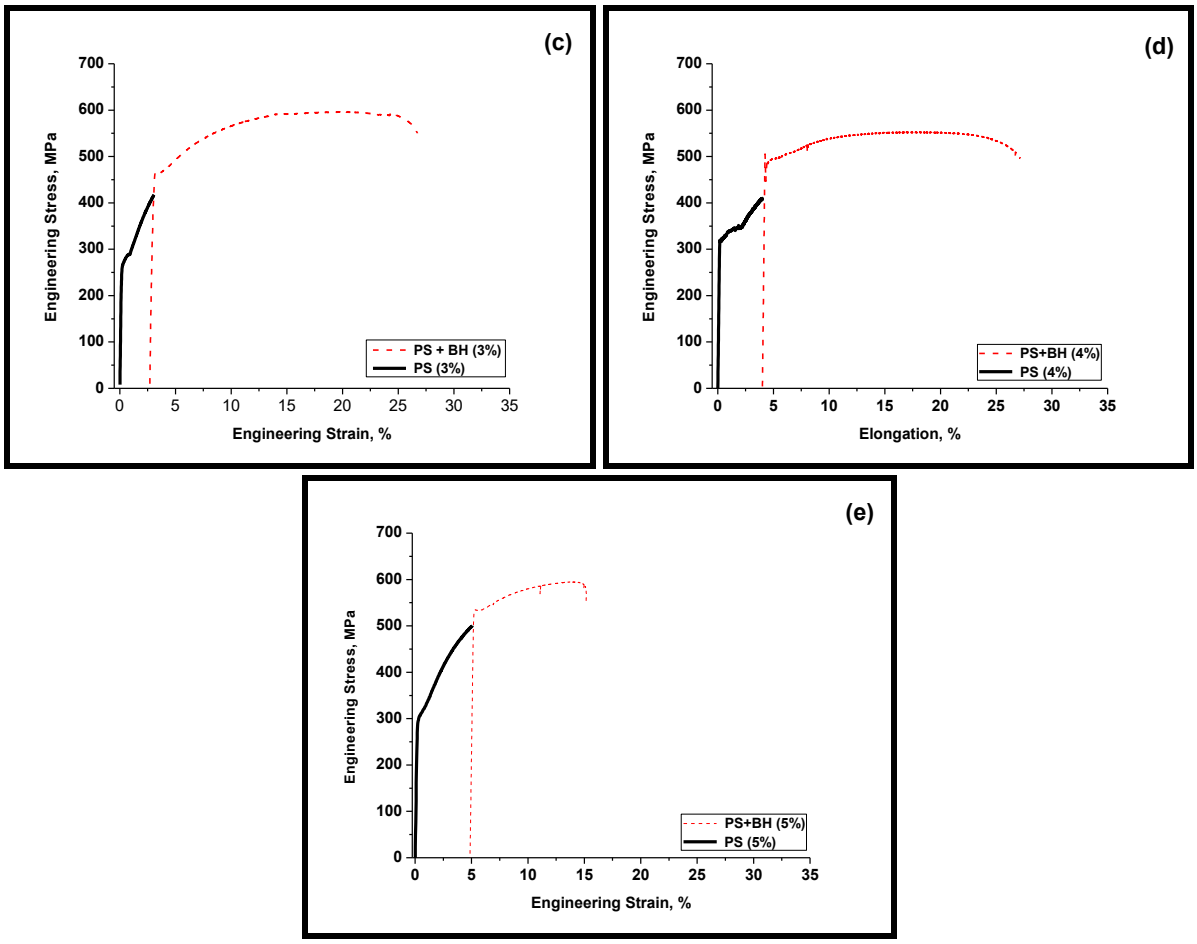

Figure 4.9: Engineering stress-strain curves of pre-strained and bake hardened CAL specimens.

The results of this tensile testing are summarized in Table 4.4.

Table 4.4: Mechanical behavior of CAL processed specimens after pre-straining and bake hardening.

.

S. No.	Pre-strain level, %	Flow Stress, MPa (Post PS but before BH)	YS, MPa (Post PS and after BH)	BHI, MPa	TE, %
1.	1	290	348	58	26
2.	2	373	445	72	25
3.	3	412	464	52	23
4.	4	425	470	50	22
5.	5	499	534	35	11

The results (Table 4.4 and Figure 4.9) show that the yield strength obtained after bake hardening treatment is always higher than the corresponding flow stress at each pr-straining level i.e. the bake hardening treatment always resulted in a positive bake hardening index, for every pre-strained value investigated in the present work. It was also observed that bake hardening index

values showed an initial increasing trend followed by a decreasing trend. Bake hardening index value improved till 2 % pre-strain (with maximum value of 72 MPa at 2% pre-straining) and thereafter, showed a continuous drop in bake hardening index (with minimum BHI value of 35 MPa at 5% pre-straining). These observations in the trend of bake hardening index with change in pre-straining values were in agreement with earlier reported work of [17–22].

4.5.2. Bake Hardening Treatment of mod-CAL processed DP590 specimens.

The pre-strained mod-CAL processed specimens were next bake hardened. Figure 4.10depicts the engineering stress-strain plots for the “pre-strained” (PS; showed in solid lines and also the “pre-strained with bake hardened” (PS+BH; showed in dotted lines) mod-CAL processed specimens.

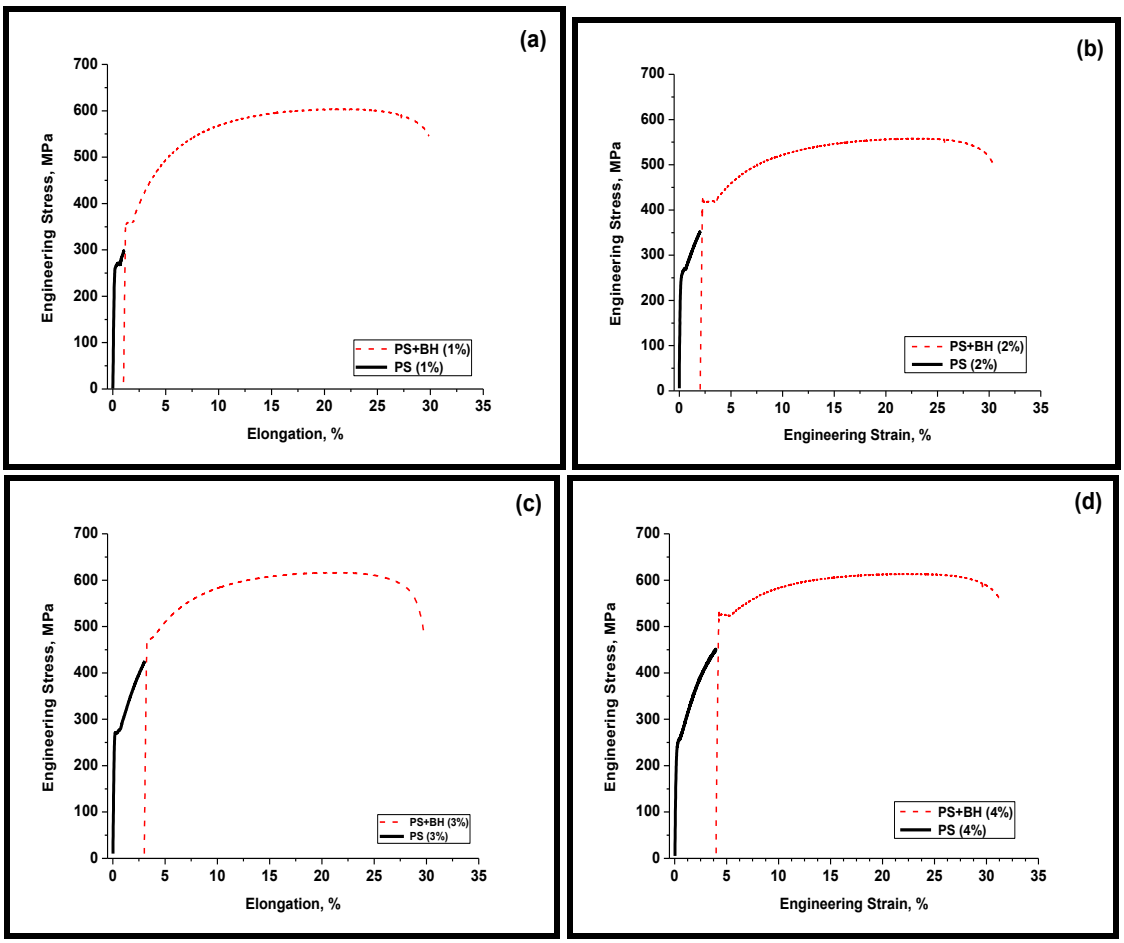

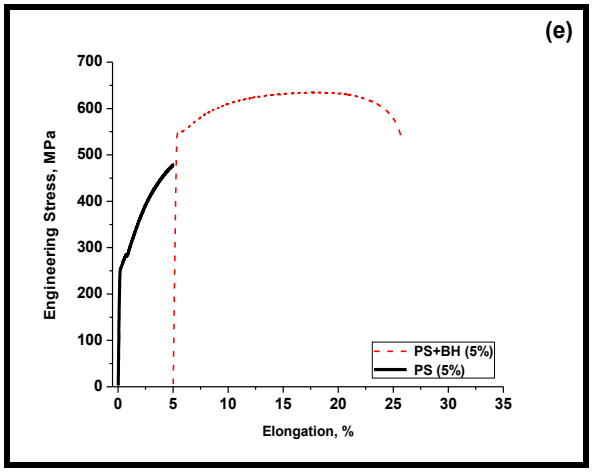

Figure 4.10: Engineering stress-strain curves of pre-strained and bake hardened mod-CAL specimens.

The results of this tensile testing are summarized in Table 4.5. The results (Table 4.5 and Figure 4.10) show that the yield strength obtained after bake hardening treatment is always higher than the corresponding flow stress at each pre-straining level, as was also seen in the case of CAL processed specimens.

Table 4.5: Mechanical behavior of mod-CAL processed specimens after pre-straining and bake hardening.

S. No.	Pre-strain level, %	Flow Stress, MPa (Post PS but before BH)	YS, MPa (Post PS but after BH)	BHI, MPa	TE, %
1.	1	298	355	57	29
2.	2	360	422	62	28
3.	3	420	483	63	27
4.	4	451	523	72	26
5.	5	488	540	52	21

However, it was further observed that for mod-CAL processed specimens, bake hardening index values showed a stable increasing trend for most of the pre-straining spectrum investigated. The bake hardening index value increased continuously with increase in pre-strain value till 4 % (maximum of 72 MPa being at 4 % pre-strain level). However, there was a gradual drop in bake hardening index at 5 % pre-strain level. Therefore, it was observed that CAL processed specimens showed the best bake hardening response in the low pre-straining regime, while mod-CAL showed a stable and improved bake hardening response in the higher pre-straining regime. Further, it was also observed that total elongation (post baking) continuously decreased with rise in pre-straining level. The results shown in Figure 4.9–4.10 and Table 4.4–4.5 and the trends

obtained thereafter, have been consolidated in Figure 4.11. Figure 4.11 shows that with increase in pre-strain level, the work hardening continuously increased which is a well reported fact [24–26]. On comparing the work hardening behavior of the two heat treated specimens (CAL and mod-CAL respectively), it was observed that CAL processed specimen showed a local maxima of work hardening (WH= 373 MPa) at 2 % pre-strain level. However, mod-CAL specimen showed the local maxima (WH= 451 MPa) at 4 % pre-strain level. As reported earlier in this section, for both CAL and mod-CAL specimens, for all, pre-straining and bake hardening conditions a positive value of bake hardening index was obtained. Further, it may be noted from Figure 4.11a–b that local maxima for work hardening and bake hardening index coincide at (i) 2 % pre-strain level for CAL and, (ii) 4 % pre-strain level for mod-CAL.

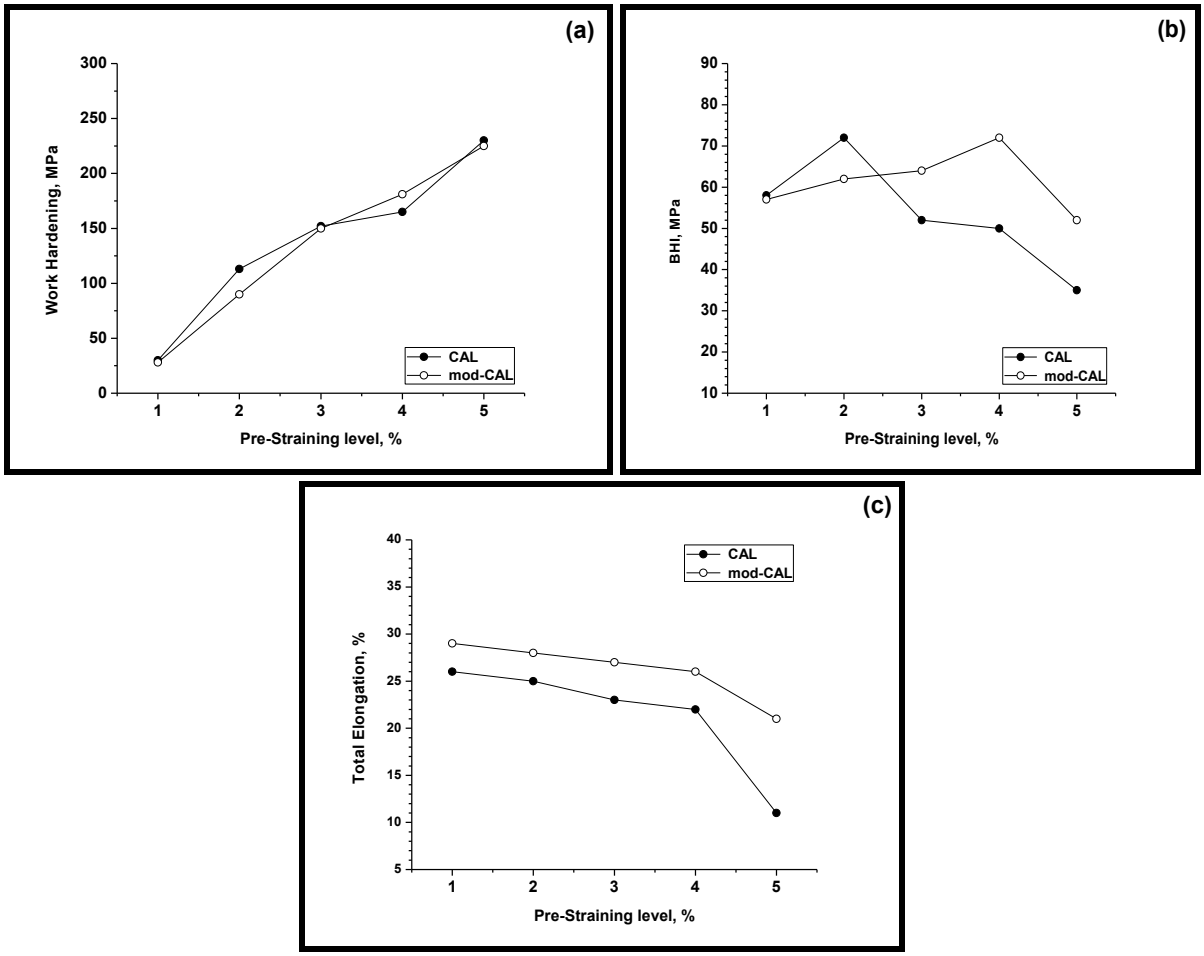

Figure 4.11: Effect of "pre-straining" only on (a) Work Hardening, and effect of "pre-straining and bake hardening on (b) Bake Hardening Index, and (c) Total Elongation.

Figure 4.11c highlights another important aspect concerning bake hardening characteristics. Though the "pre-straining with bake hardening" treatment always resulted in positive bake

hardening index values, however, an associated loss in ductility for both CAL and mod-CAL processed specimens was observed. From Figure 4.11c it was noticed that mod-CAL processed specimens showed lesser loss in ductility than the CAL processed specimens.

A detailed discussion regarding these trends obtained and the reasons thereof pertaining to the bake hardening characteristics is presented in the subsequent sections. The observed results have been analyzed with respect to the microstructure obtained from the two processes viz. CAL and mod-CAL. This analysis helped in establishing that, it was the difference in the second phase (martensite) morphology and distribution, which resulted in the marked differences in the bake hardening characteristics.

4.6. Effect of Martensite Distribution and Morphology on Bake Hardening Characteristics

This section describes the effect of second phase distribution and morphology on the bake hardening characteristics of DP steel specimens. For this, the differences in the available solute carbon content in the second phase (martensite) and differences in the lath martensite morphology and distribution have been investigated. Based on these differences, the variations seen in bake hardening response have been explained in this section.

4.6.1. Availability of Solute Carbon in Martensite Phase

In the present study, continuous increase in work hardening was observed for both the processes (viz. CAL and mod-CAL) with increase in pre-straining level (see Figure 4.11a). However, bake hardening effect did not show a similar trend. For CAL processed specimens, after an initial slight improvement in bake hardening effect, a continuous drop in BHI was observed at pre-strain values above 2 %. But, for mod-CAL processed specimens, the improvements in BHI continued even till 4 % pre-strain value. These results indicated more efficient dislocation pinning action by free solute carbon of martensite phase in the mod-CAL processed specimens. Thus, the results also showed that for CAL processed specimens, beyond 2 % pre-straining (wherein the number of mobile dislocations had increased with higher pre-strain values), effective pinning of mobile dislocations did not occur because of insufficient solute carbon in the martensite phase. These observations are in accordance with the work of Waterschoot et al (2006) on DP steels. To validate the difference in the availability of solute carbon in martensite phase, X-ray diffraction tests were conducted for bake hardened specimens pre-strained to the maximum level.

X-ray diffraction tests conclusively led to a qualitative assessment of the available solute carbon in martensite phase for both CAL as well as mod-CAL processed specimens. Solute carbon in martensite was assessed by observing the split in the peak doublet in diffractogram. The presence of a split in the peak doublet assesses the tetragonality of the martensite phase (lattice) which indirectly indicates the octahedral lattice site occupancy of solute carbon atoms in the martensite lattice [44]. In the present work, X-ray diffractograms were obtained for two specific conditions for the heat treated (CAL and mod-CAL) specimens (i) before pre-straining, and (ii) after pre-straining and bake hardening. Figure 4.12 shows the results of the X-ray diffraction test.

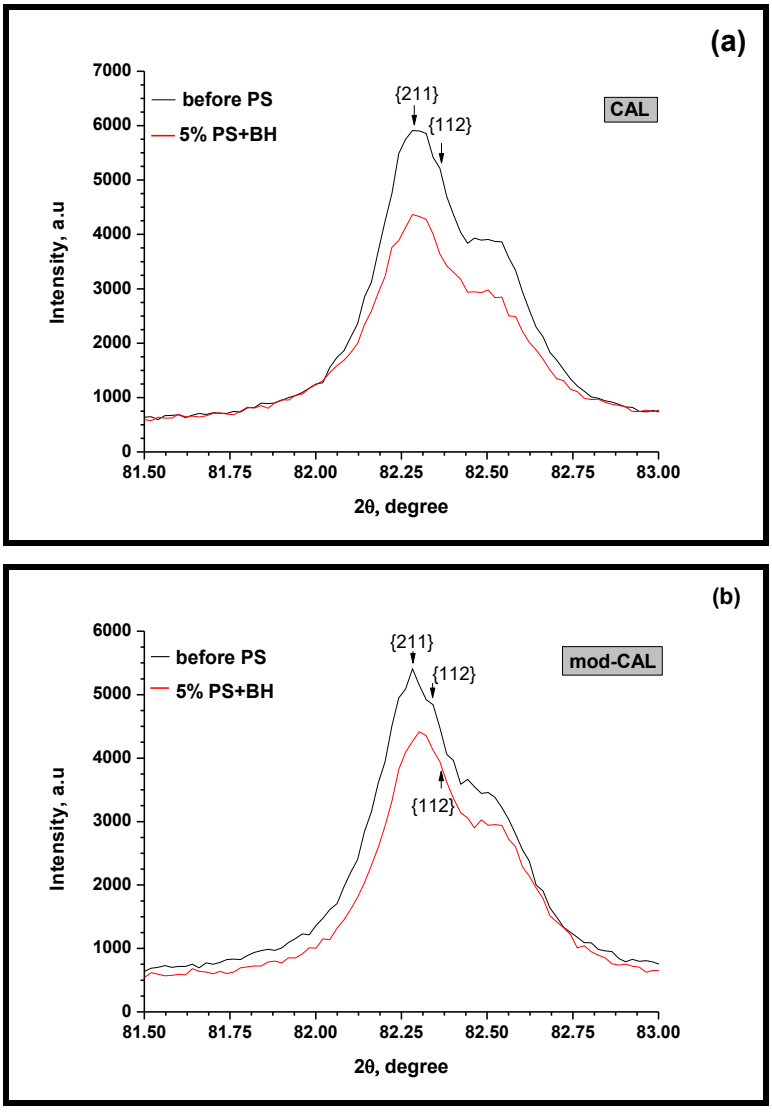

Figure 4.12: X-ray diffractograms to assess solute carbon in martensite under different conditions for (a) CAL , and (b) mod-CAL (Black arrows indicate peak doublets).

For CAL processed specimens, it was observed that a distinct split in peak doublet existed prior to pre-straining. This split in the peak doublet was absent in the post pre-straining and bake

hardened conditions. While, for mod-CAL processed specimens this split in peak doublet existed both prior to pre-straining state as well as after the pre-straining and bake hardening states. It can be observed from Figure 4.12 that for the 5 % pre-strained and bake hardened mod-CAL specimen, a peak doublet (though with a subtle second peak of {112}) still existed whereas, it was completely missing for the CAL processed specimen under similar conditions. This observation qualitatively ascertained that some solute carbon was still present in the mod-CAL specimen subjected to 5 % pre-straining and bake hardening. This solute carbon resulted in effective pinning of mobile dislocations and hence provided effective BH response even at 5 % pre-strain value. On the contrary, in case of CAL processed specimen, the absence of peak doublet after pre-straining and bake hardening indicated loss in tetragonality of martensite and thus non-availability of solute carbon in the martensite phase. Hence, for the reasons discussed, CAL processed specimens could not provide an effective bake hardening response at high pre-strain levels (i.e. beyond 2 % pre-strain level).

4.6.2. Deformation Behavior of PS and BH Specimens

This section describes the difference in properties obtained after pre-straining and bake hardening for CAL and mod-CAL specimens because of differences in the second phase distribution, grain size, and morphology. The CAL processing offered a mix of fine to medium sized second phase (martensite), mostly at or near grain boundaries, while the mod-CAL cycle showed presence of finer martensite both at/ near grain boundaries and also within ferrite grain i.e. in-grain martensite (refer to Figure 4.4). It is well reported in literature that for DP steels with the second hard phase distributed within the softer ferrite phase (in addition to its presence on the grain boundaries) leads to effective transfer of load/ strain and thereby results in improved strain partitioning and mechanical properties [24, 27, 31, 32, 45–50]. Thus, in the present work, mod-CAL processing seemed to offer a better strain partitioning between the soft and the hard microstructure constituents, which rendered good strength and ductility combination under this condition.

To understand further the effect of second phase distribution and interface morphology on the tensile deformation behavior of both CAL and mod-CAL processed specimens, interrupted tensile testing was conducted. Bake hardened specimens were subjected to interrupted tensile testing. For this purpose, 5 % pre-strained and bake-hardened specimens were chosen because of the poor ductility of CAL processed specimens.

4.6.2.1. Interrupted Tensile Testing

This test was performed to study the effect of difference in second phase distribution and interface morphology (in CAL and mod-CAL) on the deformation mechanism seen under uni-axial tensile loading of pre-strained and bake hardened specimens. It is well known that a general consequence of hardening is a resultant loss in ductility [16–22]. In the present work, the CAL processed specimen showed a drastic loss in ductility for the condition of 5 % pre-straining followed by bake hardening. Hence, 5% pre-strain value was chosen to study the mechanism of deformation.

For the test, standard tensile specimens of CAL and mod-CAL processed DP steel were provided with appropriate graduations at an interval of 2 mm along the gauge length. The gauge width of each graduation mark was recorded. Figure 4.13 shows the state of tensile specimens before interrupted tensile test was performed.

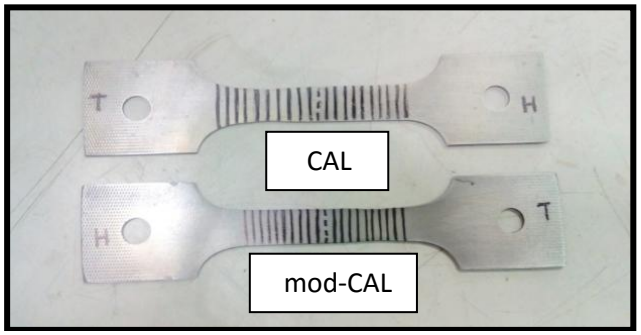

Figure 4.13: Tensile specimens with graduation marks for interrupted tensile test.

A total of ten graduations each to the left and right of a central line (dashed) were drawn. During tensile testing, the test was interrupted just when the tensile curve of the engineering stress-strain plot reached its ultimate strength i.e. just when the necking initiated. This completed the interrupted tensile test. The final gauge width at each of the graduation marks was again recorded to measure the critical true strain (change in width/ initial gauge width). After the completion of the interrupted tensile test, the necking zone (entire portion of gauge length which showed signs of decrease in width) of each specimen (CAL and mod-CAL) was cut out from the entire tensile specimen. This necking zone was further polished and grooves were cut along one of the side edges. The grooves helped in locating the position of the scanned area when deformation studies were performed under SEM. Figure 4.14 shows the necking zone obtained from the tensile specimens (interrupted test) of CAL and mod-CAL respectively.

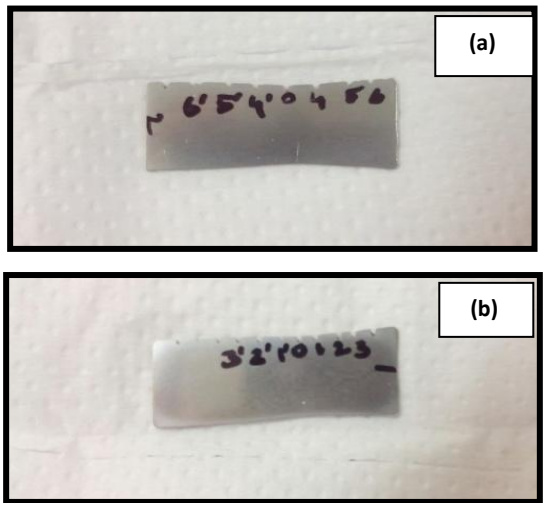

Figure 4.14: Necking zone obtained from the interrupted tensile test (a) CAL processed, (b) mod-CAL processed DP590.

From the interrupted tensile test, it was observed that necking initiated at almost the same critical true strain value for both the CAL and mod-CAL processed specimens. However, longitudinal strain developed was much different for the two cases. CAL specimen showed onset of necking at around 9 % longitudinal strain, while mod-CAL specimen showed necking at about 20 % longitudinal strain value, thus indicating the delayed nature of necking. Table 4.6 gives the values of the critical true strain observed at three different locations on the necking zone. The three zones were selected based on their proximity to the necking zone.

Table 4.6: Initial and final width measurements on the interrupted tensile test specimens.

Graduation mark on tensile specimen of		**Initial Width, mm**		**Final Width, mm**		**Critical True Strain** $(\frac{\Delta w}{Initial\ width})$	
CAL	**mod-CAL**	**CAL**	**mod-CAL**	**CAL**	**mod-CAL**	**CAL**	**mod-CAL**
5	**2**	10.23	10.03	9.06	8.54	0.14384	0.14761
4	**1**	10.23	10.04	8.60	8.45	0.15837	0.16052
0	**0**	**10.24**	**10.04**	**8.49**	**8.35**	**0.1709**	**0.16933**
• **at the onset of necking, longitudinal strain for CAL was ~ 9% and for mod-CAL was ~ 20%.**							

In the necking zone, three regions were selected for microstructure investigation based on their proximity to the critical necking area (where maximum decrease in width was observed). These three regions included the critical necking area itself (marked as graduation number “0” on both CAL and mod-CAL specimen) and two additional graduations (regions) in its vicinity (marked as “5” and “4” on CAL and as “2” and “1” on mod-CAL specimens respectively). Table 4.6

shows the critical true strain values observed at the respective graduation marks on the necking zone of the tensile specimens. Microstructural investigation of the necking zone of the CAL and mod-CAL specimens subjected to interrupted tensile testing was now conducted through scanning electron microscopy. The results of the microstructural analysis are shown in Figure 4.14.

Figure 4.15 (a, c, e) present the SEM micrographs of the necking regions marked as 5, 4, and 0 (Table 4.6 and Figure 4.13) of the CAL processed specimen. Similarly, Figure 4.15 (b, d, f) present the microstructure at the necking zone regions marked as 2, 1, and 0 of the mod-CAL processed specimen. An early micro-crack initiation was noted at grain boundary martensite/ferrite interfaces in specimen processed by CAL, resulting in loss of ductility. mod-CAL processed specimen did not show any micro-cracking evidence even in the critical neck region. However, very limited micro-void nucleation at the martensite/ferrite interfaces was noted in the mod-CAL specimen. The absence of interface cracking in the mod-CAL processed specimen implied stronger interfaces thus, resulting in better ductility in the mod-CAL processed pre-strained and bake hardened specimens [51–56]. CAL offered uniform distribution of second phase along the ferrite grain boundaries, while mod-CAL showed a more mixed distribution of second phase martensite both along ferrite grain boundary as-well as within the ferrite grains. This mixed distribution of martensite enabled better strain partitioning for mod-CAL processed specimens as compared to CAL specimens. Further, microstructure studies near fracture tip with martensite present at grain boundary showed extensive micro-crack tendency at interface for CAL cycle, whereas, mod-CAL showed micro void nucleation at the in-grain ferrite/martensite interfaces. Further, to investigate the role of varied martensite morphology on the mechanical behavior of pre-strained and bake hardened DP microstructure, microstructural evaluation near the fracture tip of interrupted tensile test specimens was now conducted at very high magnifications. Figure 4.16 shows the SEM micrographs for the CAL and mod-CAL specimens respectively. For CAL processed specimen, microstructure studies near the fracture tip revealed that martensite (typical lath type) at the grain boundaries showed extensive micro-cracking (delamination/ shearing) tendency at the interface [54–56].

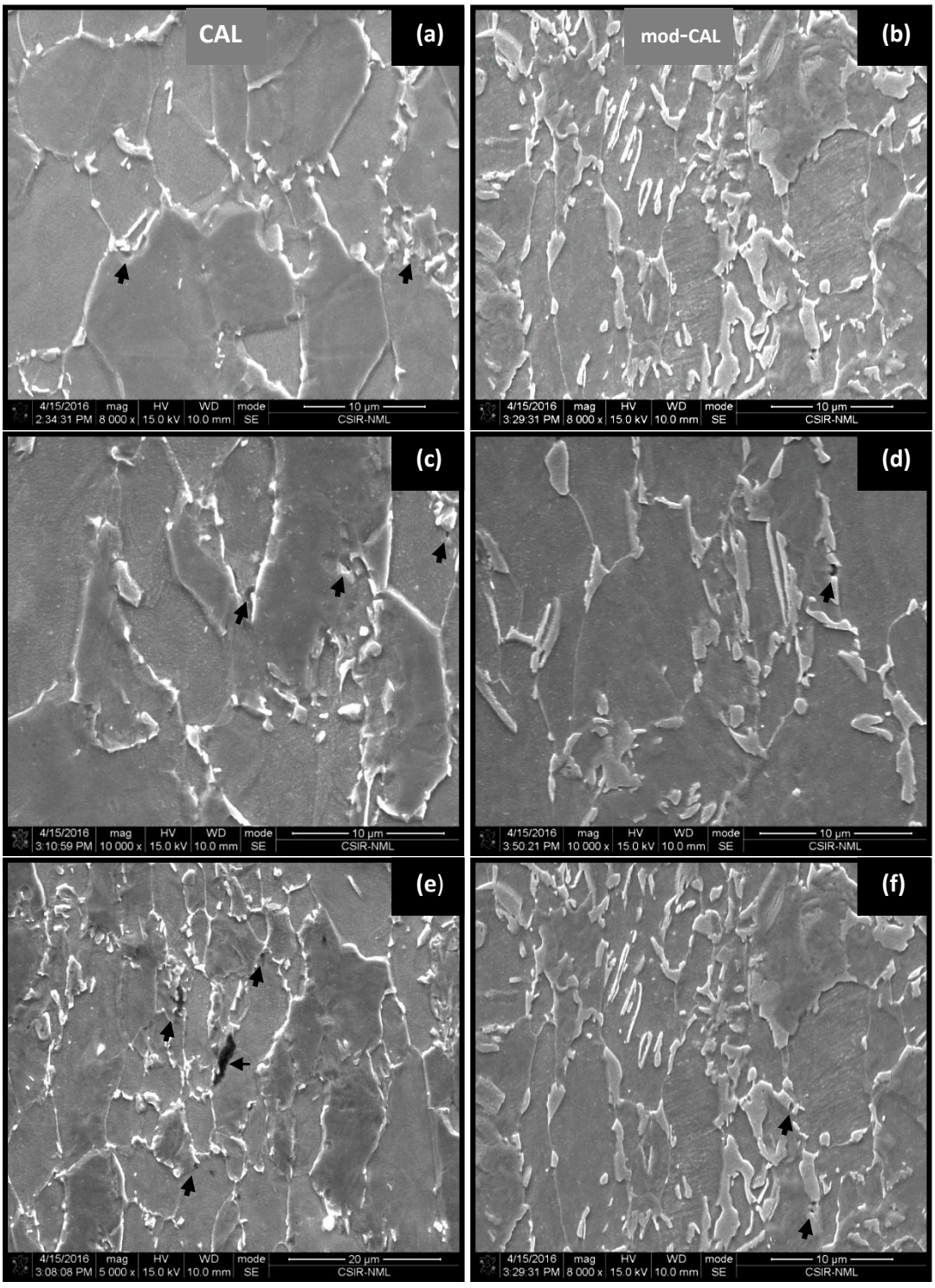

Figure 4.15: SEM microstructure of CAL and mod-CAL specimens showing micro-void/crack initiation and grain boundary shearing with increasing true strain (a, c, e) and (b, d, f) respectively (a) initiation of boundary shear for CAL, (b) very stable boundary for mod-CAL, (c) initiation of micro-void at several places and grain boundary shearing in CAL, (d) scattered micro-void nucleation witnessed in mod-CAL, (e) extensive local deformation and shear along grain boundaries, (f) relatively stable boundaries and extensive ferrite grains deformation with few micro-cracks. Arrows indicate various defect zones.

However, for the mod-CAL processed specimen, micro-void nucleation at the ferrite-martensite interfaces was noted.

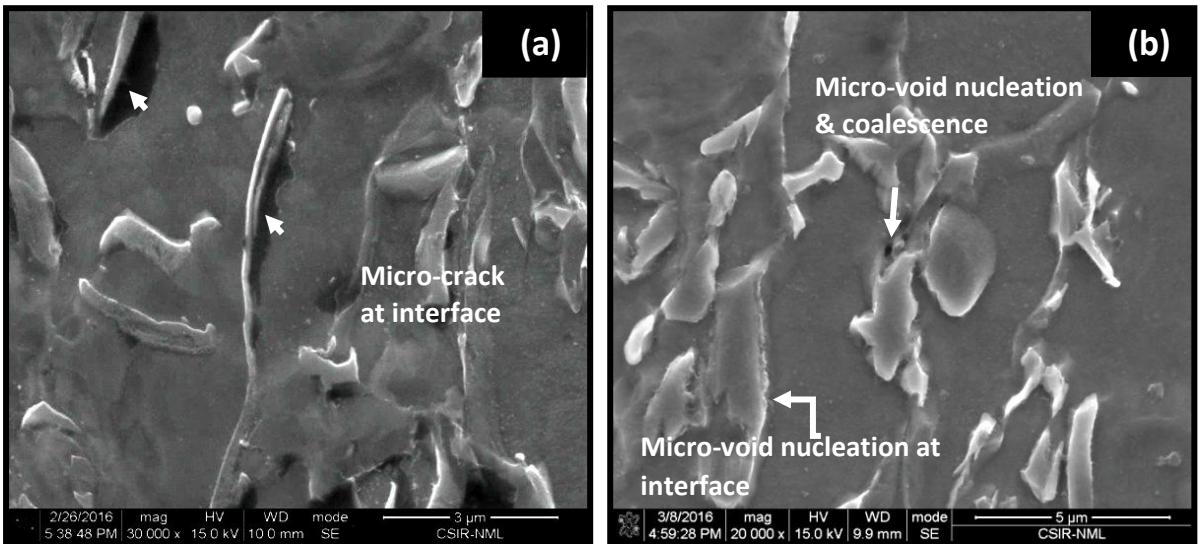

Figure 4.16: Micro-crack formation /micro-void formation in 5% pre-strained and bake hardened specimens. (a) CAL process microstructure showing extensive micro-cracking of ferrite-martensite interface and (b) mod-CAL processed microstructure shows only interface micro-void nucleation. Arrows indicate various cracks.

Moreover, irrespective of the process cycle followed grain boundary martensite showed early fracture, as can be seen in Figure 4.16. However, severity of micro-crack initiation was observed at sharp ferrite/martensite interfaces in CAL cycle, independent of its location. Further, shape of hard martensite phase was found to influence severity of micro-cracking [31, 47, 48, 51, 56, 57]. Fine lath martensite at grain boundaries as in shown in Figure 4.3 (c) was more sensitive to interface strain localization compared to oblong or polygonal shape martensite as in Figure 4.3 (d) at ferrite grain boundaries.

4.7. Aspect Ratio Evaluation

To understand the deformation behavior more accurately, plastic deformation characteristics of ferrite grains were studied. Microstructure (Figure 4.15) very distinctly showed extensive plastic deformation in the two processed steels. To distinguish the extent of plastic deformation, ferrite grain elongation in the tensile deformation direction was determined by estimating aspect ratio distribution. Aspect ratio distribution for the CAL and mod-CAL processed specimens (5 % pre-strained and bake hardened) is shown in Figure 4.17.

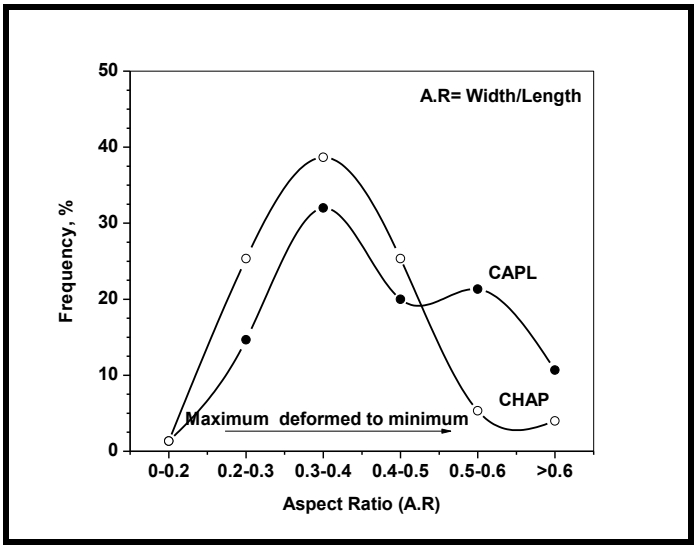

Figure 4.17: Ferrite grain shape aspect ratio distribution post tensile deformation necking of CAL and mod-CAL processed specimens.

The mod-CAL pre-strained and bake hardened specimens showed exclusive peak near smaller aspect ratio values (see Figure 4.17) values indicating that nearly all the ferrite grains underwent extensive plastic deformation. On the contrary, CAL showed bimodal distribution in aspect ratio values (see Figure 4.16) thus indicating insufficient strain partitioning between the soft (ferrite) and the hard (martensite) phases. The bimodal distribution as seen in the case of CAL (5 % pre-strained and bake hardened) specimens indicated that a few ferrite grains had deformed extensively (as shown by the first peak appearing at a lower value of aspect ratio nearly 0.3–0.4), while the remaining ferrite grains largely remained undeformed (as shown by a second peak appearing at a higher aspect ratio value nearly 0.5–0.6). This bimodal nature of ferrite grain deformation indicated early micro-crack initiation observed in the predominantly grain boundary martensite distribution seen in CAL processed DP microstructure. Thus, early initiation of necking was noticed in CAL processed (5 % pre-strained and bake hardened) specimen. Further, from the interface morphology viewpoint, the serrated lath edges along with in-grain martensite in mod-CAL processed specimens, resulted in a delayed behavior of micro-void initiation of martensite within ferrite grains. This was because interfacial crack was delayed due to the lesser localized stress concentration generated at the oblong or serrated lath edges in mod-CAL processed specimens.

Chapter 5
Conclusions

5.1. General

DP steels offer wide applicability in modern day automobile industries. So, processing of DP steels is considered as a prime area of focus. Industrial processing routes involve continuous annealing process lines to obtain DP microstructure wherein martensite is the secondary hard phase within a soft and primary ferrite matrix. Bake hardening is a finishing treatment which helps in curing of the paint coat on finished auto-body components. This treatment also improves the final yield strength or more specifically enhances the dent resistance at practically no additional production cost. Thus, improvement in processing routes to obtain DP microstructure also has a great impact on improving bake hardenability of finished components by tailoring of the second phase (martensite) distribution and morphology. The present study shows the possibility of improving bake-hardening response along with improved final ductility via modification of current industrial continuous annealing process line parameters. SEM analysis was done to characterize the second phase distribution and morphology, while, XRD and Nano-indentation test validated the results.

5.2. Results and Conclusions

As-Received Material

- The microstructure of the low carbon cold rolled (67 %) as-received material consisted of deformed pearlite (86 %) colonies and ferrite (14 %) grains.

Annealing Simulation Results

- To obtain difference in second phase distribution and morphology, two alternate heat treatment routes (CAL and mod-CAL) were used. In the conventional CAL process, annealing temperature of 790 ℃ was reached with a moderate heating rate of 10 ℃/ s, followed by isothermal holding at 790 ℃ for 60 s and finally cooling to room temperature. In the mod-CAL processing route, the peak temperature was increased to 840 ℃, the heating rate was decreased, and soaking was eliminated, followed by the same cooling route.

- These two processing routes led to a marked difference in the second phase (martensite) distribution and morphology. The CAL processed specimen showed a typical grain boundary distribution of martensite along the ferrite grain boundaries. The ferrite-martensite interface morphology was very sharp and fine. However, the mod-CAL processed specimen showed distribution of martensite along the ferrite grain boundaries and also within the ferrite grains (in-grain martensite). The ferrite-martensite interface in this case was seen to be oblong or the edges were serrated. Absence of isothermal holding or soaking at the annealing temperature led to staggered or oblong (serrated) edges of lath ferrite-martensite interfaces in mod-CAL specimen while in the conventional annealing line (CAL) the edges of the lath morphology were typically fine and smooth.

Results of Pre-straining and Bake Hardening Experiments

- Both processes showed increasing work hardenability with pre-strain, however, bake hardening behavior was different for the two cases. It showed nearly constant values for mod-CAL, whereas, a decreasing trend was observed for CAL at higher pre-strains. Bake hardening index showed maximum value of 72 MPa at 2 % pre-strain for CAL processed DP steel beyond which strength was observed to fall ~35 MPa at maximum pre-strain of 5%. On the other hand, mod-CAL processed specimen showed a peak in BH at 4% PS of about 72 MPa and did not show any sharp drop even at 5% pre-strain. Most importantly, it did not show loss in its ductility even at 5% pre-strain.
- The improvement in the bake hardening characteristics at higher pre-strain values for mod-CAL processed specimens was correlated with different contents of available solute carbon in the two processes. Nano-indentation test also confirmed higher hardness of mod-CAL processed martensite phase, thus indicating higher carbon presence in it. The average hardness of the lath martensite phase in CAL and mod-CAL processes was 350 HV and 387 HV respectively.
- The grain boundary distribution of second phase martensite in CAL microstructure showed high amount of local deformation along the ferrite-martensite interface boundary by means of interfacial crack growth and propagation while in-grain ferrite martensite lath in mod-CAL showed relatively less stress concentration at boundaries. Therefore, martensite presence at the ferrite grain boundaries seemed to increase the propensity of early micro-crack formation leading to loss of ductility in CAL processed specimens.

- The lath structures of CAL and mod-CAL were strikingly different. While CAL showed sharp/smooth interface with ferrite, mod-CAL processing produced a serrated type interface. This difference in interface also appeared to influence the fracture or de-lamination of ferrite-martensite boundaries.
- Between CAL and mod-CAL, the strain distribution behavior varied. The onset of necking in mod-CAL case was a synergistic effect of loss in ferrite phase strain hardenability and micro-void nucleation. Thus, loss in ductility with increase in pre-strain value post bake hardening treatment was far lesser when compared to CAL process. The final total elongation for CAL and mod-CAL for maximum pre-strained and bake hardened specimens were 11 % and 22 % respectively.

5.2. Major Conclusions and Recommendations

The work presented in this study establishes the fact that changes in heating rates and annealing temperatures will result in variant DP microstructure which can be tailored to our needs. Bake hardening response and its consequent loss in ductility depends not only on pre-straining level, baking temperature and baking time, but, it can now be conclusively suggested that it also depends on the second phase distribution and morphology. Thus, annealing process changes can bring significant improvements in bake hardening behavior of DP steels. The following are the major conclusions and recommendations from the present work:

- Improvement in annealing parameters (heating rates, and annealing temperature, holding time etc.) improves the bake hardening characteristics of DP steels by varying the second phase (martensite) distribution and morphology.
- For achieving higher degree of pre-straining constraints (for any futuristic complex and aesthetically demanding auto-body components), mod-CAL processing of DP steels will outperform CAL with regards to bake hardening behavior.

5.4. Scope of Future Work

In this present work, owing to certain practical limitations, bake hardening responses were judged only for a particular temperature of 170 ℃. However, with appropriate control of baking temperature and time, optimized bake hardening response for CAL processed DP steel is still widely anticipated. Another important aspect of baking is that most of the work in the present study was performed in oxidizing conditions due to which loss in carbon in form of de-carburization was inevitable.

Stricter testing conditions can be achieved by complete vaccumization of baking chamber prior to baking treatment to nullify the chances of any carbon loss thereby, further improving the bake hardening properties.

References

1. J. Galán, L. Samek , P. Verleysen , K. Verbeken, Houbaert Y, Advanced high strength steels for automotive industry, *Revista de Metalurgia* 48 (2012) 118–131.
2. R. Kuziak, R. Kawalla, S. Waengler, Advanced high strength steels for automotive industry, *Archives of Civil and Mechanical Engineering* 8 (2008) 103–117.
3. O. Kwon, K. Lee, G. Kim, K.G. Chin, New trends in advanced high strength steel developments for automotive applications, *Materials Science Forum* 638–642 (2010) 136–141.
4. S. Maggi, M. Murgia, Introduction to the metallurgic characteristics of advanced high-strength steels for automobile applications, *Welding International* 22 (2008) 610–618.
5. D.K. Matlock, J.G. Speer, Processing opportunities for new advanced high-strength sheet steels, *Materials and Manufacturing Processes* 25 (2010) 7–13.
6. D.K. Matlock, J.G. Speer, E.D. Moor, P.J. Gibbs, Recent developments in advanced high strength sheet steels for automotive applications: an overview, *Jestech* 15 (2012) 1–12.
7. O.N. Cora, M. Koç, Promises and problems of ultra/advanced high strength steel (U/AHSS) utilization in automotive industry. OTEKON'14. In: Proceedings of the 7th Otomotiv Teknolojileri Kongresi; 2014 May 26–27; Bursa (Turkey). 2014. p 1–8.
8. C.M. Tamarelli, AHSS 101: The evolving use of advanced high-strength steels for automotive applications. Steel Market Development Institute, Michigan, USA, 2000.
9. Q.U. Hao, Advanced high strength steel through paraequilibrium carbon partitioning and austenite stabilization, Ph.D Thesis, Case Western Reserve University, United States (2011).
10. N. Baluch, Z.M. Udin, C.S. Abdullah. Advanced high strength steel in auto industry: an overview, *Engineering, Technology & Applied Science Research* 4 (2014) 686–689.
11. E. Billur, T. Altan, Challenges in forming advanced high strength steels. In: Proceedings of new developments in sheet metal forming; 2012. p 285–304.
12. C. Buscha , A. Hatscher, M. Otto, S. Huinink, M. Vucetic, C. Bonk, A. Bouguecha, B.A Behrens, Properties and application of high-manganese TWIP-steels in sheet metal forming, *Procedia Engineering* 81 (2014) 939–944.

13. J. Adamczyk, A. Grajcar, Effect of heat treatment conditions on the structure and mechanical properties of DP-type steel, *Journal of Achievements in Materials and Manufacturing Engineering* 17 (2006) 305–308.
14. X. Cornet, and J.C. Herman, Method for making a multiphase hot-rolled steel strip, *U.S. Patent 0041933 A1*, March 6, 2003.
15. Q. Meng, J. Li, J. Wang, Z. Zhang, L. Zhang, Effect of water quenching process on microstructure and tensile properties of alloy cold rolled dual-phase steel, *Materials and Design*, 30 (2009) 2379–2385.
16. A.K. De, S. Vandeputte, B.C. De Cooman, Static strain aging behavior of ultra low carbon bake hardening steel, *Scripta Materialiaialia* 41 (1999) 831–837.
17. S. Das, Bake hardening in low and medium carbon steels, Ph.D Thesis, IIT Kharagpur, India (2012).
18. A. Momeni, K. Dehghani, S. Abbasi, M. Torkan, Bake hardening of a low carbon steel for automotive applications, *Metalurgija*, 13 (2007) 131–138.
19. Y. Cao, J. Ahlström, B. Karlsson, The influence of temperatures and strain rates on the mechanical behavior of dual phase steel in different conditions, *Journal of Materials Research and Technology* 4 (2015) 68–74.
20. S. Gunduz, Static strain ageing behaviour of dual phase steels, *Materials Science and Engineering A* 486 (2008) 63–71.
21. J. Zhang, R. Fu, R. Liu, X. Wei, L. Li, Bake hardening behaviour of DP and TRIP steels, *Journal of University of Science and Technology Beijing* 15 (2008) 132–137.
22. A. Ramazani, S. Bruehla, T. Gerber, W. Bleck, U. Prahl, Quantification of bake hardening effect in DP600 and TRIP700 steels, *Materials and Design* 57 (2014) 479–486.
23. L.J. Chiang, K.C Yang, I.C. Hsiao, Effects of annealing conditions on bake hardenability for ULC steels, *China Steel Technical Report* 24 (2011) 1－6.
24. W. Bleck, A. Frehn, J. Ohlert, H.M. Sonne, G. Steinbeck, Influence of temperature and pre-straining on the plastic material behaviour of modern sheet steels for autobody applications, *Materialwissenschaft und Werkstofftechnik* 35 (2004) 495-504.
25. S. Brühl, Einfluss der Martensitephase auf das Bake-Hardening-Verhalten von Dualphasen-Stählen, Ph.D Thesis, RWTH Aachen, Germany (2010).

26. W.C Jeong, Effect of prestrain on aging and bake hardening of cold-rolled, continuously annealed steel sheets. *Metallurgical and Materials Transactions A* 29 (1998) 463–467.
27. P. Chang, Temper ageing of continuously annealed low carbon dual phase steel, *Metallurgical and Materials Transactions A* 15 (1984) 73–86.
28. R.G. Davies, Early stages of yielding and strain ageing of a vanadium containing dual phase steel, *Metallurgical and Materials Transactions A* 10 (1979) 1549–55.
29. T. Waterschoot, A.K De, S Vandeputte, B.C De Cooman, Static strain aging phenomena in cold-rolled dual-phase steels, *Metallurgical and Materials Transactions A* 34 (2003) 781–91.
30. I.B. Timokhina, P.D. Hodgson, E.V. Pereloma. Transmission electron microscopy characterization of the bake hardening behavior of transformation induced plasticity steels and dual phase steels, *Metallurgical and Materials Transactions A* 38 (2007) 2442–54
31. J. Kadkhodapoura, A. Butzb, S. Ziaei-Rad, Mechanisms of void formation during tensile testing in a commercial dual-phase steel, *Acta Materialia* 59 (2011) 2575–2588.
32. H. Ghadbeigi, C. Pinna, S. Celotto, Failure mechanism in DP600 steel: Initiation, evolution and fracture, *Materials Science and. Engineering A* 588 (2013) 420-431.
33. L. Valeria, N. Hernán, N. Lorusso, G. Hernán, Effect of carbon content on microstructure and mechanical properties of dual phase steels, *Procedia Materials Science* 8 (2015) 1047-1056.
34. Q. Lai, O.Bouaziz, M.Gouné, L. Brassart, M. Verdier, G. Parry, A. Perlade, Y. Bréchet, T. Pardoen, Damage and fracture of dual-phase steels: Influence of martensite volume fraction, *Materials Science and Engineering A* 646 (2015) 322–331.
35. H. Seyedrezain, A.K. Pilkey, J.D. Boyd, Effect of pre-IC annealing treatments on the final microstructure and work hardening behavior of a dual-phase steel, *Materials Science and Engineering A* 594 (2014) 178–188.
36. S. Sharma, Simulations for pearlite-to-austenite transformation in a DP 590 steel for improved mechanical properties, M.E Thesis, Thapar University, Patiala, India (2015).

37. M. Mittal, Effect of intercritical annealing parameters on the recrystallization, austenite formation and stabilization in a dual phase steel, M.E Thesis, Thapar University, Patiala, India (2014).
38. P. Li, J. Li, Q. Meng, W. Hua, D. Xu, Effect of heating rate on ferrite recrystallization and austenite formation of cold-roll dual phase steel, *Journal of Alloys and Compounds* 578 (2013) 320–327.
39. A. Ghaheri, A.Shafyei, M Honarmand, Effects of inter-critical temperatures on martensite morphology, volume fraction and mechanical properties of dual phase steels obtained from direct and continuous annealing cycles, *Materials and Design* 62 (2014) 305–319.
40. A.P. Pierman, O. Bouazizb, T. Pardoena, P.J. Jacques, L. Brassart, The influence of microstructure and composition on the plastic behaviour of dual-phase steels, *Acta Materialia* 73 (2014) 298–311.
41. I.P. Kemp, G. Pollard, A.N. Bramley, Static strain aging in high-carbon steel wire, *Materials Science and Technology* 6 (1990), 331-337.
42. P. Watte, J. Van Humbeeck, E. Aernoudt, I. Lefever, Strain ageing in heavily drawn eutectoid steel wires, *Scripta Materialia* 34 (1996) 89–95.
43. A. Bag, K.K. Ray, E.S. Dwarkadasa, Influence of martensite content and morphology on tensile and impact properties of high-martensite dual phase steels, *Metallurgical Materials Transactions* 30 (1999) 1193–1202.
44. T. Waterschoot, K Verbeken, B.C. De Cooman, Tempering kinetics of the martensitic phase in DP steel. *Iron and Steel Institute of Japan International* 46 (2006) 138–146.
45. T. Waterschoot, Fundamentals of aging in multiphase steels: static strain aging and tempering in dual phase steels, Ph.D Thesis, University of Ghent, Ghent, Belgium, (2003).
46. Y. Yamada, Static strain aging of eutectoid carbon-steel wires, *Iron and Steel Institute of Japan International* 16 (1976) 8, 417-426.
47. S. Kim, S. Lee, Effects of martensite morphology and volume fraction on quasi-static and dynamic deformation behavior of dual phase steels, *Metallurgical Materials Transactions* 31 (2000) 1753–60.
48. F. Maresca, V.G. Kuznetsova, M.G.D. Geers, Deformation behaviour of lath martensite in multi-phase steels, *Scripta Materialia* 110 (2016), 74–77.

49. C.F. Kuang , J. Li , S.G. Zhang, J. Wang , H.F. Liu , A.A. Volinsky, Effects of quenching and tempering on the microstructure and bake hardening behavior of ferrite and dual phase steels, *Materials Science and Engineering A* 613 (2014) 178–183.
50. C.F. Kuang, S. Zhang, J. Li, J. Wang, H. Liu, Effects of pre-strain and baking parameters on the microstructure and bake hardening properties of dual phase steel, *International Journal of Minerals, Metallurgy and Materials* 21 (2014) 766–771.
51. E.V. Nesterovaa, S. Bouvierb, B. Bacroix, Microstructure evolution and mechanical behavior of a high strength dual-phase steel under monotonic loading, *Materials Characterization* 100 (2015) 152–162.
52. K. Sugimoto, M. Kobayashi, H. Matsushima, S. Hashimot, X-ray residual stress and strain induced transformation of retained austenite in TRIP aided dual phase steels, *Transactions of the Japan Society of Mechanical Engineers A* 16 (1995) 80–86.
53. W.M. Garrison Jr, N.R. Moody, Ductile fracture, *Journal of Physics and Chemistry of Solids* 48 (1987) 1035–74.
54. W.A. Spitzig, R.E. Smelser, O. Richmond, The evolution of damage and fracture in iron compacts with various initial porosities, *Acta Metallurgica* 36 (1988) 1201–11.
55. H.Qiu, H.Mori, M. Enoki, K. Teruo, Evaluation of Ductile Fracture of Structural Steels, *Iron and Steel Institute of Japan International* 39 (1999) 358–364.
56. G. LeRoy, J.D. Embury, G. Edwards, M.F. Asbhy, A model of ductile fracture based on the nucleation and growth of voids, *Acta Metallurgica* 29 (1981) 1509–22.
57. D. Kwon, Interfacial de-cohesion around spheroidal carbide particles, *Scripta Metallurgica* 22 (1988) 1161–64.
58. M. Krieger, Mechanical properties and bake hardening behaviour of cold rolled dual phase steels subjected to advanced galvanising process routes, Ph.D. Thesis, Clausthal University of Technology, Germany (2007).